isvr Institute of Sound and Vibration Research

Low and High Frequency Instabilities in Feedback Control of a Vibrating Single Degree of Freedom System

K.A. Ananthaganeshan, M.J. Brennan and S.J. Elliott

ISVR Technical Memorandum 870

September 2001

University of Southampton

SCIENTIFIC PUBLICATIONS BY THE ISVR

Technical Reports are published to promote timely dissemination of research results by ISVR personnel. This medium permits more detailed presentation than is usually acceptable for scientific journals. Responsibility for both the content and any opinions expressed rests entirely with the author(s).

Technical Memoranda are produced to enable the early or preliminary release of information by ISVR personnel where such release is deemed to the appropriate. Information contained in these memoranda may be incomplete, or form part of a continuing programme; this should be borne in mind when using or quoting from these documents.

Contract Reports are produced to record the results of scientific work carried out for sponsors, under contract. The ISVR treats these reports as confidential to sponsors and does not make them available for general circulation. Individual sponsors may, however, authorize subsequent release of the material.

UNIVERSITY OF SOUTHAMPTON

INSTITUTE OF SOUND AND VIBRATION RESEARCH

DYNAMICS GROUP

Low and High Frequency Instabilities in Feedback Control of a Vibrating Single Degree of Freedom System

by

K.A. Ananthaganeshan, M.J. Brennan and S.J. Elliott

ISVR Technical Memorandum No: 870

September 2001

Authorized for issue by
Dr M.J. Brennan
Group Chairman

Contents

Abstract

This report describes an investigation into acceleration, velocity and displacement feedback control of the vibration of a single degree of freedom system. The control strategy used is simple analogue control by feeding back absolute acceleration, velocity or displacement response. It is found that although an ideal system is unconditionally stable, the real systems, which include filters, integrators and amplifiers, are only conditionally stable.

Causes of instability at low and high frequency are investigated for a real system. It is found that low frequency phase advance is critical to the system stability and performance. The dominant source of instabilities at low frequencies is found to be the high pass filter component and simple expressions are derived to give the maximum gain that can be applied before system becomes unstable with high pass filters fitted. In a lightly damped system, increasing damping only has a marginal effect on overall system performance.

The theoretical predictions are supported by some experimental work. A relatively simple formula to analyse control time delay is also derived. Considering low and high frequency instabilities, velocity feedback control is found to be more robust and hence more attractive.

Introduction

Vibration isolators are required to protect a dedicated piece of equipment from the vibration of a structure to which it is attached [1,2]. Conventional passive forms of isolation generally involve an inherent compromise between high frequency isolation, that requires low values of damping, and limited excitation of the rigid body modes, which requires high values of isolator damping [3,4,5]. Passive isolation performance can be enhanced by coupling an active system to the existing mounts [6]. The objective of active vibration control is to reduce the vibration response of the mechanical system by automatic modification of the system dynamics [4]. The control systems used for vibration isolation purposes can be either feed forward or feedback. Feed forward control has been used extensively in active machinery vibration isolation involving a time domain least squares adaptive filter [7]. The effectiveness of this method depends on determining an appropriate reference signal, and when this signal cannot be obtained easily feedback control has to be used [4]. For periodic disturbances feed forward control may indeed be preferable as the reference signal need not be in advance of the controller output signal to satisfy causality constraints. However in many cases vibrations are not periodic in nature and it is not possible to get the information of the incoming disturbance soon enough for a feed forward control to be effective. Under these circumstances, feedback control is considered to be a better method.

The application of feedback control for vibration isolation has been well documented, for example [1, 2, 3, 5, 9, 11]. In recent years feedback control for vibration isolation is increasingly being used, the implementation of which can be either analogue or digital control. Analogue feedback control systems for vibration control have been described in references [1, 3, 5, 11].

The essential components in an active control system are a sensor (to detect the vibration), an electronic controller and actuators [4, 10, 13]. Sensors and actuators together with associated signal conditioning equipment play an important role in active vibration control, but often place limits on the control performance [13]. Devices such as accelerometers are often used as the sensing device in vibration

testing and control [4,15,16]. These devices often use piezoelectric sensing elements to achieve certain design natural frequencies, weight and sensitivity characteristics [16]. They are generally charge generating devices, which require high input impedance signal conditioning instruments to interface between them and recording device [15,16]. Charge amplifiers are such devices, which convert the generated charge into an output voltage that can be measured or recorded. These signal-conditioning devices often consist of filters to reject unwanted signals. The term filtering is used to describe the process of removing a certain band of frequencies from a signal and permitting others to be transmitted [19]. These kinds of filters often introduce extra phase shift at certain bands of frequencies, which are sometimes critical to the stability of the feedback vibration control system [2,11]. Ren et al. [9] studied the phase lag introduced by A/D, D/A converters, and actuators in an active feedback control system and suggested that a phase-lead compensation net work can be employed to over come this problem.

Actuators are used in active vibration control to generate a secondary vibrational response, which could reduce the overall response by destructive interference with the original response of the system caused by primary source of vibration [4]. Such actuators in practice can be configured either to react off the base structure or function as an inertial actuator [3]. The choice actuator configuration also influences the available stability limit [3]. In general, the design of a feedback controller involves a trade-off between performance (the attenuation of the disturbance) and robust stability (the ability to remain stable under changing conditions) [8]. However the choice of controller, to a certain extent, depends on the system considered for control.

This report deals with feedback control of a single degree of freedom (SDOF) system. It particularly looks at high and low frequency stability issues. Following this introduction, the concept of feedback control of vibration is presented in section 2 using an idealised system for acceleration, velocity and displacement feedback control. The distinctions between a real and an ideal system are also discussed in section 2. Section 3 deals with low frequency instabilities and section 4 deals with high frequency instabilities. In section 5 experimental work is presented and discussed. Finally in section 6 concluding remarks are given.

2. Feedback control of a single degree of freedom system

2.1 Basic concept

Consider a SDOF system modelled as a lumped mass- spring-damper system with feedback control applied as shown in Fig 2.1. A passive mount with stiffness k and damping coefficient c supports a rigid mass m, which is excited by a primary force f_p. It is assumed that the mounts are mass-less. An electromagnetic control shaker generating the control force f_s is also installed between the mass and base structure in parallel with the passive mount to achieve a reduction in the response of the mass. The control system uses direct negative feedback control. In other words the signal measured by the sensor mounted on the equipment is used to produce the control force. This control force, which can be proportional to acceleration, velocity or displacement, is produced via the controller which has a gain $-H$. It is this concept that is investigated in this section. Accelerance, mobility and receptance are considered as the frequency response functions for acceleration, velocity and displacement feedback control system respectively.

2.1.1 System without control

For the system in figure 2.1, the differential equation describing the motion in the absence of feedback control is,

$$m\ddot{x}(t) + c\dot{x}(t) + kx(t) = f_p(t) \tag{2.1}$$

Where,

m - mass of the system

c - damping coefficient

k - stiffness of the mount

$x(t)$ - instantaneous displacement

$f_p(t)$- disturbing/exciting force.

By assuming zero initial conditions and taking Laplace transforms gives,

$$\frac{\ddot{X}(s)}{F_p(s)} = \frac{s^2}{ms^2 + cs + k} \tag{2.2}$$

The corresponding frequency response function can be obtained by substituting $s = j\omega$ in equation (2.2) to give,

$$\frac{\ddot{X}(j\omega)}{F_p(j\omega)} = \frac{-\omega^2}{m\left(\omega_n^2 - \omega^2 + j2\zeta\omega_n\omega\right)} \tag{2.3}$$

where

$\omega_n = \sqrt{\frac{k}{m}}$ is the undamped natural frequency and $\zeta = \frac{c}{2m\omega_n}$ is the damping ratio.

Letting $\Omega = \frac{\omega}{\omega_n}$ equation (2.3) can be written as,

$$\frac{\ddot{X}(j\Omega)}{F_p(j\Omega)} \times m = \frac{-\Omega^2}{\left(1 - \Omega^2 + j2\zeta\Omega\right)} \tag{2.4}$$

where $\frac{\ddot{X}(j\Omega)}{F_p(j\Omega)} \times m$ is the non-dimensional accelerance.

Similarly mobility and receptance can be written in the Laplace domain as,

$\frac{\dot{X}(s)}{F_p(s)} = \frac{s}{ms^2 + cs + k}$ and $\frac{X(s)}{F_p(s)} = \frac{1}{ms^2 + cs + k}$ respectively.

The non-dimensional mobility and the non-dimensional receptance of the system can be written as,

$$\frac{\dot{X}(j\Omega)}{F_p(j\Omega)} \times c = \frac{j2\zeta\Omega}{\left(1 - \Omega^2 + j2\zeta\Omega\right)} \tag{2.5}$$

where $\frac{\dot{X}(j\Omega)}{F_p(j\Omega)} \times c$ is the non-dimensional mobility, and

$$\frac{X(j\Omega)}{F_p(j\Omega)} \times k = \frac{1}{\left(1 - \Omega^2 + j2\zeta\Omega\right)} \tag{2.6}$$

where $\frac{X(j\Omega)}{F_p(j\Omega)} \times k$ is the non-dimensional receptance.

2.1.2 System with feedback control

Now consider the system with feedback control, the differential equation describing the motion of the system becomes,

$$m\ddot{x}(t) + c\dot{x}(t) + kx(t) = f_p(t) - f_S(t) \tag{2.7}$$

where,

$f_s(t)$ is the secondary or control force.

Acceleration feedback control is considered first. The control force, which is proportional to the acceleration, can be written as,

$$f_s(t) = g_a \ddot{x}(t) \tag{2.8}$$

where g_a is the gain for acceleration feedback control.

From equations (2.7) and (2.8) the non-dimensional accelerance in the frequency domain can be written as,

$$\frac{\ddot{X}(j\Omega)}{F_p(j\Omega)} \times m = \frac{-\Omega^2}{\left(1 - \left(1 + \frac{g_a}{m}\right)\Omega^2 + j2\zeta\Omega\right)} \tag{2.9}$$

where $\frac{g_a}{m}$ is the non-dimensional gain for acceleration feedback control.

Similarly for velocity feedback control, the control force, which is proportional to the velocity, can be written as,

$$f_s(t) = g_v \dot{x}(t) \tag{2.10}$$

where g_v is the gain for the velocity feedback control.

From equations (2.7) and (2.10) the non-dimensional mobility in the frequency domain can be written as,

$$\frac{\dot{X}(j\Omega)}{F_p(j\Omega)} \times c = \frac{j2\zeta\Omega}{\left(1 - \Omega^2 + j2\zeta\Omega\left(1 + \frac{g_V}{c}\right)\right)} \tag{2.11}$$

where $\frac{g_V}{c}$ is the non-dimensional gain for velocity feedback control.

For displacement feedback control, the control force, which is proportional to the displacement, can be written as,

$$f_S(t) = g_d x(t) \tag{2.12}$$

where g_d is the gain for displacement feedback control.

From equations (2.7) and (2.12) the non-dimensional receptance in the frequency domain can be written as,

$$\frac{X(j\Omega)}{F_p(j\Omega)} \times k = \frac{1}{\left(\left(1+\frac{g_d}{k}\right) - \Omega^2 + j2\zeta\Omega\right)} \tag{2.13}$$

where $\frac{g_d}{k}$ is the non-dimensional gain for displacement feedback control.

Figures 2.2, 2.3 and 2.4 show the non-dimensional accelerance, mobility and receptance for acceleration, velocity and displacement feedback control respectively as a function of non-dimensional frequency for various gains. A damping ratio of 0.05 was considered for all these cases. The accelerance plot in figure 2.2 shows that the response at the original resonance frequency reduces considerably. But the response has a resonance peak at a lower frequency than the original system as the gain is increased. Comparing equations (2.4) and (2.9) it can be seen that increasing the gain in acceleration feedback control effectively adds mass to the system. Equations (2.5) and (2.11) suggest that velocity feedback control increases the effective damping. Hence the response is reduced at the natural frequency of the system, which is shown in figure 2.3 for various gains.

In the case of displacement feedback, it is seen from equations (2.6) and (2.13) that the system tends to behave as if the stiffness is increased. Figure 2.4 shows the receptance of the system for various feedback control gains.

All these three cases show that the response of the uncontrolled system at the original resonance frequency (i.e. the plant) reduces considerably under active control. Also the system resonance shifts to below or above the original resonance frequency in acceleration and displacement feedback control respectively and remains the same for velocity feedback control. This phenomenon can be explained by considering the equivalent resonance frequency and damping ratio.

For acceleration feedback the equivalent resonance frequency and damping ratio are given by, $\omega_{n\_equ} = \sqrt{\frac{k}{(m+g_a)}}$ and $\zeta_{equ} = \frac{c}{2\sqrt{(m+g_a)k}}$. Similarly for velocity feedback this becomes, $\omega_{n\_equ} = \sqrt{\frac{k}{m}}$ and $\zeta_{equ} = \frac{c+g_v}{2\sqrt{mk}}$. For displacement feedback this becomes, $\omega_{n\_equ} = \sqrt{\frac{k+g_d}{m}}$ and $\zeta_{equ} = \frac{c}{2\sqrt{m(k+g_d)}}$. It can be seen from the above expressions that for acceleration feedback control, as the gain is increased, ω_{n_equ} and ζ_{equ} decreases thus the resonance frequency shifts down and the peak becomes narrower. For velocity feedback ω_{n_equ} remains the same while ζ_{equ} increases, thus the peak response reduces while the resonance frequency remains the same as the gain is increased. Similarly for displacement feedback ω_{n_equ} increases while ζ_{equ} reduces as the gain is increased.

2.1.3 Block diagram representation of control system

In practice accelerometers are used to obtain the plant response. The signals from these sensors can be integrated once or twice to obtain the velocity or the displacement response respectively. Therefore it is appropriate to consider accelerance as the plant frequency response function. Here the term plant refers to the system response without feedback control. Equation (2.2) represents the plant transfer function, and from equation (2.4) this can be expressed in the frequency domain as,

$$G_P(j\Omega) = \frac{-\Omega^2}{m(1-\Omega^2 + j2\zeta\Omega)} \qquad (2.14)$$

The block diagram representation for acceleration, velocity and displacement feedback control systems are shown in figures 2.5(a), 2.5(b) and 2.5(c) respectively. It can be seen that acceleration, velocity and displacement are considered as the system output response for acceleration, velocity and displacement feedback control respectively. From equation (2.7), it can be seen that the plant experiences the difference between the primary disturbance and the control force, and its response is acceleration. This can be integrated once to give velocity and twice to give the displacement response as shown in figures 2.5(b) and 2.5(c). Single integration is

represented in the frequency domain by $\frac{1}{j\omega}$ and the double integration by $\frac{-1}{\omega^2}$ (or in the Laplace domain by $\frac{1}{s}$ and $\frac{1}{s^2}$ respectively).

The feedback loop in the block diagrams *H(s)* or *H(jω)* consists simply of a gain, which amplifies the output signal to produce the control force. Throughout this report, the product of the forward path functions for example $G_p(s)\frac{1}{s}$ or $G_p(j\omega)\frac{1}{j\omega}$ in figure 2.5(b), will be referred to as *G(s)* or *G(jω)* and the feedback path as *H(s) or H(jω)*.

2.2 Stability of an ideal system

The ideal feedback system is one where an integrator can be represented in the frequency domain by $\frac{1}{j\omega}$ (or in Laplace domain by $\frac{1}{s}$), the combination of the power amplifier and the shaker, which generates the secondary force by a pure gain and the accelerometer is assumed to provide the true acceleration of the plant. In this section the stability of such an ideal system is analysed.

The vibration responses presented in section 2.1 show that the plant response at its original resonance frequency reduces with acceleration, velocity and displacement feedback control. However the closed loop response does not provide information on the maximum attainable gain of a stable system.

The stability of a control system can be analysed using root-locus techniques or Nyquist criteria [24]. Root locus methods offer a broad over view of the system stability but do not give a definite answer as to the stability of a feedback control system in all cases. However this method does offer a sophisticated graphical technique for system analysis and design.

Consider the feedback system shown in figures 2.5(a, b & c), the closed loop response can be written as,

$$\frac{Output}{F_p(s)} = \frac{G(s)}{1+G(s)H(s)} \qquad (2.15)$$

where the output can be acceleration, velocity or displacement depending on the control type used. The characteristic equation of the system is given by,

$$1+G(s)H(s)=0 \tag{2.16}$$

If the gain (K) is separated then equation (2.16) can be written as,

$$1+KG(s)H_1(s)=0 \tag{2.17}$$

where $H(s)=KH_1(s)$

The root locus is defined as the locus of the roots of equation (2.17) when the gain K is increased from zero to infinity. A system is said to be stable for any gain if the entire root locus is in the left half of the Laplace plane (s plane).

The product *G(s)H(s)* is said to be the corresponding open loop transfer function and can be interpreted as the frequency response function by substituting for $s = j\omega$.

Equation (2.17) can be expressed in the frequency domain as,

$G(j\omega)H(j\omega)=-1$ or in terms of non-dimensional frequency as

$$KG(j\Omega)H_1(j\Omega)=-1 \tag{2.18}$$

The Nyquist criterion states that the system is stable if and only if the open loop frequency response function *G(jΩ)H(jΩ)* does not enclose the (-1,0) point in the complex *G(jΩ)H(jΩ)* plane [2]. Thus the stability of the system can be studied by considering the magnitude of the open loop frequency response function when it crosses the negative real axis in the complex *G(jΩ)H(jΩ)* plane.

From equation (2.18), this occurs when the magnitude of *G(jΩ)H(jΩ)* is equal to one and the phase is equal to -180°.

2.2.1 Acceleration feedback control

Acceleration feed back control is considered first. From equation (2.8) and from figure 2.5(a)

$$H(j\Omega)=\frac{F_s(j\Omega)}{\ddot{X}(j\Omega)}=g_a \tag{2.18}$$

From equation (2.14) the forward path frequency response function is given by

$$G(j\Omega)=\frac{-\Omega^2}{m\left(1-\Omega^2+j2\zeta\Omega\right)}=G_P(j\Omega) \tag{2.19}$$

Combining equations (2.18) and (2.19) the open loop frequency response function becomes,

$$G(j\Omega)H(j\Omega) = \left(\frac{g_a}{m}\right)\frac{-\Omega^2}{(1-\Omega^2 + j2\zeta\Omega)} \tag{2.20}$$

where $\left(\frac{g_a}{m}\right)$ is the non-dimensional gain for acceleration feedback control.

The open loop transfer function can be written as,

$G(s)H(s) = \left(\frac{g_a}{m}\right)\frac{s^2}{(s^2 + j2\zeta\omega_n s + \omega_n^2)}$ which can be used to form the characteristic equation from which root locus can be drawn.

Rearranging equation (2.20) into real and imaginary parts gives,

$$G(\,j\Omega)H(\,j\Omega) = -\left(\frac{g_a}{m}\right)\left\{\frac{\Omega^2(1-\Omega^2)}{(1-\Omega^2)^2 + (2\zeta\Omega)^2} - j\frac{2\zeta\Omega^3}{(1-\Omega^2)^2 + (2\zeta\Omega)^2}\right\} \tag{2.21}$$

The frequency at which the Nyquist plot crosses the negative real axis is called the phase cross over frequency. When this occurs the imaginary part of equation (2.21) is zero. It occurs at $\Omega = 0$. The magnitude of the real part then becomes,

$\mathrm{Re}\{G(j\Omega)H(j\Omega)\} = 0$

Thus the system is unconditionally stable.

Figure 2.6 shows the root locus of the acceleration feedback control system for a damping ratio of 0.05 and a resonance frequency of 20.5 Hz. It is seen that for all values of gain the system is in the left half of s plane hence stable. Figure 2.7 shows the Nyquist plot of the open loop frequency response function for acceleration feedback control. It can be seen that it does not cross the negative real axis and thereby does not enclose the (–1,0) point of the Nyquist plane. In addition, when Ω tends to infinity, the magnitude of the real part is $\frac{g_a}{m}$. It is seen that the plot asymptotically leaves from the origin along the negative real axis and return to the positive real axis away from the origin.

2.2.2 Velocity feedback control

In velocity feedback control, the feedback path frequency response function becomes,

$$H(j\Omega) = \frac{F_s(j\Omega)}{\dot{X}(j\Omega)} = g_v \tag{2.22}$$

From figure 2.5(b) the forward path frequency response function can be written as,

$$G(j\Omega) = G_P(j\Omega)\frac{1}{j\omega} \tag{2.23}$$

Therefore the open loop frequency response function now becomes,

$$G(\,j\Omega)H(\,j\Omega) = \left(\frac{g_v}{m\omega_n}\right)\left(\frac{j\Omega}{(1-\Omega^2)+j(2\zeta\Omega)}\right) \tag{2.24}$$

The corresponding open loop transfer function is given by,

$$G(s)H(s) = \left(\frac{g_v}{c}\right)\frac{2\zeta\omega_n s}{(s^2 + j2\zeta\omega_n s + \omega_n^2)} \tag{2.25}$$

Rearranging equation (2.24) into real and imaginary parts and substituting for $\frac{c}{2\zeta} = m\omega_n$ gives,

$$G(\,j\Omega)H(\,j\Omega) = \left(\frac{2\zeta g_v}{c}\right)\left\{\frac{2\zeta\Omega^2}{\left(1-\Omega^2\right)^2+(2\zeta\Omega)^2} + j\frac{\Omega\left(1-\Omega^2\right)}{\left(1-\Omega^2\right)^2+(2\zeta\Omega)^2}\right\} \tag{2.26}$$

The Nyquist plot crosses the real axis when the imaginary part of equation (2.26) is zero. This gives, $\Omega = 0$ *or* $\Omega = 1$

When $\Omega = 0$

The real part of $G(\,j\Omega)H(\,j\Omega) = 0$ and

When $\Omega = 1$

Real part of $G(\,j\Omega)H(\,j\Omega) = \frac{g_v}{c}$

Since this is positive the system with velocity feedback control is unconditionally stable.

Figure 2.8 shows the root locus of the velocity feedback control system for a damping ratio of 0.05 and a resonance frequency of 20.5 Hz. It is seen that for all values of gains the system is on the left half of s plane hence stable. The Nyquist plot for velocity feedback is shown in figure 2.9, where it is evident that the Nyquist plot is completely in the right half of the Nyquist plane. In addition it crosses the real axis when the magnitude is zero and $\frac{g_V}{c}$. From equation (2.26), when Ω tends to infinity, the real and imaginary parts of the open loop frequency response function $G(j\Omega)H(j\Omega)$ are zero. Thus the Nyquist plot leaves and returns to the origin along the imaginary axis.

2.2.3 Displacement feedback control

For displacement feedback control, the feedback path frequency response function is,

$$H(j\Omega) = \frac{F_s(j\Omega)}{X(j\Omega)} = g_d \tag{2.27}$$

From figure 2.5(c) forward path frequency response function is given by

$$G(j\Omega) = G_P(j\Omega)\left(\frac{-1}{\omega^2}\right) \tag{2.28}$$

Therefore the open loop frequency response function now becomes,

$$G(\,j\Omega)H(\,j\Omega) = \left(\frac{g_d}{m\omega_n^2}\right)\left(\frac{1}{(1-\Omega^2)+j(2\zeta\Omega)}\right) \tag{2.29}$$

The corresponding open loop transfer function can be written as,

$$G(s)H(s) = \left(\frac{g_d}{k}\right)\frac{\omega_n^2}{(s^2 + j2\zeta\omega_n s + \omega_n^2)} \tag{2.30}$$

Rearranging equation (2.29) into real and imaginary parts and substituting for $k = m\omega_n^2$ gives,

$$G(\,j\Omega)H(\,j\Omega) = \left(\frac{g_d}{k}\right)\left\{\frac{(1-\Omega^2)}{(1-\Omega^2)^2+(2\zeta\Omega)^2} + j\frac{(2\zeta\Omega)}{(1-\Omega^2)^2+(2\zeta\Omega)^2}\right\} \tag{2.31}$$

The Nyquist plot crosses the real axis when imaginary part of equation (2.31) is zero. This gives, Ω =0. When this occurs,

The real part of $G(\,j\Omega)H(\,j\Omega) = \frac{g_d}{k}$

Since this is positive the system with displacement feedback control is also unconditionally stable.

Figure 2.10 shows the root locus of the displacement feedback control system for a damping ratio of 0.05 and a resonance frequency of 20.5 Hz. It is seen that for all values of gains the system is in the left half of s plane and hence stable. The Nyquist plot for the displacement feedback is shown in figure 2.11. From equation (2.31) it can be seen that when Ω tends to infinity the real and imaginary parts of the open loop frequency response function $G(j\Omega)H(j\Omega)$ are zero. Thus the Nyquist plot leaves and returns to the origin of the Nyquist plane along the real axis.

2.3 Real system

Although the ideal systems discussed above are unconditionally stable the real systems may go unstable. The reasons for this are investigated in sections 3 and 4. In this section, the components of a real system are outlined and the ways in which they differ from the ideal system is discussed. Figure 2.12 shows a block diagram representation of the real system. Individual components and their mathematical models are discussed below.

2.3.1 Charge amplifier

In a real system the charge amplifier such as the B&K type 2635 may perform the function of integration and double integration. The charge amplifier may also perform a number of other tasks, which include,

- Matching measurement instrumentation input sensitivity to that of the accelerometer output,
- Low and high frequency filtering to reject unwanted signals (high and low pass filters).

As mentioned in section 2.1 accelerometers are generally used to obtain the response in a real system. The output charge from a piezo-electric accelerometer is converted to a voltage by the charge amplifier, with the output voltage being directly proportional to the input charge. The very high resistance of the charge amplifier reduces the problem of charge leakage from the piezo-electric crystal and its very high capacitance completely dominates the effect of the cable capacitance. The electronic integration of the accelerometer output by the charge amplifier can be represented by $\frac{1}{(1+j\tau_i\omega)}$ (Refer to appendix 3). Also contained in the charge amplifier are high and low pass filters to reject the unwanted signals at low and high frequencies. The mathematical model of a high pass filter takes the form of $\frac{j\omega}{(1+j\tau_c\omega)}$ and a low pass filter takes the form of $\frac{1}{(1+j\tau_l\omega)}$. The details of these models are also given in the appendix 3. The constants τ_i, τ_c and τ_l are called time constants. Their inverses are called corner frequencies.

i.e. $\omega_i = \frac{1}{\tau_i}$, $\omega_c = \frac{1}{\tau_c}$ and $\omega_l = \frac{1}{\tau_l}$.

Consider the model of the integrator,

$$Int(j\omega) = \frac{1}{(1 + j\tau_i\omega)} \tag{2.32}$$

Where *Int* denotes the integrator. Equation (2.32) can be written as,

$$Int(j\Omega) = \frac{1}{(1 + j\alpha\Omega)} \tag{2.33}$$

Where $\Omega = \frac{\omega}{\omega_n}$ and $\alpha = \frac{\omega_n}{\omega_i}$ where ω_n is the original natural frequency of the SDOF under control.

In this model α can be used as a measure of the separation of the corner frequency of the integrator to the natural frequency of the plant. If α is large enough and as frequency increases the integrator can be approximated to

$$Int(j\Omega) \approx \frac{1}{(j\alpha\Omega)} \tag{2.34}$$

Hence almost pure integration is performed at higher frequencies. However at low frequencies the model described by equation (2.33) is valid. This introduces a phase delay of $\tan^{-1}(\alpha\Omega)$ at lower frequencies, whereas in the ideal system it remains at $-\frac{\pi}{2}$. Therefore the integrator deviates from the ideal case at low frequencies. Figure 2.13 shows the characteristics of ideal and real integrators, where for convenience α = 1 is used. The magnitude and phase plots show that the real system varies considerably from the ideal integrator at low frequencies. The magnitude plot suggests that at low frequencies no integration is performed. That means that there would be acceleration feedback control in this frequency region. However the extra phase delay of the real integrator suggests that the system will behave neither like velocity feedback control nor like acceleration feedback control.

A model of the double integrator is simply the square of a single integrator. Hence its frequency response function can be written as

$$dInt(j\Omega) = \frac{1}{(1 + j\alpha\Omega)^2} \tag{2.35}$$

Where *dInt* denote the double integrator

Now consider the model of a high pass filter

$$hp(j\omega)=\frac{j\omega}{(1+j\tau_c\omega)} \tag{2.36}$$

where hp denotes high pass filter. Substituting for $\Omega=\frac{\omega}{\omega_n}$ and $\beta=\frac{\omega_n}{\omega_c}$ equation (2.36) can be written as,

$$hp(j\Omega)=\frac{j\omega_n\Omega}{(1+j\beta\Omega)} \tag{2.37}$$

Similarly for a low pass filter, the mathematical model can be written as,

$$lp(j\Omega)=\frac{1}{(1+j\gamma\Omega)} \tag{2.38}$$

where $\gamma=\frac{\omega_n}{\omega_l}$.

Figures 2.14 and 2.15 shows the characteristics of high and low pass filters for $\beta = 1$ and $\gamma = 1$ respectively. The characteristics of a high pass filter shows that it introduces a considerable phase advance at low frequencies. In addition it attenuates the signal at low frequencies. Therefore it generally introduces a low frequency problem. The characteristics of low pass filter shows that it introduces considerable phase delay at high frequencies and in addition it attenuates high frequency signals. Therefore it generally introduces a high frequency problem.

2.3.2 Power amplifier

The power amplifier in the real system is used to control the feedback gain. An ideal power amplifier produces a pure gain, which is independent of frequency, but this can be expensive. Most commercial power amplifiers have a high pass filter incorporated. From the model of the high pass filter discussed in the previous section, a real power amplifier will introduce a low frequency problem. A first order high pass filter is assumed in the analysis described in this report.

2.3.3 Time delay

In real systems, time delay may present. This is particularly dominant in digital control systems and is relatively insignificant in analogue control systems. Pure time delay in the frequency domain can be represented as $e^{-j\omega T}$ where T is the delay time.

The presence of a control time delay affects the feedback frequency response function. For example, the presence of time delay in a velocity feedback system means the feedback path frequency response function is,

$$H(j\omega) = \frac{F_s(j\omega)}{\dot{X}(j\omega)} = g_v e^{-j\omega T} \tag{2.39}$$

Or it can be written in terms of non-dimensional frequency as

$$H(j\Omega) = \frac{F_s(j\Omega)}{\dot{X}(j\Omega)} = g_v e^{-j2\pi\tau\Omega} \tag{2.40}$$

where $\tau = \frac{T}{T_n}$ and T_n is the natural period of the plant.

The effect of time delay is to alter the open loop frequency response function.

Equation (2.40) shows that the presence of time delay does not alter the magnitude but introduces a phase lag. This phase lag, which is a function of frequency, becomes significant at high frequencies. Hence the time delay introduces a high frequency problem.

2.3.4 Accelerometer and secondary shakers.

An accelerometer is an electromechanical transducer, which outputs a voltage or charge that is proportional to the acceleration of the object to which it is attached. It is the most widely used vibration measurement transducer due to its small size, range of sensitivities and large frequency range. An accelerometer can be modelled as a single degree of freedom system [16] as shown in figure 2.16.

From figure 2.16, the equation describing the motion of the seismic mass is,

$$m\ddot{z}(t) + c\dot{z}(t) + kz(t) = f(t) - m\ddot{x}(t) \tag{2.41}$$

where $z(t) = x(t) - y(t)$ and $f(t)$ is a constant usually gravity force because of the seismic mass is sealed in a case.

Assuming harmonic response i.e. $x(t) = X_o e^{j\omega t}$ and $z(t) = Z_o e^{j\omega t}$, equation (2.41) can be written as,

$$Z_o = \frac{-m\omega^2 X_o}{k(1 - \Omega_a^2 + j2\zeta_a\Omega_a)} \tag{2.42}$$

where

Ω_a –non-dimensional frequency ω/ω_{na},

ω_{na} - accelerometer resonance frequency

ζ_a – damping in the accelerometer

Noting that

$\ddot{x}(t) = -X_o\omega^2 e^{j\omega t} = A_o e^{j\omega t}$ Where $A_o = -X_o\omega^2$ and if $\omega_{na} >> \omega$, the equation (2.42) can be approximated to

$$Z_o = \frac{A_o m}{k} \tag{2.43}$$

Thus at low frequencies the accelerometer only introduces a pure gain. At higher frequencies, however, the accelerometer resonance may cause a problem. Hence this is also a high frequency problem.

A secondary force shaker is required to produce the control force. In this report an electrodynamic shaker is considered. The effect of mass (moving assembly), springs (flexures) and damping gives a frequency response characteristic to the shaker. The frequency response is dominated by the mass and stiffness of the flexures and at very high frequencies, the resonance of the moving element itself [15]. This resonance may cause instabilities in a control system at very high frequencies.

2.3.5 Discussion

Based on the characteristics of various components discussed above, the real system may vary considerably from the ideal system. Therefore the stability limits (the maximum attainable gain in a real system) and the sources of instability (which of the electrical components leads to instability) have to be established. It is assumed that the high and low pass filters and real integrators are separable in charge amplifiers as this enables an analysis of the different components to identify which of them causes instability. Interestingly, from the characteristics of these components, some of them are dominant at low frequencies and others at higher frequencies. Accordingly they can be classified as low and high frequency sources of instability. From the characteristics discussed in this section, the power amplifier (specifically the high pass filter of the power amplifier) and high pass filter and real integrator of charge amplifier are potential sources of instability at low frequencies. The low pass filter in the charge amplifier, time delay, actuators and accelerometers fall into the group of high frequency sources of instabilities. The next section deals with the low frequency sources of instability.

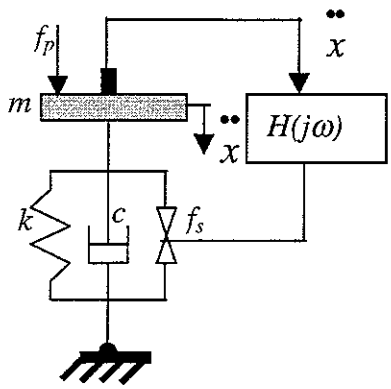

Figure 2.1 A simplified model of a SDOF system with feedback control

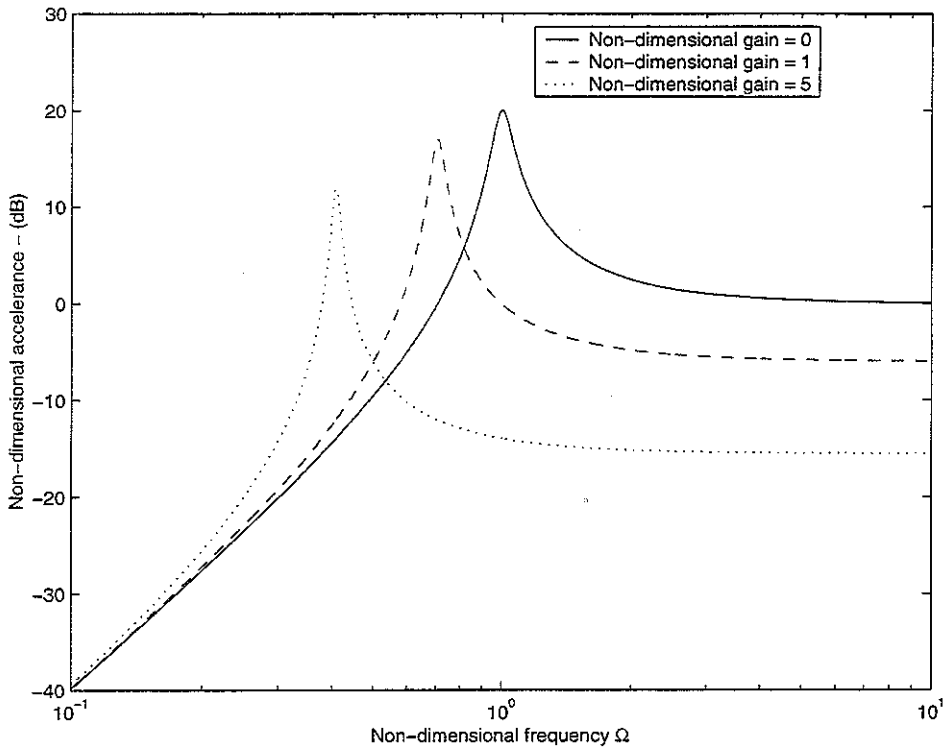

Figure 2.2Closed loop response of a SDOF system with acceleration feedback control $\zeta = 0.05$

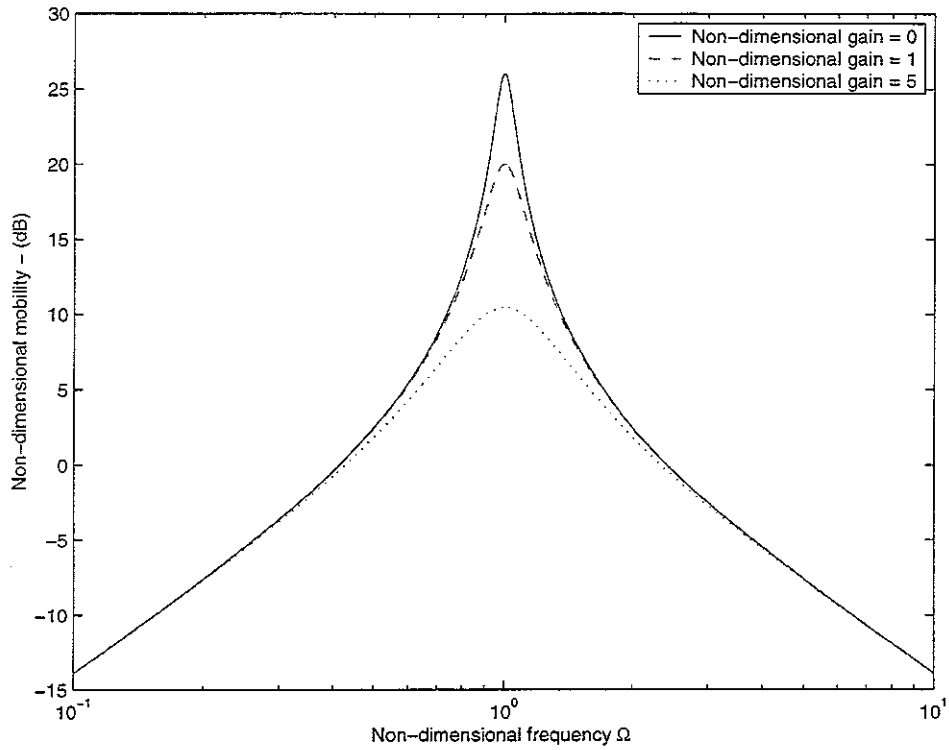

Figure 2.3 Closed loop response of a SDOF system with velocity feedback control $\zeta = 0.05$

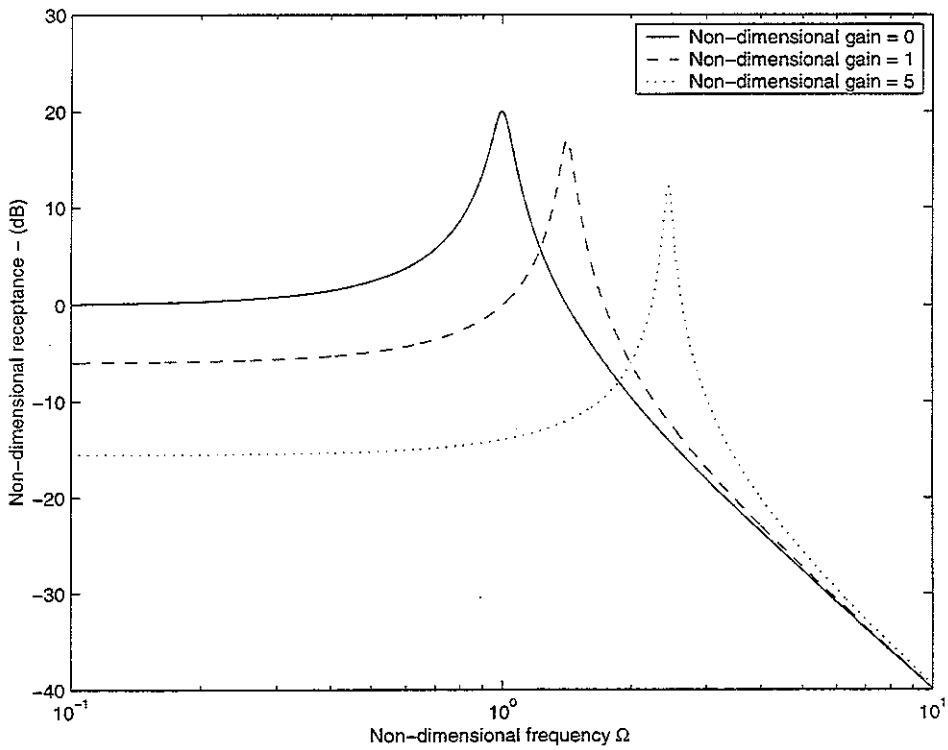

Figure 2.4 Closed loop response of a SDOF system with displacement feedback control $\zeta = 0.05$

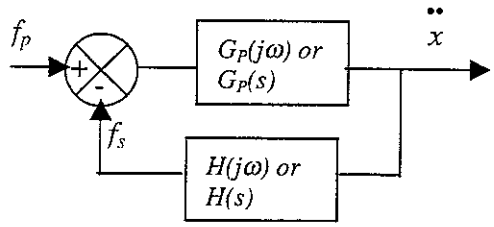

(a) Acceleration feedback control system

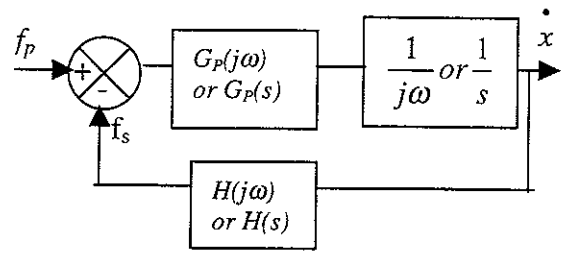

(b) Velocity feedback control system

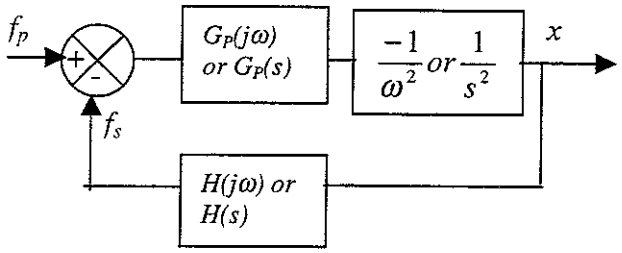

(c) Displacement feedback control system

Figure 2.5 Block diagram representation of acceleration, velocity and displacement feedback control systems.

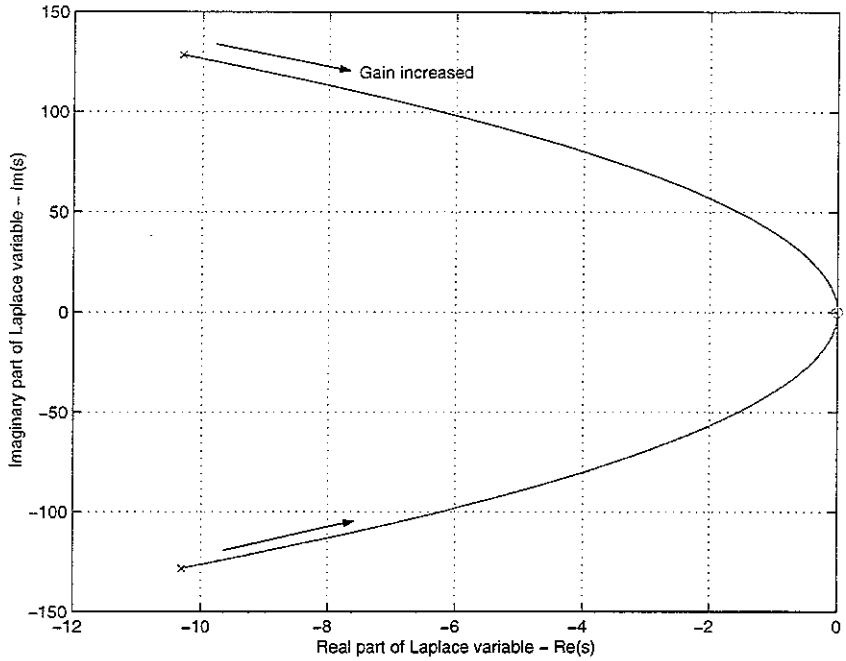

Figure 2.6 Root locus of a SDOF system with acceleration feedback control $\zeta = 0.05$ and $\omega_n = 20.5$ Hz. ('X' denotes open loop poles and 'O' denotes open loop zeros)

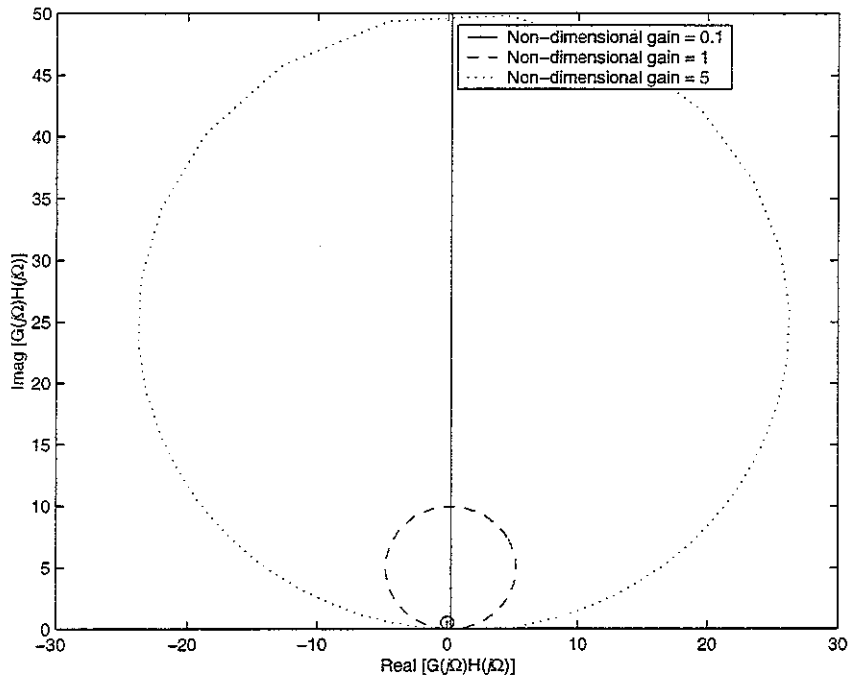

Figure 2.7 Nyquist open loop response plot of a SDOF system with acceleration feedback control $\zeta = 0.05$

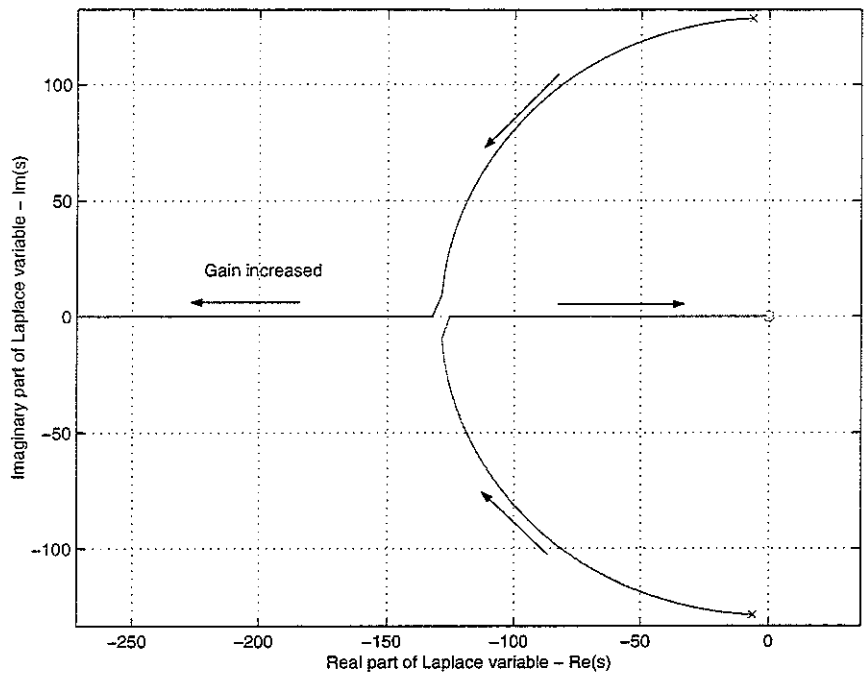

Figure 2.8 Root locus of a SDOF system with velocity feedback control $\zeta = 0.05$ and $\omega_n = 20.5$ Hz. ('X' denotes open loop poles and 'O' denotes open loop zeros)

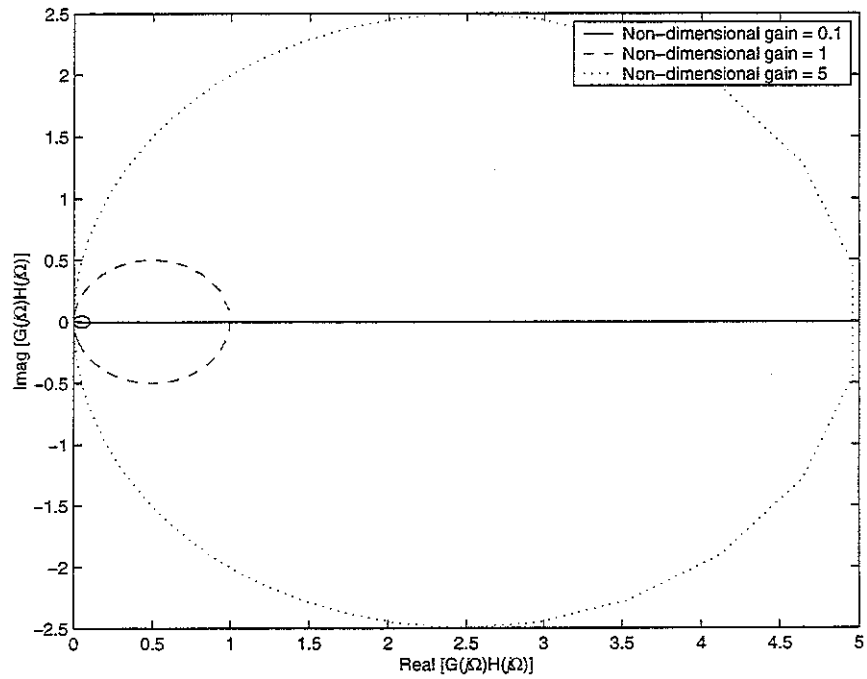

Figure2. 9 Nyquist open loop response plot of a SDOF system with velocity feedback control $\zeta = 0.05$

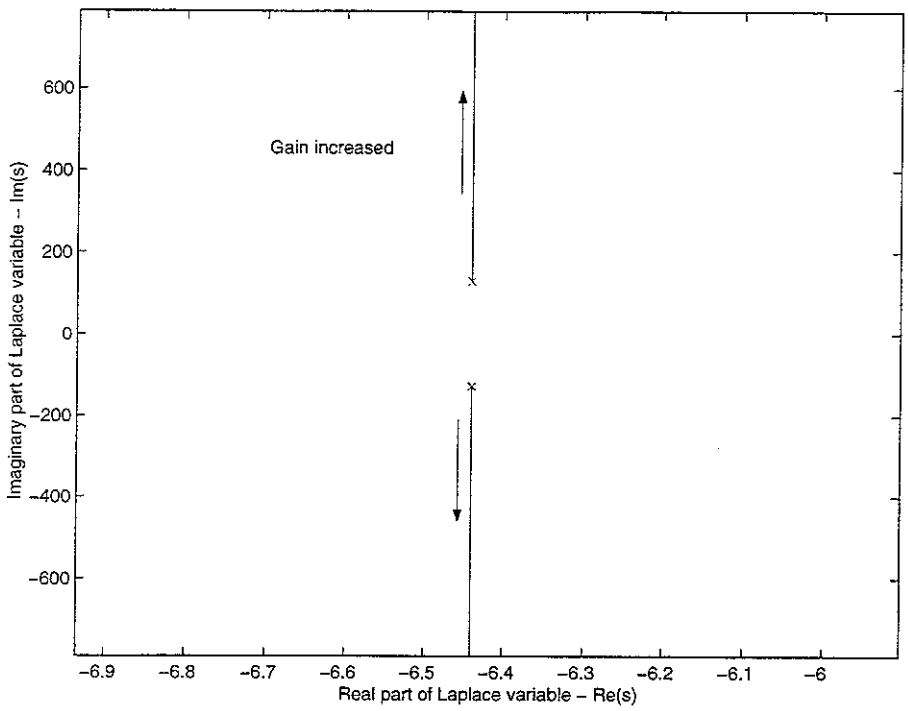

Figure 2.10 Root locus of a SDOF system with displacement feedback control $\zeta = 0.05$ *and* $\omega_n = 20.5$ *Hz. ('X' denotes open loop poles and 'O' denotes open loop zeros)*

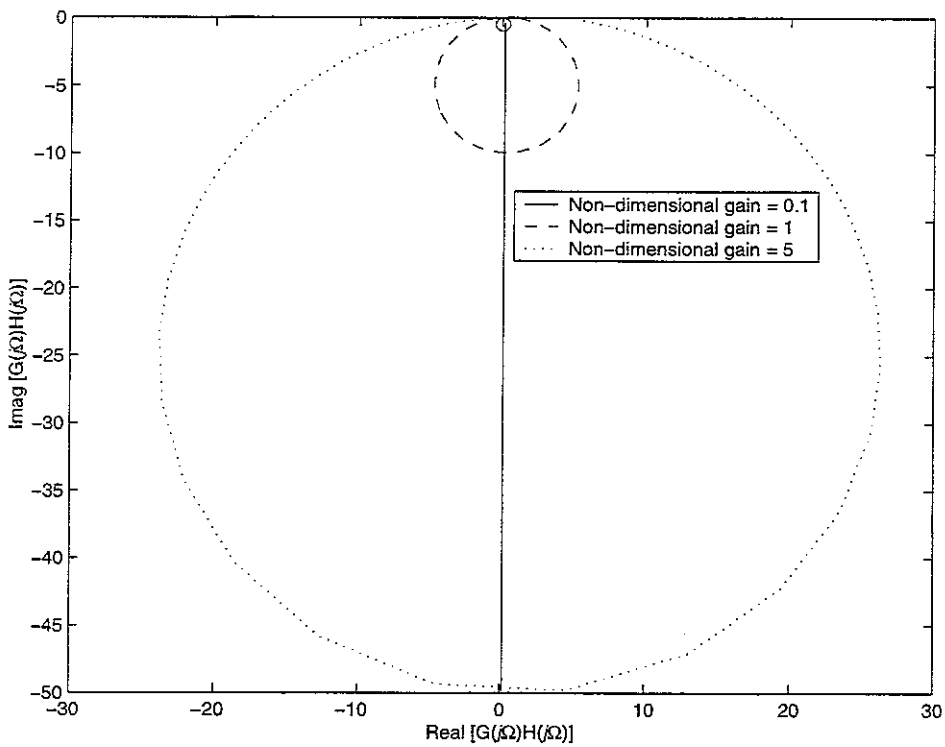

Figure 2.11 Nyquist open loop response plot of a SDOF system with displacement feedback control $\zeta = 0.05$

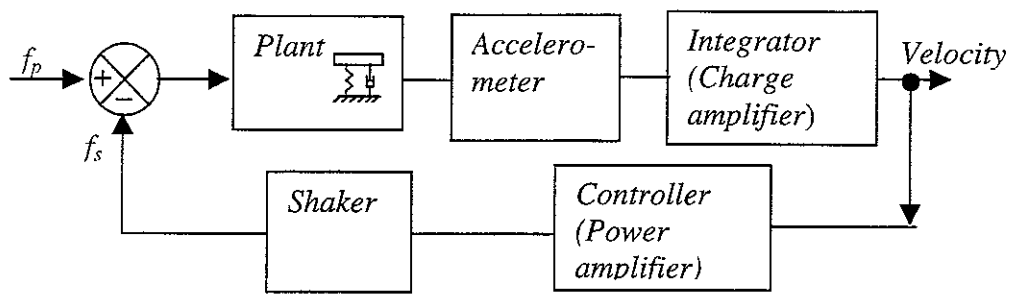

Figure 2. 12 Block diagram representation of a real closed loop system with velocity feedback control

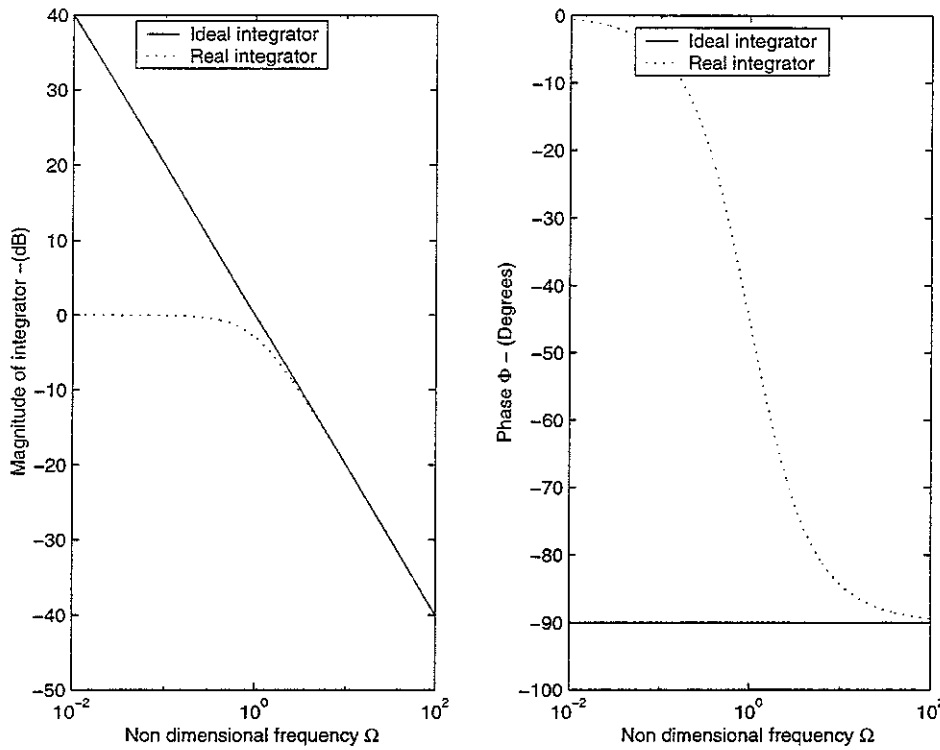

(a) Amplitude *(b) phase*

Figure 2.13 Ideal and real integrators $\alpha = 1$

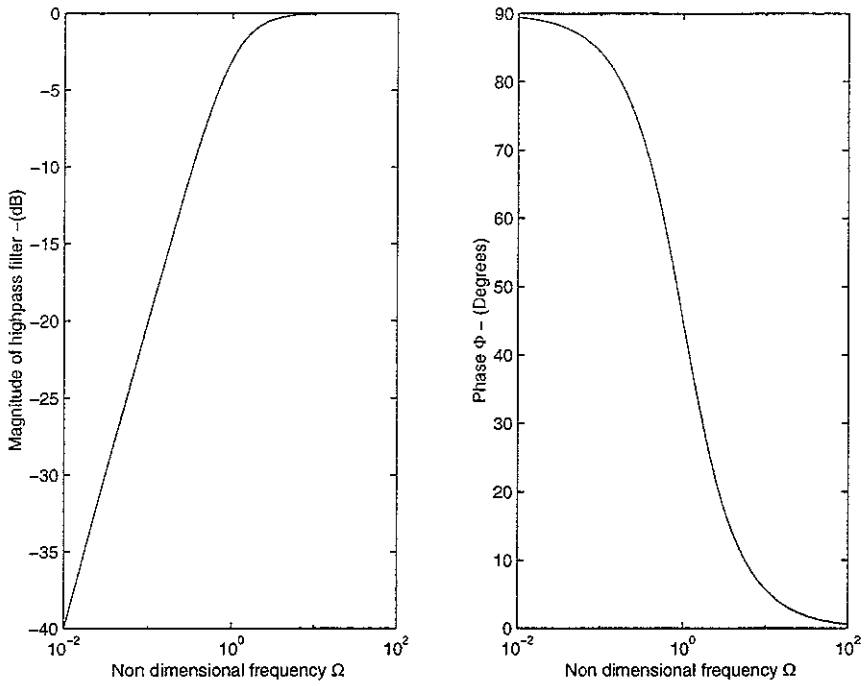

(a) Amplitude *(b) phase*

Figure 2.14 High pass filter characteristics $\beta = 1$

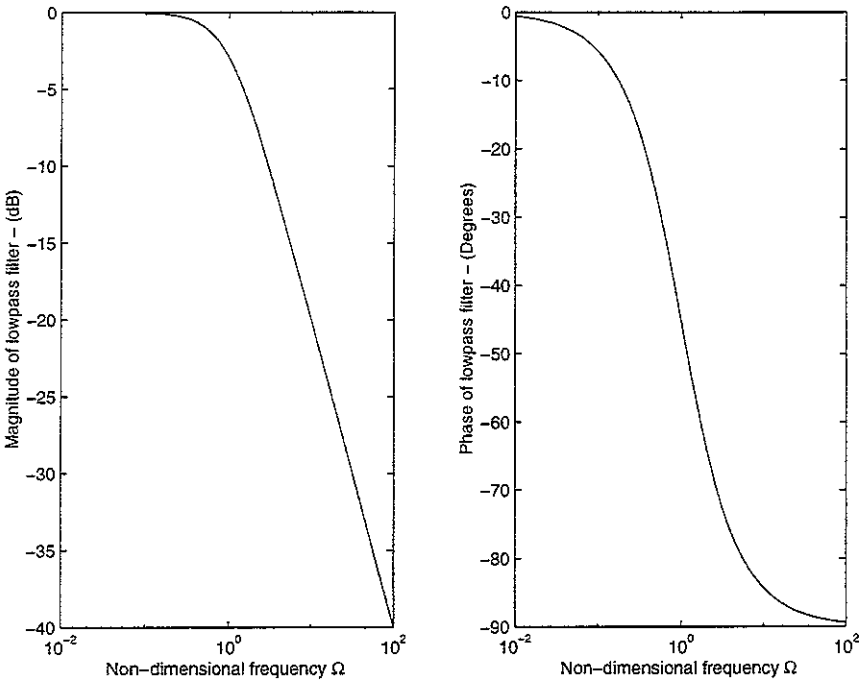

(a) Amplitude *(b) phase*

Figure 2.15 Low pass filter characteristics $\gamma = 1$

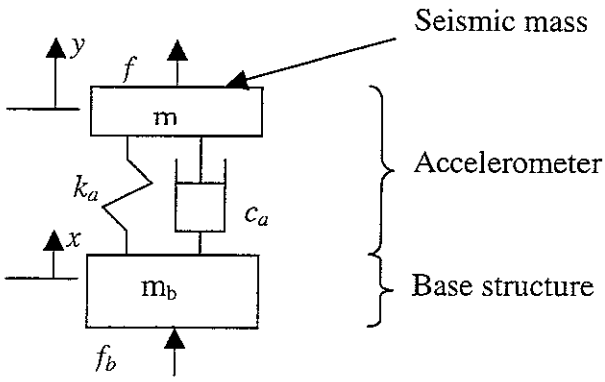

(a) Schematic diagram

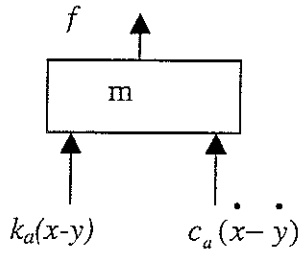

(b) Free body diagram

Figure 2.16 Accelerometer model

3. Low frequency instabilities

3.1 Introduction

Theoretically the Nyquist plot of an open loop frequency response function crosses the negative real axis when the phase is ± 180 degrees. Thus if the Nyquist plot crosses the negative real axis, then the system may go unstable, when the gain is increased such that Real $[G(j\omega)H(j\omega)]$=-1. It was established in section 2 that the real integrators and the high pass filter in the charge and power amplifiers are the potential sources of instabilities at low frequencies. With the introduction of charge and power amplifiers into the feedback control system, both forward frequency response function $G(j\omega)$ and feedback frequency response function $H(j\omega)$ are changed from the ideal. The number of open loop poles and zeros may be increased by the addition of instruments and hence the root locus may cross over into the right half of the s-plane for some range of gain. In general the addition of a pole makes the system less stable. Therefore the unconditional stability of the SDOF system discussed in section 2 is no longer guaranteed. Thus the real systems require investigation, and this section identifies the dominant source of instability and the maximum gain attainable for such systems.

It is assumed that the integrator and the high pass filter in the charge amplifier and high pass filter in the power amplifier are separable. This is helpful in the investigation of the relative influence of each component in the system. The charge amplifier is assumed to be able to take the following forms.

- Ideal integrator with high pass filter – to study the effect of the high pass filter
- Real integrator without high pass filter – to study the effect of the real integrator
- Real integrator and high pass filter – to study the combined effect.

Similarly the power amplifier is assumed to take the following forms,

- Power amplifier with a pure gain
- Power amplifier with a high pass filter incorporated

Since the charge amplifier is installed in the forward path and power amplifier in the feedback path, the conditions of the charge amplifier affects the forward path

frequency response function $G(j\omega)$ and the power amplifier affects the feedback path frequency response function $H(j\omega)$. Hence the overall open loop frequency response function varies for each case. Three charge amplifier conditions and two-power amplifier conditions gives six combinations of instrument conditions. In table 3.1, these instruments conditions together with the ideal case, which was considered in section 2 are tabulated for acceleration, velocity and displacement feedback control. The maximum attainable gains for these cases are determined in the next section.

3.2 Analysis of maximum gain

From figure 3.1 the forward path frequency response function for velocity feedback can be defined as

$$G(j\omega) = G_P(j\omega)hp_1(j\omega)Int(j\omega)g_c \qquad (3.1)$$

In terms of non-dimensional frequency, this can be written as,

$$G(j\Omega) = G_P(j\Omega)hp_1(j\Omega)Int(j\Omega)g_c \qquad (3.2)$$

Where g_c is the combined gain of the charge amplifier and accelerometer.

Similarly the feedback path frequency response function can be written in terms of non-dimensional frequency as,

$$H(j\Omega) = g_p g_s hp_2(j\Omega) \qquad (3.3)$$

where g_p is the gain of power amplifier, which can be written as g_a in the case of acceleration feedback control, g_v in velocity feedback control and g_d in displacement feedback control, and g_s is the gain of control force shaker.

Therefore the open loop frequency response function becomes,

$$G(j\Omega)H(j\Omega) = g_p g_c g_s G_P(j\Omega)hp_1(j\Omega)Int(j\Omega)hp_2(j\Omega) \qquad (3.4)$$

Note that g_p is the physical gain that is set in the feedback path power amplifier.

For acceleration feedback control $Int(j\Omega)$ is replaced by 1 and for displacement feedback by $dInt(j\Omega)$.

The frequency response function of the components as a function of non-dimensional frequency can be written as follows,

Ideal integrator $= \dfrac{1}{j\Omega\omega_n}$

Ideal double integrator $= \dfrac{-1}{\Omega^2\omega_n^2}$

Real integrator $= \dfrac{1}{(1+j\alpha\Omega)}$

Real double integrator $= \dfrac{1}{(1+j\alpha\Omega)^2}$

High pass filter in the charge amplifier $= \dfrac{j\omega_n\Omega}{(1+j\beta\Omega)}$

High pass filter in the power amplifier $= \dfrac{j\omega_n\Omega}{(1+j\delta\Omega)}$

where $\alpha = \dfrac{\omega_n}{\omega_i}$ $\beta = \dfrac{\omega_n}{\omega_h}$ and $\delta = \dfrac{\omega_n}{\omega_{hp}}$

For the purpose of simplicity $\alpha = \beta = \delta$ is assumed.

A few cases from those presented in table 3.1 are discussed here in detail. The cases A1, A2 and A3 were considered in section 2 and were shown to be unconditionally stable. This is reported in table 3.2.

Consider case B1 from table 3.1, where the system consists of acceleration feedback control with a high pass filter and gain of the charge amplifier in the forward path and pure a gain power amplifier and shaker gain in the feedback path.

The open loop frequency response function can be written as,

$$G(j\Omega)H(j\Omega) = \left(\frac{-\Omega^2}{m\left((1-\Omega^2)+j2\zeta\Omega\right)}\right)\left(\frac{j\omega_n\Omega}{1+j\alpha\Omega}\right)g_c g_p g_s \qquad (3.5)$$

For convenience the total gain is defined as $g_{total} = \dfrac{g_c g_p g_s \omega_n}{m}$. Equation (3.5) can be arranged into real $\mathrm{Re}(G(j\Omega)H(j\Omega))$ and imaginary $\mathrm{Im}(G(j\Omega)H(j\Omega))$ parts as follows,

$$\mathrm{Re}(G(j\Omega)H(j\Omega)) = g_{total}\frac{-\Omega^4\left(2\zeta+\alpha\left(1-\Omega^2\right)\right)}{\left(\left(1-\Omega^2\right)^2+(2\zeta\Omega)^2\right)\left(1+\alpha^2\Omega^2\right)} \qquad (3.6)$$

$$\mathrm{Im}(G(j\Omega)H(j\Omega)) = g_{total}\frac{\Omega^3\left(2\alpha\zeta\Omega^2+\Omega^2-1\right)}{\left(\left(1-\Omega^2\right)^2+(2\zeta\Omega)^2\right)\left(1+\alpha^2\Omega^2\right)} \qquad (3.7)$$

The system becomes unstable when the Nyquist plot passes through (-1,0). The corresponding gain when this occurs is the maximum gain that can be attained. The frequency when the imaginary part of the open loop frequency response is zero is found by setting equation (3.7) to zero to give,

$$\Omega^2 = \frac{1}{1+2\zeta\alpha} \tag{3.8}$$

Substituting equation (3.8) in equation (3.5) and equating to –1 gives,

$g_{total\_max} = 2\zeta\left(2\zeta\alpha+\alpha^2+1\right)$. For low damping i.e. $\zeta << 1$ and for a high pass filter corner frequency much less than the resonance frequency of the plant i.e. $\alpha >> 1$ this becomes,

$$g_{total\_max} = 2\zeta\alpha^2 \tag{3.9}$$

Note that for systems with low damping i.e. $\zeta << 1$, the total gain is very small since it includes damping. For a given system the maximum attainable total gain can be found from equation (3.9). The corresponding maximum physical gain g_p can be found from the following relationship;

$$g_{total\_max} = \frac{g_c g_s \omega_n g_{p\_max}}{m} \tag{3.10}$$

Now consider case B2, which is a system with velocity feedback control with a high pass filter and gain of the charge amplifier in the forward path and a pure gain power amplifier and shaker gain in the feedback path.

The open loop frequency response function can be written as,

$$G(j\Omega)H(j\Omega) = \left(\frac{-\Omega^2}{m\left(\left(1-\Omega^2\right)+j2\zeta\Omega\right)}\right)\left(\frac{j\omega_n\Omega}{1+j\alpha\Omega}\right)\left(\frac{1}{j\omega_n\Omega}\right)g_c g_p g_s \tag{3.11}$$

In a similar way to case B1 we let $g_{total} = \frac{g_c g_p g_s}{m}$. Note that for convenience the same notation for total gain is used for acceleration and velocity feedback control, although they are different in their composition.

Equation (3.11) can be arranged into real and imaginary parts as follows,

$$\mathrm{Re}(G(j\Omega)H(j\Omega)) = g_{total}\frac{\Omega^2\left(2\zeta\alpha\Omega^2+\left(\Omega^2-1\right)\right)}{\left(\left(1-\Omega^2\right)^2+\left(2\zeta\Omega\right)^2\right)\left(1+\alpha^2\Omega^2\right)} \tag{3.12}$$

$$\mathrm{Im}(G(j\Omega)H(j\Omega)) = g_{total}\frac{\Omega^3\left(2\zeta+\alpha\left(1-\Omega^2\right)\right)}{\left(\left(1-\Omega^2\right)^2+\left(2\zeta\Omega\right)^2\right)\left(1+\alpha^2\Omega^2\right)} \tag{3.13}$$

The system becomes unstable when the Nyquist passes through (-1,0). Therefore when equation (3.13) is set to zero,

$$\Omega^2 = \frac{\alpha+2\zeta}{\alpha} \tag{3.14}$$

Substituting equation (3.14) into equation (3.12) gives,

$$\mathrm{Re}(G(j\Omega)H(j\Omega)) = g_{total}\frac{2\zeta+\alpha}{2\zeta(2\zeta\alpha+\alpha^2+1)}$$

Since this is positive, the Nyquist plot will not cross the negative real axis and so the system is unconditionally stable.

For case B3, which is displacement feedback, consisting of a high pass filter and charge amplifier gain in the forward path, and pure gain power amplifier and shaker gain in the feedback path, the open loop frequency response function can be written as,

$$G(j\Omega)H(j\Omega) = \left(\frac{-\Omega^2}{m(1-\Omega^2)+j2\zeta\Omega}\right)\left(\frac{j\omega_n\Omega}{1+j\alpha\Omega}\right)\left(\frac{-1}{\omega_n^2\Omega^2}\right)g_c g_p g_s \qquad (3.15)$$

Letting $g_{total} = \frac{g_c g_p g_s}{m\omega_n}$ equation (3.17) can be arranged into real and imaginary parts as follows,

$$\mathrm{Re}(G(j\Omega)H(j\Omega)) = g_{total}\frac{\Omega^2(2\zeta-\alpha(\Omega^2-1))}{((1-\Omega^2)^2+(2\zeta\Omega)^2)(1+\alpha^2\Omega^2)} \qquad (3.16)$$

$$\mathrm{Im}(G(j\Omega)H(j\Omega)) = g_{total}\frac{\Omega(2\zeta\alpha\Omega^2-(1-\Omega^2))}{((1-\Omega^2)^2+(2\zeta\Omega)^2)(1+\alpha^2\Omega^2)} \qquad (3.17)$$

When the imaginary part of equation (3.17) is zero,

$$\Omega^2 = \frac{1}{1+2\zeta\alpha} \qquad (3.18)$$

Substituting equation (3.18) into equation (3.16) gives,

$$\mathrm{Re}(G(j\Omega)H(j\Omega)) = g_{total}\frac{2\zeta\alpha+1}{2\zeta(2\zeta\alpha+\alpha^2+1)}$$

Since this is positive the system is unconditionally stable as in case B2.

From table 3.1 it can be seen that cases (A1 & C1), (B1, D1 &F1), (B2 & C2), (D2, E2 & F2), (C3 & E3) and (D3 & F3) are mathematically similar.

Figures 3.2, 3.4 and 3.6 shows the root locus plot for the cases B1, B2 and B3 respectively. It is seen that increasing gain alters the root locus of the ideal system presented in section 2. Further more the acceleration feedback system becomes unstable with an increasing gain. Figures 3.3, 3.5 and 3.7 show the open loop Nyquist plots for cases B1, B2 and B3 respectively. The figures are plotted for $\alpha = 10$, $\alpha = 15$, $\alpha = 20$ respectively and for gains 10, 22, and 40, which were the maximum respective gains for case B1. It is seen from figure 3.3 that for the acceleration feedback system,

the Nyquist plot passes through the (-1,0) point of the Nyquist plane. However the corresponding velocity feedback system is almost completely in the right half of the Nyquist plane. Part of the Nyquist plot for the corresponding displacement feedback system, however, lies in the left half of the Nyquist plane but does not cross the negative real axis. Hence it is a stable system. The analysis for the maximum gain for the rest of the cases can be found in appendix 1. Table 3.2 gives the maximum non-dimensional gains for the systems shown in table 3.1 as a function of damping ratio ζ and α. An approximation for $\zeta << 1$ and $\alpha >> 1$ is also given in table 3.2. The maximum *physical* gain can be found by equating the total gain to the corresponding relationship in terms of individual component gains given in table 3.3. It is evident from table 3.2 that the maximum non-dimensional gain for the acceleration feedback control system is small compared with the corresponding maximum non-dimensional gains for velocity and displacement systems. Thus velocity and displacement feedback control have much lager stability limits compared to the acceleration feedback control system. Comparing velocity and displacement feedback control systems, the displacement feedback allows a larger gain than the corresponding velocity feedback control system.

In addition, considering cases C2 & C3 from table 3.2 (no high pass filter and real integrator) and cases D2 & D3 (high pass filter and real integrator), it is evident that adding a high pass filter makes the unconditionally stable system conditionally stable with a finite gain limit. It is further evident from cases C3 and E3, which both have an overall open loop frequency response function $G_P(j\Omega)\frac{g_p g_c g_s}{(1+j\alpha\Omega)^2}$, that the high pass filter effects in case E3 are virtually cancelled out leaving only a real integrator effect present. Because of this, although there is a high pass filter in this system it is unconditionally stable. It is also clear that the addition of high pass filters, further reduces the stability limits. This is seen from cases D2, G2 and D3, G3 for velocity and displacement feedback control respectively.

3.3 Closed loop responses of real systems

It was determined in section 3.2 that the high pass filter is the source of instability at low frequencies. Although the Nyquist plot of the open loop frequency response function provides information on the stability of the system it does not provide information on the actual behaviour of the system. The closed loop response gives the information about the system behaviour when it is implemented. This information is vital in judging the performance of a system.

In this the section the closed loop response of the real systems for acceleration, velocity and displacement feedback control are considered. Since the acceleration feedback control system is not viable in terms of stability it is not considered for closed loop response. A system with a real power amplifier, which consists of a gain and a high pass filter, and charge amplifier, which consists of a real integrator and a high pass filter, is considered.

3.3.1 Velocity feedback control

Consider the velocity feedback control of the single degree of freedom discussed in section 2. From figure 3.1 the closed loop frequency response function *(CLFRF)* can be written as,

$$CLFRF = \frac{G(j\Omega)}{1+G(j\Omega)H(j\Omega)} \tag{3.19}$$

where,

$$G(j\Omega) = g_c G_P(j\Omega)\frac{j\omega_n\Omega}{(1+j\alpha\Omega)^2} \text{ and } H(j\Omega) = g_p g_s \frac{j\omega_n\Omega}{(1+j\alpha\Omega)} \tag{3.20,3.21}$$

This gives,

$$CLFRF = \left(\frac{g_c\omega_n}{m}\right)\left(\frac{-j\Omega^3(1+j\alpha\Omega)}{(1-\Omega^2+j2\zeta\Omega)(1+j\alpha\Omega)^3+g_{total}\Omega^4}\right) \tag{3.22}$$

where $g_{total} = \dfrac{g_p g_c g_s \omega_n^2}{m}$

The closed loop frequency response function *CLFRF*, which is the mobility for velocity feedback control, can be non-dimensionalised. Substituting maximum gain $g_{total\_max} = \dfrac{8\alpha^4}{9}$ (table 3.2 case G2) in equation (3.20) and rearranging gives,

$$CLFRF\left(\frac{m}{g_c\omega_n}\right)=\left(\frac{-j\Omega^3(1+j\alpha\Omega)}{(1-\Omega^2+j2\zeta\Omega)(1+j\alpha\Omega)^3+\frac{8\alpha^4}{9}\Omega^4}\right) \qquad (3.23)$$

In equation (3.23), all the parameters in the RHS are in non-dimensional form. Thus the LHS, which denotes the mobility is also non-dimensional.

Figure 3.8 shows the non-dimensional mobility as a function of non-dimensional frequency for $\alpha = 10$ and $\zeta = 0.05$ for various gains. It is seen from the figure that in contrast to the ideal behaviour of the velocity feedback control system, the resonance frequency under real conditions, shifts to a lower frequency as the gain is increased. Figure 3.9 shows the change in mean square response for $10 \le \alpha \le 100$ in the frequency band of $0.1 \le \Omega \le 10$ with half the maximum gain $\frac{1}{2} g_{total\_max} = \frac{4\alpha^4}{9}$ applied. The mean square response can be used as a measure of overall performance. It can be seen from figure 3.9 that as α is increased a considerable change in mean square response is observed, thus providing a better system. It is observed from the open loop frequency response that increasing α increases the stability limit. From the change in mean square response plot, it is also seen that an increase in α results in a better performance. Thus increasing α, which is a measure of separation of the natural frequency to the corner frequency of the high pass filter of the electrical components, increases the stability. In addition, by comparing the change in mean square response plot for damping ratios 0.01 and 0.05 that although damping improves the performance, it is not a dominant factor.

3.3.2 Displacement feedback control

The forward path frequency response function for displacement feedback control becomes,

$$G(j\Omega) = \frac{-\Omega^2}{m(1-\Omega^2+j2\zeta\Omega)} \times \frac{jg_c\omega_n\Omega}{(1+j\alpha\Omega)^3} \qquad (3.24)$$

Substituting equation (3.24) and (3.21) into equation (3.19) the closed loop frequency response function (*CLFRF*) for displacement feedback control becomes,

$$CLFRF = \left(\frac{g_c\omega_n}{m}\right)\left(\frac{-j\Omega^3(1+j\alpha\Omega)}{(1-\Omega^2+j2\zeta\Omega)(1+j\alpha\Omega)^4+g_{total}\Omega^4}\right) \qquad (3.25)$$

where $g_{total} = \frac{g_p g_c g_s \omega_n^2}{m}$, substituting the maximum gain $g_{total\_max} = 4\alpha^4$ into equation (3.26) and rearranging gives the non-dimensional receptance,

$$CLFRF\left(\frac{m}{g_c \omega_n}\right) = \left(\frac{-j\Omega^3(1+j\alpha\Omega)}{(1-\Omega^2+j2\zeta\Omega)(1+j\alpha\Omega)^4+4\alpha^4\Omega^4}\right) \qquad (3.26)$$

Figure 3.10 shows the non-dimensional receptance as a function of non-dimensional frequency for $\alpha = 10$ and $\zeta = 0.05$ for various gains. It is seen from the figure that in contrast to the ideal behaviour of displacement feedback control system, a second peak is starting to form at low frequencies. Figure 3.11 shows the change in mean square response for $10 \le \alpha \le 100$ in the frequency band of $0.1 \le \Omega \le 10$ with half the maximum gain $\frac{1}{2} g_{total\_max} = 2\alpha^4$ applied. It can be seen from figure 3.8 that as α is increased a considerable change in mean square response is observed. It is also observed from the open loop frequency response that increasing α increases the stability limit. Similar to velocity feedback control, although damping improves the stability it does not improve the performance considerably.

Both velocity and displacement feedback control systems perform well in closed loop. Their gains for a stable system are considerably higher compared to acceleration feedback control. The maximum gain that can be achieved for a given α is higher in displacement feedback compared to the other two.

3.4 System with more high pass filter components

It has been established that the high pass filter is the source of instability at low frequency. The mathematical model of the high pass filter considered so far takes the form $\frac{j\omega_n\Omega}{(1+j\alpha\Omega)}$. However it is possible to have higher order filters. For simplicity filters which have the form $\left(\frac{j\omega_n\Omega}{1+j\alpha\Omega}\right)^m$ are considered. Systems with m = 1, m =2 are given in table 3.2, for example for velocity feedback control, cases D2 and G2 respectively. Therefore the systems with m = 3 and m = 4 are considered in this section. For simplicity an undamped system is considered.

3.4.1 Velocity feedback control

The open loop frequency response function for velocity feedback control can be written as,

$$G(j\omega)H(j\omega) = \left(\frac{g_c g_p g_s}{m}\right)\left(\frac{-\Omega^2}{1-\Omega^2}\right)\left(\frac{1}{1+j\alpha\Omega}\right)\left(\frac{j\omega_n\Omega}{1+j\alpha\Omega}\right)^m \qquad (3.27)$$

Table 3.4 shows the maximum gain for different number of high pass filters. The details of calculations are given in appendix 1. Consider a system with f_n = 20 Hz then ω_n = 125.7 rad/sec, figure 3.12 shows the maximum gain of this system as a function of α for m = 1 to 4. It is seen that the gain reduces considerably when a higher number of high pass filters installed.

3.4.2 Displacement feedback control

The open loop frequency response function for displacement feedback control can be written as,

$$G(j\omega)H(j\omega) = \left(\frac{g_c g_p g_s}{m}\right)\left(\frac{-\Omega^2}{1-\Omega^2}\right)\left(\frac{1}{1+j\alpha\Omega}\right)^2\left(\frac{j\omega_n\Omega}{1+j\alpha\Omega}\right)^m \qquad (3.28)$$

Table 3.5 shows the maximum gain for different number of high pass filters. Considering a system with f_n = 20 Hz, figure 3.13 shows the maximum gain of this system as a function of α for m = 1 to 4. It is seen that the maximum gain reduces considerably when a higher number of high pass filters installed.

3.5 Discussion

It can be seen from the analysis in this section that in an acceleration feedback control system far less gain is possible than the other two configurations. In the real system, comparing the maximum gain attainable for velocity and displacement feedback control, it is evident that for displacement feedback control a higher gain than for velocity feedback is possible. It is also evident that the overall performance, quantified by the change in mean square response, is not very different for these two systems. Although the system damping helps to improve the closed loop performance, it is not a dominant factor.

It is clear that the high pass filter component is the dominant source of instability at low frequency. The real integrator does not affect the performance greatly compared with an ideal integrator. It is also evident that when higher numbers of high pass filters are installed the maximum gain reduces.

Table 3.1 Mathematical models of different combinations of power amplifier and charge amplifier for acceleration, velocity and displacement feedback control

Charge amplifier settings considered	Acceleration feedback *1*	Velocity feedback *2*	Displacement feedback *3*
Pure gain power amplifier - g_p			
[A] No high pass filter and Ideal integrator *(Ideal condition)*	-	$\frac{1}{j\omega}$	$-\frac{1}{\omega^2}$
[B] High pass filter and ideal integrator (if applicable)	$\frac{jg_c\omega}{(1+j\tau_c\omega)}$	$\frac{jg_c\omega}{(1+j\tau_c\omega)}\frac{1}{j\omega}$	$-\frac{jg_c\omega}{(1+j\tau_c\omega)}\frac{1}{\omega^2}$
[C] No high pass filter and real integrator (if applicable)	-	$\frac{g_c}{(1+j\tau_i\omega)}$	$\frac{g_c}{(1+j\tau_i\omega)^2}$
[D] High pass filter and real integrator	$\frac{jg_c\omega}{(1+j\tau_c\omega)}$	$\frac{jg_c\omega}{(1+j\tau_c\omega)}\times\frac{1}{(1+j\tau_i\omega)}$	$\frac{jg_c\omega}{(1+j\tau_c\omega)}\times\frac{1}{(1+j\tau_i\omega)^2}$
Real power amplifier $\frac{jg_p\omega}{(1+j\tau_p\omega)}$			
[E] High pass filter and ideal integrator (if applicable)	$\frac{jg_c\omega}{(1+j\tau_c\omega)}$	$\frac{jg_c\omega}{(1+j\tau_c\omega)}\frac{1}{j\omega}$	$-\frac{jg_c\omega}{(1+j\tau_c\omega)}\frac{1}{\omega^2}$
[F] No high pass filter and real integrator (if applicable)	-	$\frac{g_c}{(1+j\tau_i\omega)}$	$\frac{g_c}{(1+j\tau_i\omega)^2}$
[G] High pass filter and real integrator	$\frac{jg_c\omega}{(1+j\tau_c\omega)}$	$\frac{jg_c\omega}{(1+j\tau_c\omega)}\times\frac{1}{(1+j\tau_i\omega)}$	$\frac{jg_c\omega}{(1+j\tau_c\omega)}\times\frac{1}{(1+j\tau_i\omega)^2}$

Table 3. 2 Maximum non-dimensional gain for the cases considered in table 3.1

Charge amplifier settings considered	Acceleration feedback *1*	Velocity feedback *2*	Displacement feedback *3*
Pure gain power amplifier - g_p			
[A] No high pass filter and Ideal integrator *(Ideal condition)*	*Unconditionally Stable*	*Unconditionally Stable*	*Unconditionally Stable*
[B] High pass filter and ideal integrator (if applicable)	$g_{max} = 2\zeta\left(1+\zeta\alpha+\alpha^2\right)$ $g_{max} \approx 2\alpha^2\zeta$	*Unconditionally Stable*	*Unconditionally Stable*
[C] No high pass filter and real integrator (if applicable)	*Unconditionally stable*	*Unconditionally stable*	*Unconditionally stable*
[D] High pass filter and real integrator	$g_{max} = 2\zeta\left(1+\zeta\alpha+\alpha^2\right)$ $g_{max} \approx 2\zeta\alpha^2$	$g_{max} = \frac{2\alpha\left\{4\alpha^2\zeta^2+(\alpha^2-1)^2\right\}}{(\alpha^2-1)}$ $g_{max} \approx 2\alpha^3$	$g_{max} = \frac{8\alpha\left\{12\alpha^2\zeta^2+(3\alpha^2-1)^2\right\}}{3(3\alpha^2-1)}$ $g_{max} \approx 8\alpha^3$
Real power amplifier $\frac{jg_p\omega}{\left(1+j\tau_p\omega\right)}$			
[E] High pass filter and ideal integrator (if applicable)	$g_{max} = \frac{\alpha\zeta(2\alpha\zeta+\alpha^2+1)^2}{(\alpha+\zeta)^2}$ $g_{max} \approx \alpha^3\zeta$	$g_{max} = \frac{2\alpha\left\{4\alpha^2\zeta^2+(\alpha^2-1)^2\right\}}{(\alpha^2-1)}$ $g_{max} \approx 2\alpha^3$	*Unconditionally stable*
[F] No high pass filter and real integrator (if applicable)	$g_{max} = 2\zeta\left(1+\zeta\alpha+\alpha^2\right)$ $g_{max} \approx 2\zeta\alpha^2$	$g_{max} = \frac{2\alpha\left\{4\alpha^2\zeta^2+(\alpha^2-1)^2\right\}}{(\alpha^2-1)}$ $g_{max} \approx 2\alpha^3$	$g_{max} = \frac{8\alpha\left\{12\alpha^2\zeta^2+(3\alpha^2-1)^2\right\}}{3(3\alpha^2-1)}$ $g_{max} \approx 8\alpha^3$

[G] High pass filter and real integrator	$g_{max}=\dfrac{\alpha\zeta(2\alpha\zeta+\alpha^2+1)^2}{(\alpha+\zeta)^2}$ $g_{max}\approx\alpha^3\zeta$	$g_{max}=\dfrac{8\alpha^2\{12\alpha^2\zeta^2+(\alpha^2-3)^2\}}{9(\alpha^2-3)}$ $g_{max}\approx\dfrac{8\alpha^4}{9}$	$g_{max}=\dfrac{4\alpha^2\{4\alpha^2\zeta^2+(\alpha^2-1)^2\}}{(\alpha^2-1)}$ $g_{max}\approx 4\alpha^4$

Table 3. 3 Total gain as a function of individual gain settings of components for the cases considered in table 3.1

Instrument settings considered	Velocity feedback **1**	Displacement feedback **2**	Acceleration feedback **3**
Pure gain Power amplifier- g_p			
B] High pass filter and ideal integrator (if applicable)	$g_{total} = \frac{g_c g_p g_s \omega_n}{m}$ $\Omega_{cri}^2 = \frac{1}{2\alpha\zeta + 1}$	$g_{total} = \frac{g_c g_p g_s}{m}$ *Unconditionally stable*	$g_{total} = \frac{g_c g_p g_s}{m\omega_n}$ *Unconditionally stable*
C] No high pass filter and real integrator (if applicable)	$g_{total} = \frac{g_c g_p g_s}{m}$ *Unconditionally stable*	$g_{total} = \frac{g_c g_p g_s}{m}$ *Unconditionally stable*	$g_{total} = \frac{g_c g_p g_s}{m}$ *Unconditionally stable*
D] High pass filter and real integrator	$g_{total} = \frac{g_c g_p g_s \omega_n}{m}$ $\Omega_{cri}^2 = \frac{1}{2\alpha\zeta + 1}$	$g_{total} = \frac{g_c g_p g_s \omega_n}{m}$ $\Omega_{cri}^2 = \frac{1}{\alpha^2}$ for $\alpha >> 1 \& \zeta << 1$	$g_{total} = \frac{g_c g_p g_s \omega_n}{m}$ $\Omega_{cri}^2 = \frac{1}{3\alpha^2}$ for $\alpha >> 1 \& \zeta << 1$
Real power amplifier $\frac{jg_p\omega}{(1 + j\tau_p\omega)}$			
E] High pass filter and ideal integrator (if applicable)	$g_{total} = \frac{g_c g_p g_s \omega_n^2}{m}$ $\Omega_{cri}^2 = \frac{\alpha + \zeta}{\alpha(\alpha\zeta + 1)}$	$g_{total} = \frac{g_c g_p g_s \omega_n}{m}$ $\Omega_{cri}^2 = \frac{1}{\alpha^2}$ for $\alpha >> 1 \& \zeta << 1$	$g_{total} = \frac{g_c g_p g_s}{m}$ *Unconditionally stable*
F] No high pass filter and real integrator (if applicable)	$g_{total} = \frac{g_c g_p g_s \omega_n}{m}$ $\Omega_{cri}^2 = \frac{1}{2\alpha\zeta + 1}$	$g_{total} = \frac{g_c g_p g_s \omega_n}{m}$ $\Omega_{cri}^2 = \frac{1}{\alpha^2}$ for $\alpha >> 1 \& \zeta << 1$	$g_{total} = \frac{g_c g_p g_s \omega_n}{m}$ $\Omega_{cri}^2 = \frac{1}{3\alpha^2}$ for $\alpha >> 1 \& \zeta << 1$
G] High pass filter and real integrator	$g_{total} = \frac{g_c g_p g_s \omega_n^2}{m}$ $\Omega_{cri}^2 = \frac{\alpha + \zeta}{\alpha(\alpha\zeta + 1)}$	$g_{total} = \frac{g_c g_p g_s \omega_n^2}{m}$ $\Omega_{cri}^2 = \frac{3}{\alpha^2}$ for $\alpha >> 1 \& \zeta << 1$	$g_{total} = \frac{g_c g_p g_s \omega_n^2}{m}$ $\Omega_{cri}^2 = \frac{1}{\alpha^2}$ for $\alpha >> 1 \& \zeta << 1$

Table 3.4 Maximum gain for an undamped velocity feedback control system as a function of α for higher number of high pass filter components.

Order of high pass filter	Critical frequency Ω^2	Maximum gain Where $g_{max} = \frac{g_c g_s g_p}{m}$	Approximate Maximum gain for $\alpha >> 1$, Where $g_{max} = \frac{g_c g_s g_p}{m}$
n = 1	$\frac{1}{\alpha^2}$	$g_{max} = \frac{2\alpha(\alpha^2 - 1)}{\omega_n}$	$g_{max} \approx \frac{2\alpha^3}{\omega_n}$
n = 2	$\frac{3}{\alpha^2}$	$g_{max} = \frac{8\alpha^2(\alpha^2 - 3)}{9\omega_n^2}$	$g_{max} \approx \frac{8\alpha^4}{9\omega_n^2}$
n = 3	$\left(\frac{\sqrt{2}+1}{\alpha}\right)^2$	$g_{max} \approx \frac{8\alpha^3(\alpha^2 - 6)}{14\omega_n^3}$	$g_{max} \approx \frac{8\alpha^5}{14\omega_n^3}$
n = 4	$\left(\frac{2\sqrt{5}+5}{\alpha^2}\right)$	$g_{max} \approx \frac{8\alpha^4(\alpha^2 - 9)}{19\omega_n^4}$	$g_{max} \approx \frac{8\alpha^6}{19\omega_n^4}$

Table 3.4 Maximum gain for an undamped displacement feedback control system as a function of α for higher number of high pass filter components.

Order of high pass filter	Critical frequency Ω^2	Maximum gain Where $g_{max} = \frac{g_c g_s g_p}{m}$	Approximate Maximum gain for $\alpha >> 1$, Where $g_{max} = \frac{g_c g_s g_p}{m}$
n = 1	$\frac{1}{3\alpha^2}$	$g_{max} = \frac{8\alpha(3\alpha^2 - 1)}{3\omega_n}$	$g_{max} \approx \frac{8\alpha^3}{\omega_n}$
n = 2	$\frac{1}{\alpha^2}$	$g_{max} = \frac{4\alpha^2(\alpha^2 - 1)}{\omega_n^2}$	$g_{max} \approx \frac{4\alpha^4}{\omega_n^2}$
n = 3	$\left(\frac{2\sqrt{5}+5}{5\alpha^2}\right)$	$g_{max} \approx \frac{32\alpha^3(\alpha^2 - 2)}{11\omega_n^3}$	$g_{max} \approx \frac{32\alpha^5}{11\omega_n^3}$
n = 4	$\frac{3}{\alpha^2}$	$g_{max} \approx \frac{64\alpha^4(\alpha^2 - 3)}{27\omega_n^4}$	$g_{max} \approx \frac{64\alpha^6}{27\omega_n^4}$

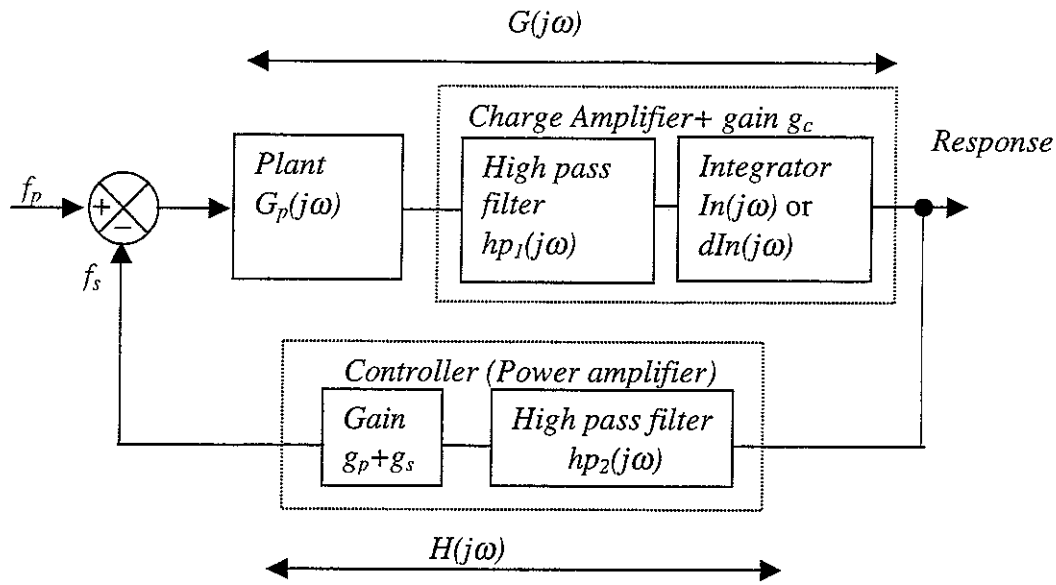

Figure 3.1 Simplified model of real system for feedback control

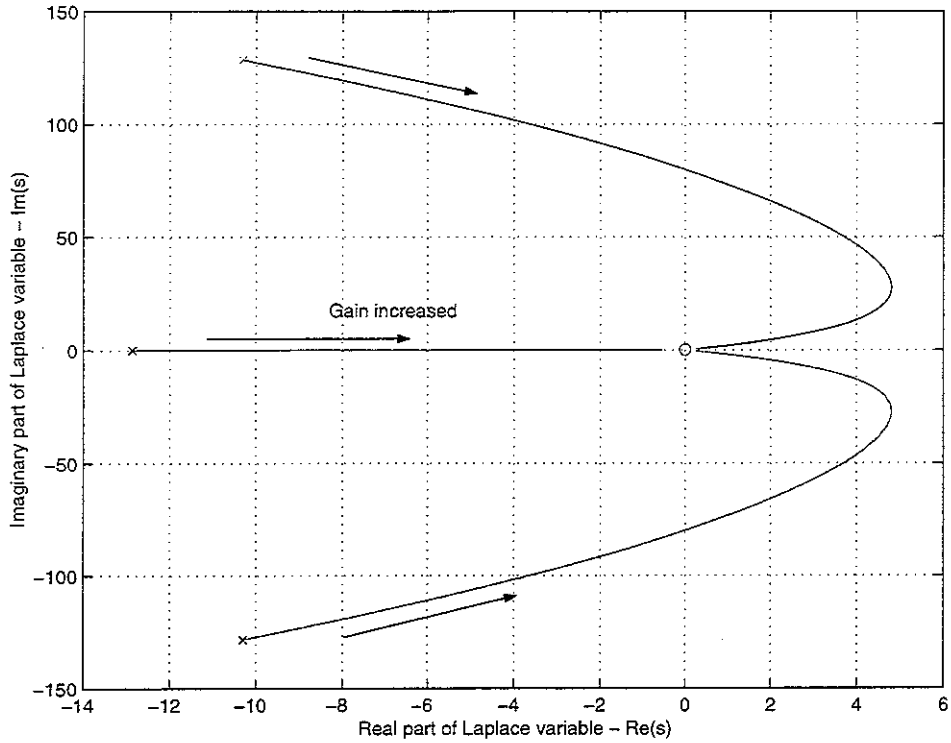

Figure 3.2 Root locus for acceleration feedback control (case B1) - $\zeta = 0.05$ and $f_n = 20$ Hz

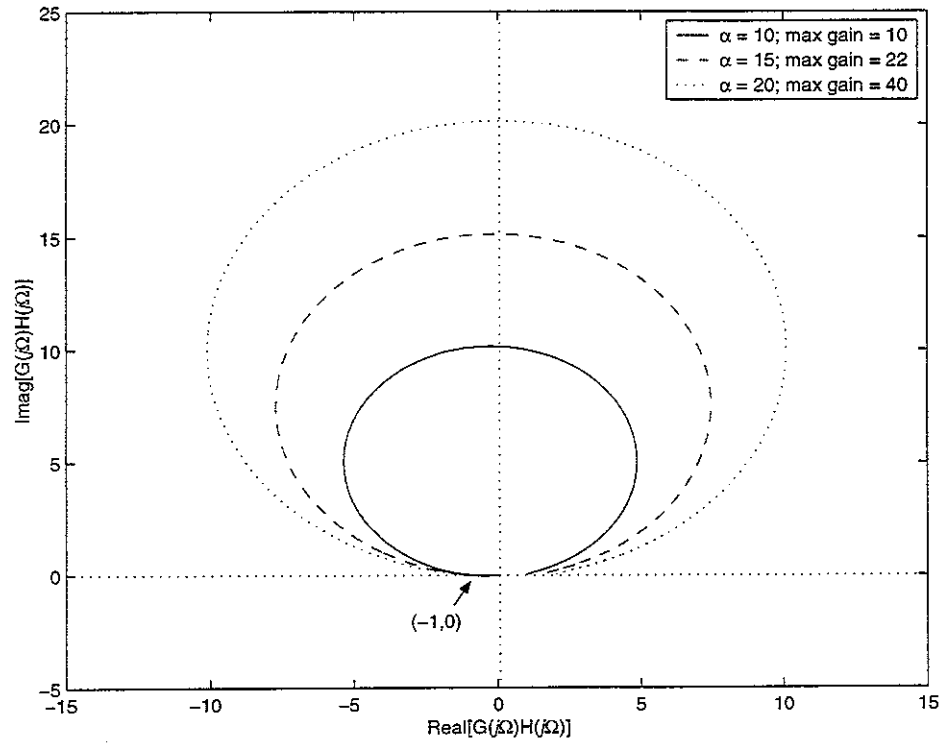

Figure 3.3 The Nyquist plot for acceleration feedback control with $\zeta = 0.05$ (case B1).

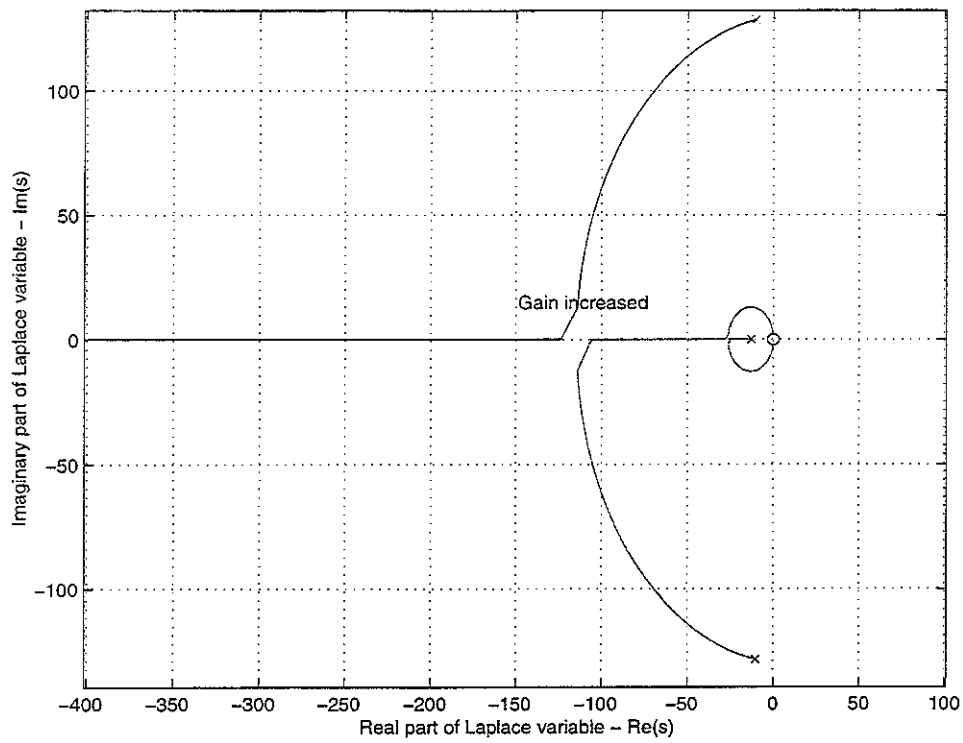

Figure 3.4, Root locus for velocity feedback control (case B2) - $\zeta = 0.05$ and $f_n = 20$ Hz

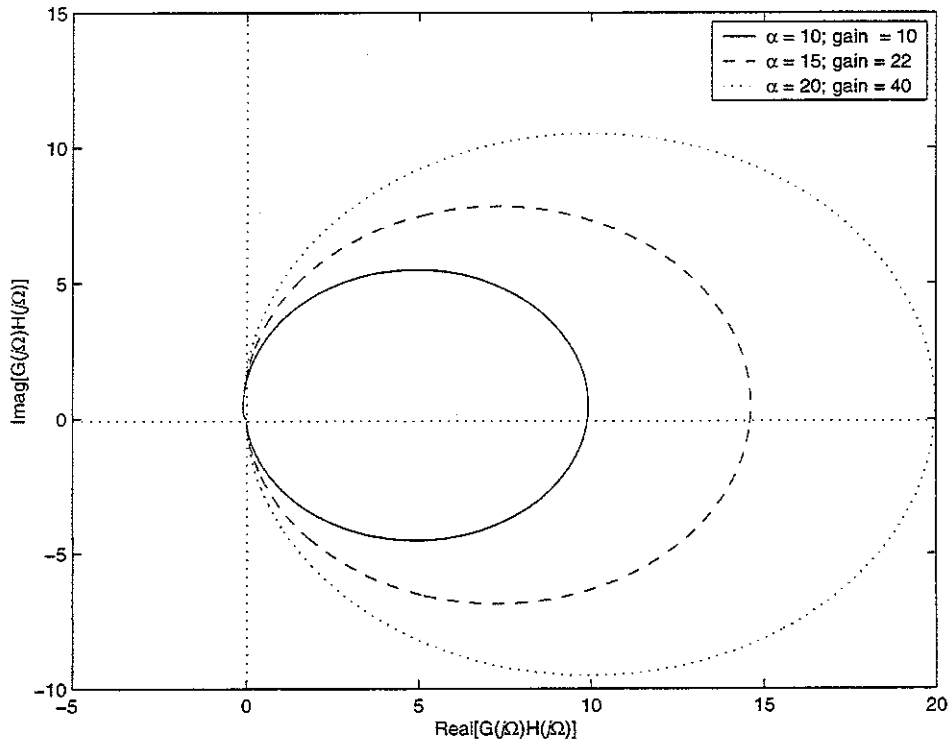

Figure 3.5 The Nyquist plot for velocity feedback control with $\zeta = 0.05$. (Case B2)

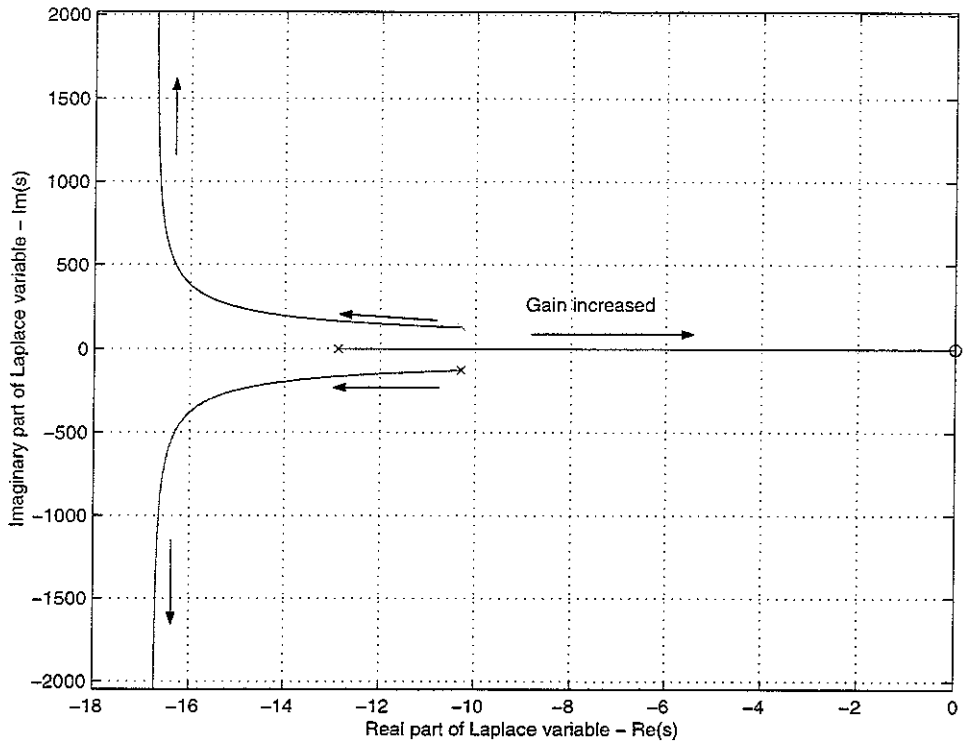

Figure 3.6 Root locus for displacement feedback control (case B3) - $\zeta = 0.05$ and $f_n = 20$ Hz

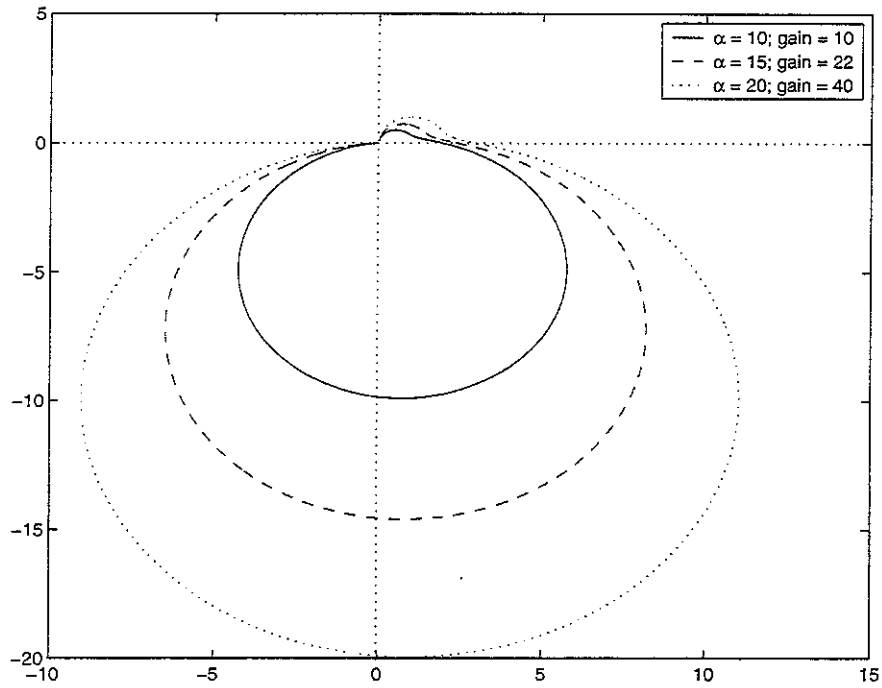

Figure 3.7 The Nyquist plot for displacement feedback control with $\zeta = 0.05$. (Case B3)

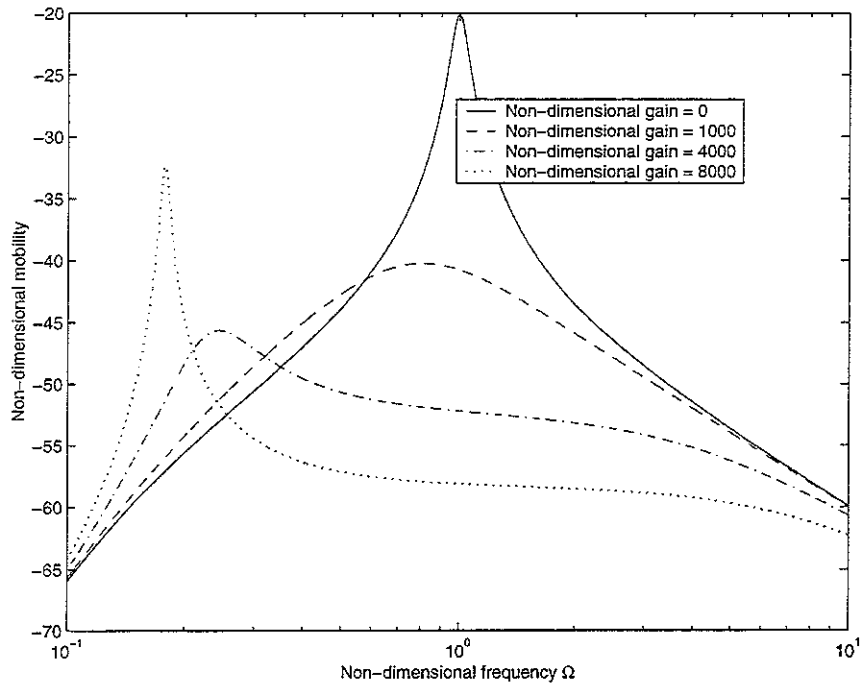

Figure 3.8 Closed loop response of SDOF for velocity feedback control - case G2 (ζ = 0.05. Gains 0, 1000, 4000, 8000 ($<g_{total\_max}=\frac{8\alpha^4}{9}$) and α = 10)

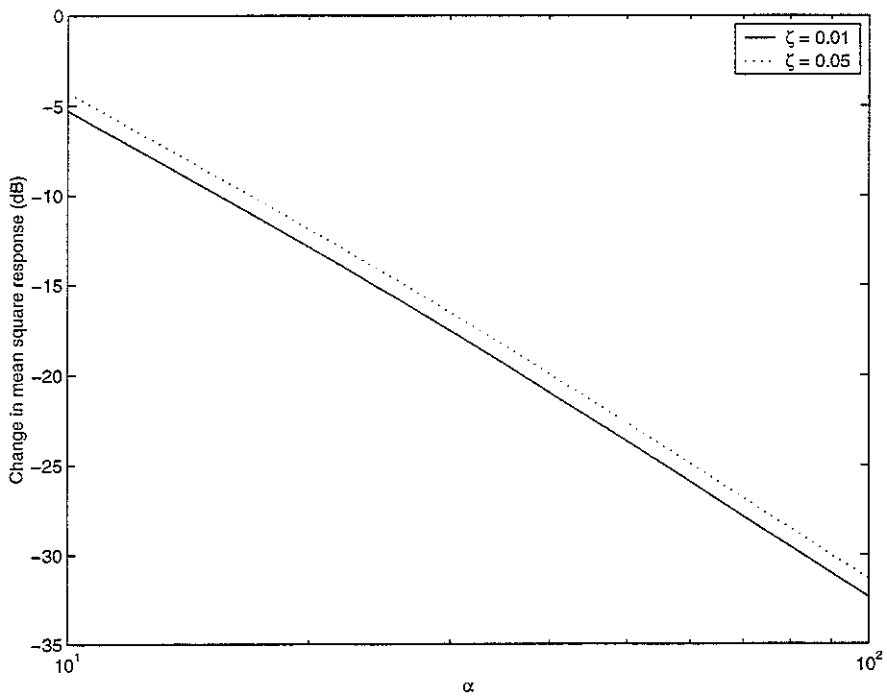

Figure 3.9 Change in mean square response for velocity feedback control of SDOF. (ζ=0.01, 0.05, frequency band $0.1 \le \Omega \le 10$ and a gain of $0.5\times\frac{8\alpha^4}{9}$ for each α)

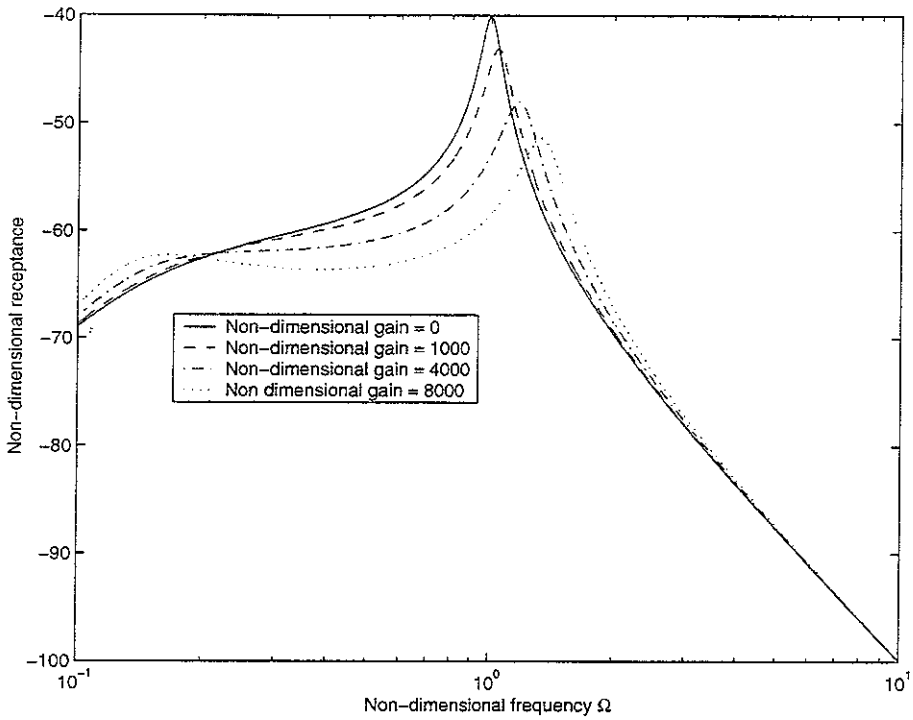

Figure 3.10 Closed loop response of SDOF in displacement feedback control - case G3 ($\zeta = 0.05$. Gains – 0, 1000, 4000, 8000 ($<g_{max}=4\alpha^4$) and $\alpha = 10$)

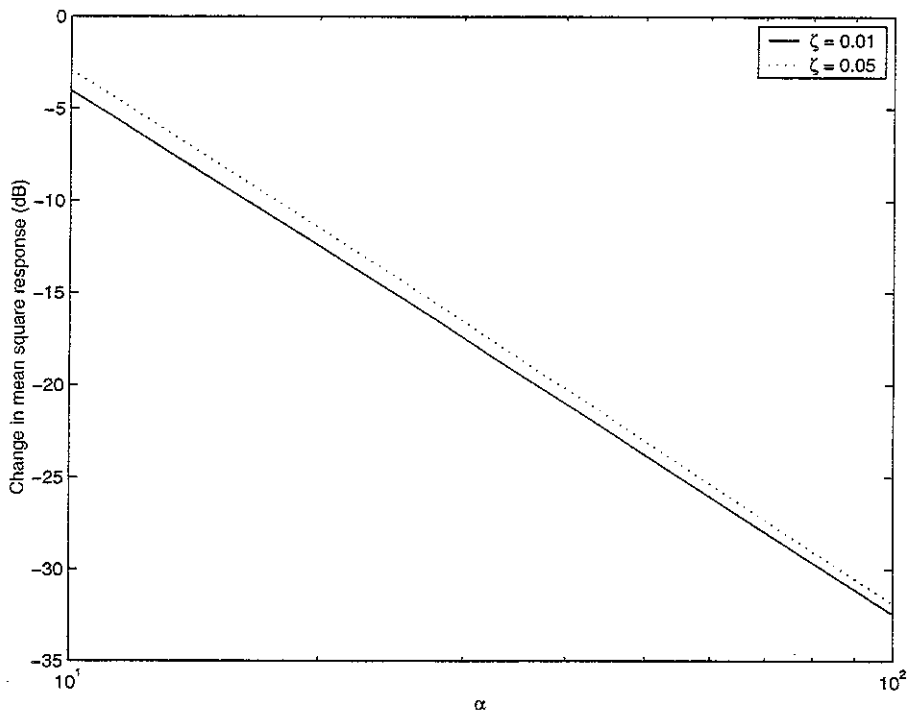

Figure 3.11 Change in mean square responses in displacement feedback control of SDOF. (ζ=0.01, 0.05, frequency band $0.1 \leq \Omega \leq 10$ and a gain of half the maximum $0.5\times 4\alpha^4$)

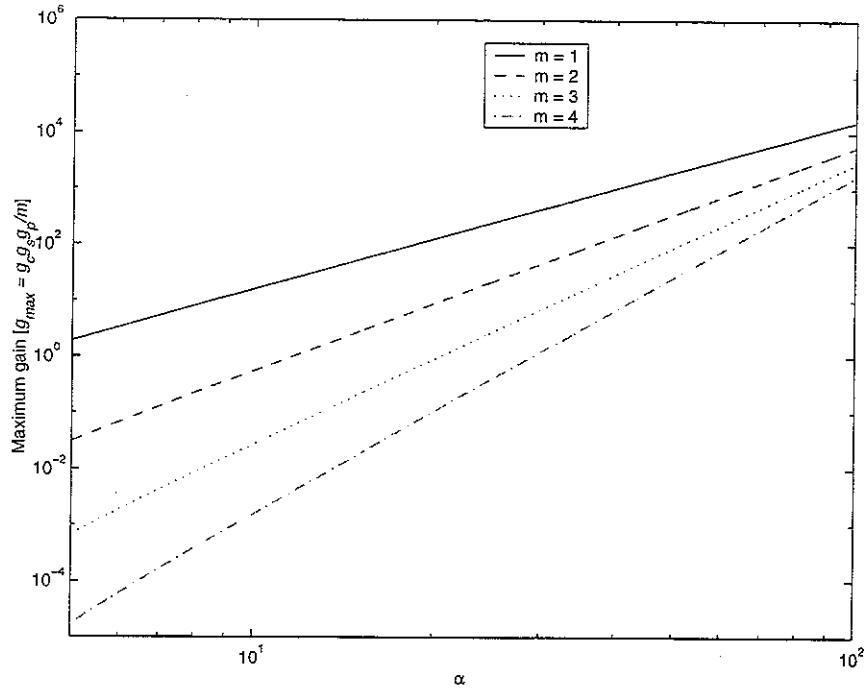

Figure 3.12 Maximum gain for different number of high pass filter components with α *for an undamped velocity feedback control system-* f_n *= 20 Hz.*

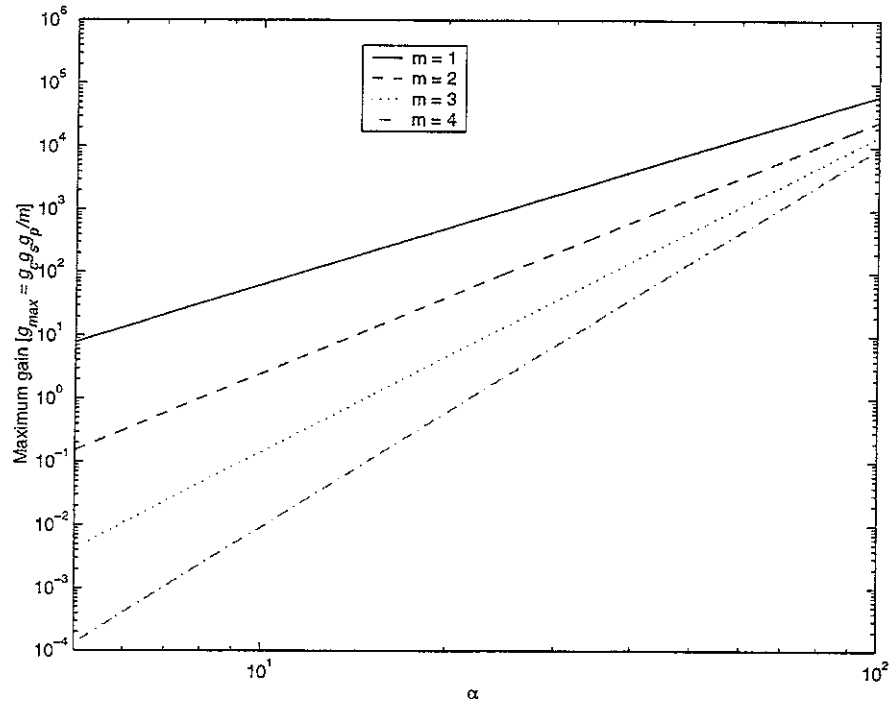

Figure 3.13 Maximum gain for different number of high pass filter components with α *for an undamped displacement feedback control system-* f_n *= 20 Hz .*

4 High frequency instabilities

4.1 Introduction

In this section the sources of high frequency instabilities in the feedback control of the SDOF system are investigated. As mentioned in section 2, high frequency instabilities in the active feedback control system arise from four sources. They are,

1. Time delay
2. Low pass filter module of the charge amplifier.
3. Control force shakers
4. Accelerometers

In this section time delay and effect of low pass filters are discussed in detail and some mention is made of the other two. Time delay is considered first.

4.2 Time delay

The delay is represented as $e^{-j\omega T}$ where T is the delay time. Delays in feedback control mainly come from digital control systems where there is some processing to be done by a computer. Therefore a delay such as this is unlikely to influence an analogue control system. However for completeness it is investigated here.

The delay term affects the feedback frequency response function. For example consider an ideal velocity feedback control system with time delay. The feedback frequency response function becomes,

$$H(j\omega) = g_v e^{-j\omega T} \tag{4.1}$$

where $g_v = g_p g_s$ (g_p, g_s - gains of power amplifier and secondary shaker respectively)

The open loop frequency response function for a SDOF system with velocity feedback and time delay in the control loop now becomes,

$$G(j\Omega)H(j\Omega) = \frac{g_v}{c} \times \frac{j2\zeta\Omega e^{-j2\pi\Omega\tau}}{1-\Omega^2 + j2\zeta\Omega} \tag{4.2}$$

where $\omega_n = \sqrt{\frac{k}{m}}$ is the resonance frequency, $\zeta = \frac{c}{2m\omega_n}$, is the damping ratio, $\Omega = \frac{\omega}{\omega_n}$ is the non-dimensional frequency and $\tau = \frac{T}{T_n}$ is the non-dimensional time delay, where T_n is the natural period.

The open loop frequency response function given in equation (4.2) is plotted in the form of a Nyquist plot for various time delays and for damping ratio $\zeta = 0.05$ and $\frac{g_v}{c} = 1$, and is shown in figure 4.1b. The figure shows how the delay affects the stability of a single degree of freedom system. The open loop response of a system with no time delay lies completely in the right half of the Nyquist plane and as time delay is increased the orientation of the plot changes in a clockwise direction. It becomes unstable with a non-dimensional time delay of 0.5. It is also interesting to note that the second frequency at which the Nyquist plot crosses the real axis is important in this case. With a non-dimensional time delay of 0.5, the frequencies 0.9, 1.0 and 1.1 are also marked in the figure 4.1b. Interestingly this shows how rapidly the frequency changes for a system, which passes through (-1,0) point of the Nyquist plane. For a system with non-dimensional time delay 0.5, it is stable for $\Omega = 0.9$, on the verge of instability for $\Omega = 1.0$ and unstable for $\Omega = 1.1$. Therefore when critical frequency is estimated a slightly lower estimation does not do any harm, whereas a slightly over estimation means an unstable system. Similar plots for acceleration and displacement feedback control are shown in figures 4.1a and 4.1c with $\frac{g_a}{m} = 1$ and $\frac{g_d}{k} = 1$ respectively. It is interesting to note that acceleration feedback control system may go unstable with the second frequency at which the Nyquist plot crosses the real axis of the Nyquist plane whereas it is the first frequency for the displacement feedback control.

In this section the effect of time delay in acceleration, velocity and displacement feedback control are discussed. The maximum gains for a given time delay and the closed loop responses are analysed.

4.2.1 acceleration feedback control with time delay

The open loop frequency response function of an ideal acceleration feedback control with time delay can be written as,

$$G(j\Omega)H(j\Omega) = \frac{g_a}{m} \times \frac{-\Omega^2 e^{-j2\pi\Omega\tau}}{1-\Omega^2 + j2\zeta\Omega} \tag{4.3}$$

Equation (4.3) can be rearranged into real and imaginary parts to give,

$$G(j\Omega)H(j\Omega) = -\frac{g_a\Omega^2}{m}\left\{\frac{(\Omega^2-1)\cos(2\pi\tau\Omega) - 2\zeta\Omega\sin(2\pi\tau\Omega}{4\zeta^2\Omega^2 + (\Omega^2-1)^2}\right\} + \frac{jg_a\Omega^2}{m}\left\{\frac{(\Omega^2-1)\sin(2\pi\tau\Omega) + 2\zeta\Omega\cos(2\pi\tau\Omega)}{4\zeta^2\Omega^2 + (\Omega^2-1)^2}\right\} \tag{4.4}$$

To determine the relationship between the critical frequency Ω_{crit} at which the system goes unstable and the time delay, the imaginary part is set to zero to give,

$$\mathrm{Im}\{G(j\Omega)H(j\Omega)\} = 0, \text{ which results in } \tan(2\pi\tau\Omega_{crit}) = -\frac{2\zeta\Omega_{crit}}{1-\Omega_{crit}^2}$$

Let

$$f(\Omega) = \tan(2\pi\tau\Omega_{crit}) = -\frac{2\zeta\Omega_{crit}}{1-\Omega_{crit}^2} \tag{4.5}$$

Equation (4.5) can be written in alternative form as,

$\tan(\pi - 2\pi\tau\Omega_{crit}) = \frac{2\zeta\Omega_{crit}}{1-\Omega_{crit}^2}$. For low damping, i.e. when $\zeta \to 0$;

$\tan(\pi - 2\pi\tau\Omega_{crit}) \to 0$ which gives,

$$\Omega_{crit} = \frac{1}{2\tau} \tag{4.6}$$

From equation 4.5 the critical frequency depends on the damping ratio (ζ) and non-dimensional time delay (τ). A graphical representation of solution to this equation is shown in figure 4.2a for τ = 0.1. The second frequency at which the graph crosses the real axis is important for acceleration feedback control and is the critical frequency. Figure 4.3a shows the critical frequency as a function of damping ratio and non-dimensional time delay. It is evident from this figure that the dependence of the critical

frequency on the time delay is much greater than for the damping ratio. Thus for low damping, the approximation given in equation 4.6 can be used. Figure 4.4a shows this approximation graphically together with the numerical solutions to equation (4.5) for damping ratios 0.01, 0.05 and 0.1 respectively. It can be seen that this approximation is in good agreement with the numerical solution. For a time delay $0 < \tau \leq 0.15$ and damping ratio $0 < \zeta \leq 0.1$ the approximation given by equation (4.6) is in good agreement with the numerical solutions.

Substituting the approximate critical frequency given by equation (4.6) into the real part of equation (4.4) and equating to –1 to find maximum non-dimensional gain $\frac{g_a}{m}$, before the system becomes unstable gives,

$$\frac{g_{a\_\max}}{m} = 1 - 4\tau^2 \qquad (4.7)$$

It is evident from equation (4.7) that the maximum attainable gain is less than unity. Figure 4.5a shows the maximum non-dimensional gain as a function of time delay.

It can be seen that the maximum gain reduces considerably as the time delay becomes significant. Although the open loop frequency response function provides a means of finding the point of stability, it does not provide much information on the system performance. This requires the closed loop frequency response and change in mean square response to be studied. Figure 4.6a shows the closed loop frequency response function for a damping ratio of 0.05 and for various time delays. The maximum gain given in equation (4.7) was used in the simulations. This shows that when the feedback gain is increased the response reduces at its original resonance frequency but the new resonance frequency is shifted to a higher frequency and multiple resonance also occur. These resonance peaks are the undesirable effect of the time delay. Figure 4.7a shows the change in mean square response for a frequency band of $0.01 \leq \Omega \leq 100$ as a function of time delay for maximum gain given by equation (4.7). It is seen that as the time delay increases the overall performance tends to that of the original system and with a non-dimensional time delay $\tau = 0.051$ the system becomes ineffective. This means that for even a small time delay the acceleration feedback system does not help to reduce the overall vibration performance.

4.2.2 Velocity feedback control with time delay

The open loop frequency response function with velocity feedback control is given by equation (4.2), which can be rearranged into real and imaginary parts to give,

$$G(j\Omega)H(j\Omega) = \frac{2g_v\zeta\Omega}{c}\left\{\frac{2\zeta\Omega\cos(2\pi\tau\Omega) - (\Omega^2-1)\sin(2\pi\tau\Omega}{4\zeta^2\Omega^2 + (\Omega^2-1)^2}\right\} - \frac{-j2g_v\zeta\Omega}{c}\left\{\frac{(\Omega^2-1)\cos(2\pi\tau\Omega) + 2\zeta\Omega\sin(2\pi\tau\Omega)}{4\zeta^2\Omega^2 + (\Omega^2-1)^2}\right\} \quad (4.8)$$

To determine the relationship between the critical frequency $\Omega_{crit,}$ at which the system goes unstable, and the time delay, the imaginary part is set to zero to give,

$\mathrm{Im}\{G(j\Omega)H(j\Omega)\} = 0$, which results in $\tan(2\pi\tau\Omega) = \dfrac{1-\Omega^2}{2\zeta\Omega}$

Let

$$f(\Omega) = \tan(2\pi\tau\Omega) = \frac{1-\Omega^2}{2\zeta\Omega} \quad (4.9)$$

Equation (4.9) can be written in the following form,

$$\tan\left(\frac{\pi}{2} - 2\pi\tau\Omega_{\text{crit}}\right) = \frac{2\zeta\Omega_{\text{crit}}}{1-\Omega_{crit}^2} \quad (4.10)$$

When $\zeta \to 0$ in equation (4.10), $\tan\left(\dfrac{\pi}{2} - 2\pi\tau\Omega_{\text{crit}}\right) \to 0$ which results in,

$$\Omega_{crit} = \frac{1}{4\tau} \quad (4.11)$$

As seen in equation (4.9), frequency at which the Nyquist plot crosses the real axis depends on the damping ratio and non-dimensional time delay. A graphical representation of the solutions of equation (4.9) for various damping ratios is shown in figure 4.2b. The solid line in figure 4.2b shows the *tan* function (LHS of equation 4.9) and other lines shows the RHS of equation (4.9) for various damping ratios ζ and a non-dimensional time delay of 0.1.

Figure 4.3b shows the numerical solution (critical frequency) of equation (4.9) as function of damping ratio and non-dimensional time delay. It is seen from figure 4.3b that the critical frequency is influenced much more by the time delay than the damping ratio. For a given time delay and low damping, the critical frequency can be taken as the asymptote frequency of the *tan* function (equation 4.11). For higher damping the equation (4.9) has to be solved numerically. Figure 4.4b shows the approximate critical frequency and the numerical solutions to equation (4.9) for damping ratios 0.01, 0.05 and 0.1 respectively. It is seen that the approximate solution is in good agreement with numerical solutions. It can be observed that for a time delay $0 < \tau \leq 0.15$ and damping ratio $0 < \zeta \leq 0.1$ the approximation given by equation (4.11) is in good agreement with the numerical solutions.

To determine the maximum gain the real part of the open loop response function given by equation (4.8) should be set to –1 and the frequency set to the critical frequency. This gives,

$$\frac{g_{v\_max}}{c} = \frac{-\left(4\zeta^2\Omega_{crit}^2 + \left(\Omega_{crit}^2 - 1\right)^2\right)}{2\Omega_{crit}\zeta\left\{2\zeta\Omega_{crit}\cos(2\pi\tau\Omega_{crit}) + \left(1-\Omega_{crit}^2\right)\sin(2\pi\tau\Omega_{crit})\right\}} \tag{4.12}$$

When $\tau \leq 0.15$, $\Omega_{crit} \approx \frac{1}{4\tau}$ and equation (4.12) reduces to

$$\frac{g_{v\_max}}{c} = \frac{-\left(64\tau^2\zeta^2 + \left(16\tau^2 - 1\right)^2\right)}{8\tau\zeta\left(16\tau^2 - 1\right)} \tag{4.13}$$

For $\zeta << 1$ this becomes,

$$\frac{g_{v\_max}}{c} \approx \frac{\left(1-16\tau^2\right)}{8\tau\zeta} \tag{4.14}$$

which for a small time delay, $\tau << 1$ reduces further to,

$$\frac{g_{v\_max}}{c} = \frac{1}{8\tau\zeta} \tag{4.15}$$

Figure 4.5b shows the maximum gain $\frac{g_{v\_max}\zeta}{c}$ as a function of time delay for the time delay range $\tau \leq 0.15$. It is seen that the maximum gain reduces considerably as the time

delay increases. Figure 4.6b shows the closed loop frequency response function for a damping ratio of 0.05 and for various time delays. The maximum gain given in equation (4.14) was used for these simulations. This shows that when the feedback gain is increased the response reduces but the resonance frequency is shifted to a higher frequency. These resonance peaks are the undesirable effect of the time delay. Figure 4.7b shows the change in mean square response for a frequency band of $0.01 \le \Omega \le 100$ as a function of time delay for maximum gain given by equation (4.14). It is seen that as the time delay increases the overall performance tends to that of the original system. But for time delay less than 0.15 the system is still effective.

4.2.3 Displacement feedback control with time delay

The open loop frequency response function with time delay of an ideal displacement feedback control can be written as,

$$G(j\Omega)H(j\Omega) = \frac{g_d}{k} \times \frac{e^{-j2\pi\Omega\tau}}{1-\Omega^2 + j2\zeta\Omega} \tag{4.16}$$

Equation (4.16) can be rearranged into real and imaginary parts to give,

$$G(j\Omega)H(j\Omega) = \frac{g_d}{k}\left\{\frac{(\Omega^2-1)\cos(2\pi\tau\Omega) - 2\zeta\Omega\sin(2\pi\tau\Omega}{4\zeta^2\Omega^2 + (\Omega^2-1)^2}\right\} - \frac{jg_d}{k}\left\{\frac{(\Omega^2-1)\sin(2\pi\tau\Omega) + 2\zeta\Omega\cos(2\pi\tau\Omega)}{4\zeta^2\Omega^2 + (\Omega^2-1)^2}\right\} \tag{4.17}$$

To determine the relationship between the critical frequency Ω_{crit} at which the system goes unstable and the time delay, the imaginary part is set to zero to give,

$\mathrm{Im}\{G(j\Omega)H(j\Omega)\} = 0$, which results in $\tan(2\pi\tau\Omega_{crit}) = -\dfrac{2\zeta\Omega_{crit}}{1-\Omega_{crit}^2}$. Let

$$f(\Omega) = \tan(2\pi\tau\Omega_{crit}) = -\frac{2\zeta\Omega_{crit}}{1-\Omega_{crit}^2} \tag{4.18}$$

It is to be noted from figure 4.1c that the critical frequency is the first crossing (real axis) frequency of the Nyquist plot. This is in contrast to the acceleration and displacement feedback control systems discussed in section 4.2.1 and 4.2.2.

Figure 4.3c shows this first crossing frequency (critical frequency) as a function of time delay and damping ratio. It is seen that the critical frequency is influenced much more by the time delay than the damping ratio. In addition it is also evident that the magnitude of the critical frequency is much smaller than the acceleration and velocity feedback control discussed previously. Hence for a small time delay the equation (4.18) can be approximated as,

$$\tan(2\pi\tau\Omega_{crit}) \approx 2\pi\tau\Omega_{crit} = -\frac{2\zeta\Omega_{crit}}{1-\Omega_{crit}^2} \tag{4.19}$$

From equation (4.19) the approximate critical frequency can be written as,

$$\Omega_{crit}^2 = 1+\frac{\zeta}{\pi\tau} \tag{4.20}$$

Unlike acceleration and velocity feedback control this approximate critical frequency depends on the time delay and damping ratio. Figure 4.4c shows the numerical solution and approximate estimation of critical frequency for damping ratios 0.01, 0.05 and 0.1 respectively. It is seen that the estimation is in reasonable agreement with the numerical solutions. For time delay $0 < \tau \leq 0.15$ and damping ratio $0 < \zeta \leq 0.1$ the approximation given by equation (4.20) is in reasonable agreement with the numerical solutions.

Substituting the approximate critical frequency given by equation (4.20) into the real part of equation (4.17) and equating to –1 to find maximum non-dimensional gain $\frac{g_d}{k}$ gives,

$$\frac{g_{d\_\max}}{k} = \frac{\zeta}{\pi\tau} \tag{4.21}$$

Figure 4.5c shows the maximum non-dimensional gain as a function of time delay. Figure 4.6c shows the closed loop frequency response function for a damping ratio of 0.05 and for various time delays. The maximum gain given in equation (4.21) was used for these simulations. This shows that when feedback gain is increased the responses reduce at the original resonance frequency but the resonance frequency is initially shifted to a higher frequency and then to a lower frequency. This is due to the choice of damping since $\zeta = 0.05$ was considered and $\tau = 0.01$ is less than the damping ratio hence it gives a much higher gain than the other cases. However these resonance peaks are the

undesirable effect of the time delay. Figure 4.7b shows the change in mean square response for a frequency band of $0.01 \leq \Omega \leq 100$ as a function of time delay for maximum gain given by equation (4.21). It is seen that as the time delay increases the overall performance reaches to that of the original system with non-dimensional time delay 0.07 and thereafter it becomes ineffective.

4.3 Low pass filter

As mentioned in section 2 the low pass filter in the charge amplifier, which is used to filter out the high frequency unwanted signals, is a potential source of instability at higher frequencies. In this section the effect of this low pass filter in velocity and displacement feedback control is analysed. Two factors have to be explored. First whether the low pass filter affects the stability and if so what is the maximum gain. As the purpose is to investigate the effect of the low pass filter, which is dominant at high frequency, it was assumed that the effect of high pass filter is negligible. In other words the system behaves as if no high pass filter connected. An ideal integrator was assumed. It should be noted that such a system without a low pass filter is unconditionally stable.

4.3.1 Effect of the low pass filter on acceleration feedback control

With a low pass filter the open loop frequency response function for a SDOF system with acceleration feedback control becomes,

$$G(j\Omega)H(j\Omega)=\frac{-\Omega^2}{m\left(1-\Omega^2+j2\zeta\Omega\right)}\times\frac{g_a}{\left(1+j\gamma\Omega\right)} \qquad (4.22)$$

where γ is the ratio of the natural frequency of the system to the corner frequency of the low pass filter.

This system is mathematically equivalent to case B2 presented in table 3.1 and table 3.2. From the analysis presented in section 3.2, the system is unconditionally stable. Hence the low pass filter does not affect the stability of the acceleration feedback control system.

4.3.1 Effect of the low pass filter on velocity feedback control

With a low pass filter the open loop frequency response function of a SDOF system with velocity feedback becomes,

$$G(j\Omega)H(j\Omega)=\frac{-\Omega^2}{m\left(1-\Omega^2+j2\zeta\Omega\right)}\times\frac{g_v}{j\omega_n\Omega}\times\frac{1}{(1+j\gamma\Omega)} \tag{4.23}$$

where γ is the ratio of the natural frequency of the system to the corner frequency of the low pass filter. Equation (4.23) can be rewritten as,

$$G(j\omega)H(j\omega)=\frac{2g_v\zeta}{c}\times\left(\frac{j\Omega}{1-\Omega^2+j2\zeta\Omega}\right)\times\left(\frac{1}{1+j\gamma\Omega}\right) \tag{4.24}$$

This system is mathematically equivalent to case E3 presented in table 3.1 and table 3.2. From the analysis presented in appendix 1 for case E3, the system is unconditionally stable.

Hence a low pass filter does not affect the stability of the velocity feedback control system.

4.3.2 Effect of the low pass filter on displacement feedback control

Similar to the velocity feedback control system, a low pass filter in an ideal displacement feedback control system is considered. The ideal system is unconditionally stable for displacement feedback control. Because of this it is relatively simple to see whether the addition of a low pass filter has any significant effect in displacement feedback control. The open loop frequency response function becomes,

$$G(j\Omega)H(j\Omega)=\frac{g_d}{k}\times\left(\frac{1}{1-\Omega^2+j2\zeta\Omega}\right)\times\left(\frac{1}{1+j\gamma\Omega}\right) \tag{4.25}$$

which can be expressed in real and imaginary parts as,

$$\mathrm{Re}\{G(j\Omega)H(j\Omega)\}=-\frac{g_d}{k}\times\frac{\left[2\gamma\zeta\Omega^2+\left(\Omega^2-1\right)\right]}{\left[4\zeta^2\Omega^2+\left(1-\Omega^2\right)^2\right]\left[1+\gamma^2\Omega^2\right]} \tag{4.26}$$

$$\mathrm{Im}\{G(j\Omega)H(j\Omega)\}=-\frac{g_d}{k}\times\frac{j\Omega\left[2\zeta-\gamma\left(\Omega^2-1\right)\right]}{\left[4\zeta^2\Omega^2+\left(1-\Omega^2\right)^2\right]\left[1+\gamma^2\Omega^2\right]} \tag{4.27}$$

The Nyquist plot crosses the real axis when imaginary part is zero, which gives a frequency of,

$\Omega^2 = \frac{2\zeta + \gamma}{\gamma} = 1 + \frac{2\zeta}{\gamma}$. (This is similar to equation 4.20)

The real part at this frequency is $\left(-\frac{g_d}{k} \frac{\gamma}{2\zeta\left(\gamma^2 + 2\zeta\gamma + 1\right)} \right)$,

The maximum gain occurs when the real part is equal to –1, which results in

$$\frac{g_{d\_\max}}{k} = \frac{2\zeta\left(\gamma^2 + 2\zeta\gamma + 1\right)}{\gamma} \tag{4.28}$$

For $\zeta << 1$ and $\gamma << 1$ equation (4.28) can be written as,

$$\frac{g_{d\_\max}}{k} \approx \frac{2\zeta}{\gamma} \tag{4.29}$$

Therefore addition of a low pass filter in a displacement feedback control system makes the unconditionally stable system, conditionally stable.

It is also interesting to note that small time delay can be approximated to low pass filter effect in displacement feedback control system.

Non-dimensional time delay is represented by $e^{-j2\pi\tau\Omega}$ which is for a small time delay can be approximated as,

$$e^{-j2\pi\tau\Omega} = \frac{1}{1 + j2\pi\tau\Omega} \tag{4.30}$$

Let $\gamma' = 2\pi\tau$ then treating delay as a low pass filter the maximum gain from equation (4.29) can be written as

$\frac{g_{\max}}{k} \approx \frac{2\zeta}{\gamma'} = \frac{\zeta}{\pi\tau}$ which is equivalent to the gain given in equation (4.21)

Hence a small time delay in displacement feedback can be related to a low pass filter.

4.4 Combined system (low and high pass filters)

Consider an analogue velocity feedback control system with high and low pass filters and power amplifier. Since an analogue system is considered, the effect of control time delay is not included. The purpose of the low pass filter is to filter out high frequency unwanted signals and high pass filter is to filter out low frequency unwanted signals. Hence their corner frequencies should be significantly apart. Since α is defined for the high pass filter

as the plant natural frequency to the high pass filter corner frequency ratio, a similar definition for low pass filter (γ) can be written as $\gamma = k\alpha$, where k is less than one. The open loop frequency response function for combined system can be written as,

$$G(j\Omega)H(j\Omega) = \left(\frac{g_p g_c g_s}{m}\right)\left(\frac{-\Omega^2}{1-\Omega^2+j2\zeta\Omega}\right)\left(\frac{j\omega_n\Omega}{(1+j\alpha\Omega)}\right)^2\left(\frac{1}{1+j\alpha\Omega}\right)\left(\frac{1}{1+jk\alpha\Omega}\right) \quad (4.32)$$

where $\left(\frac{j\omega_n\Omega}{(1+j\alpha\Omega)}\right)^2$ represents the high pass filters in the charge amplifier and power amplifier, $\left(\frac{1}{1+j\alpha\Omega}\right)$ represents the real integrator and $\left(\frac{1}{1+jk\alpha\Omega}\right)$ represents the low pass filter.

Consider the system with negligible damping then the equation (4.17) can be written as.

$$G(j\Omega)H(j\Omega) = \left(\frac{g_p g_c g_s}{m}\right)\left(\frac{-\Omega^2}{1-\Omega^2}\right)\left(\frac{j\omega_n\Omega}{(1+j\alpha\Omega)}\right)^2\left(\frac{1}{1+j\alpha\Omega}\right)\left(\frac{1}{1+jk\alpha\Omega}\right) \quad (4.33)$$

This can be written in real and imaginary parts as follows,

$$\mathrm{Im}(G(j\Omega)H(j\Omega)) = \left(\frac{g_p g_c g_s \omega_n^2}{m}\right)\frac{\alpha\Omega^5\left(\Omega^2\alpha^2(3k+1)-(k+3)\right)}{\left(1+\Omega^2\alpha^2\right)^3\left(1+k^2\alpha^2\Omega^2\right)\left(\Omega^2-1\right)} \quad (4.34)$$

$$\mathrm{Re}(G(j\Omega)H(j\Omega)) = -\left(\frac{g_p g_c g_s \omega_n^2}{m}\right)\frac{\Omega^4\left(k\alpha^4\Omega^4-3\alpha^2\Omega^2(k+1)+1\right)}{\left(1+\Omega^2\alpha^2\right)^3\left(1+k^2\alpha^2\Omega^2\right)\left(\Omega^2-1\right)} \quad (4.35)$$

As previously, the gains of the components are grouped together, so $g = \left(\frac{g_p g_c g_s \omega_n^2}{m}\right)$

When the Nyquist plot crosses the real axis the imaginary part is zero, this gives,

$\Omega^2 = \frac{k+3}{(3k+1)\alpha^2}$. At this frequency the real part becomes,

$$\mathrm{Re}(G(j\Omega)H(j\Omega)) = -g\frac{(k+3)^2(3k+1)}{8\alpha^2\left(\alpha^2(3k+1)-(k+3)\right)(k+1)^3} \quad (4.36)$$

The maximum total gain can then be obtained by equating the real part to –1, which gives,

$$g_{max} = \frac{8\alpha^2\left(\alpha^2(3k+1)-(k+3)\right)(k+1)^3}{(k+3)^2(3k+1)} \tag{4.37}$$

If $k << 1$ and $\alpha >> 1$ then the equation (4.22) can be approximated as,

$$g_{max} = \frac{8\alpha^4}{9} \tag{4.38}$$

This is the same as the gain for the velocity feedback system defined by case G2 in table 3.2. Therefore if k is sufficiently small then the low pass filter will not affect the velocity feedback control.

It was seen in section 4.3 that the low pass filter affects the displacement feedback system even for the ideal case. Hence the real case is not investigated.

4.5 Effects of accelerometers and secondary force shakers

As mentioned in section 2 the accelerometers and secondary shakers can cause instability at higher frequencies. The resonance frequency of the accelerometer together with additional phase shift may cause the system to go unstable. Therefore the range over which the accelerometer functions as a linear transducer and the operation frequency range of the feedback system have to be considered. Similarly a resonance of the moving element of control actuator, which generally occurs at a high frequency, can produce a non- proportional control force. A system, which is theoretically stable, may go unstable because of this phenomenon. Therefore prior knowledge of the characteristics of these transducers and the operating range of the feedback system can only help to avoid unexpected instabilities.

4.6 Discussion

It can be seen from the analysis presented in this section that time delay, if present, is potentially the dominant source of instability at high frequencies. Increasing the time delay reduces the overall performance of the control system. The maximum gain that can be achieved in the acceleration, velocity and displacement feedback control systems considered can be approximately calculated using the relatively simple formulae derived.

It is also evident that the velocity and displacement feedback control system permit higher gain than the acceleration feedback control system with delay. However the overall performances suggest that acceleration and displacement feedback control systems are ineffective with even small time delays. The velocity feedback control system functions reasonably well up to a non-dimensional time delay of 0.15.

The low pass filter set to filter out high frequency components well above the natural frequency of the mechanical system, does not seriously affect the acceleration and velocity feedback control systems. An analysis of the ideal displacement feedback control system with a low pass filter shows that the low pass filter affects this system. Hence it appears that a realistic velocity feedback control system is more robust.

Although velocity and displacement feedback control systems are theoretically comparable except when there is time delay in the control system, velocity feedback is more robust. Because the accelerometer signal is integrated twice to obtain the displacement feedback signal, at higher frequencies the displacement signal becomes very small, with a reduced signal to noise ratio. This noise, affects the quality of the displacement feedback control more so than in velocity feedback control. Hence among the three configurations the velocity feedback control is considered to be more attractive.

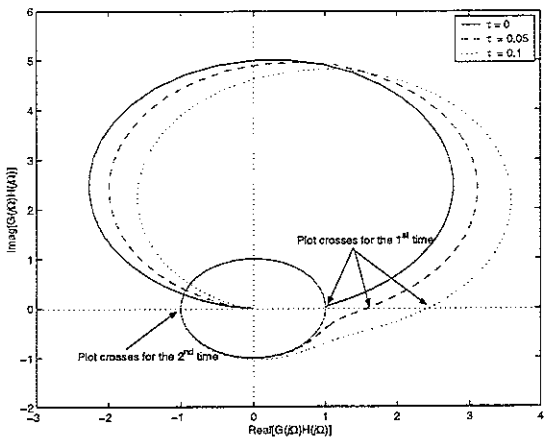

(a) Acceleration feedback control with $\frac{g_a}{m} = 1$ and $\zeta = 0.05$.

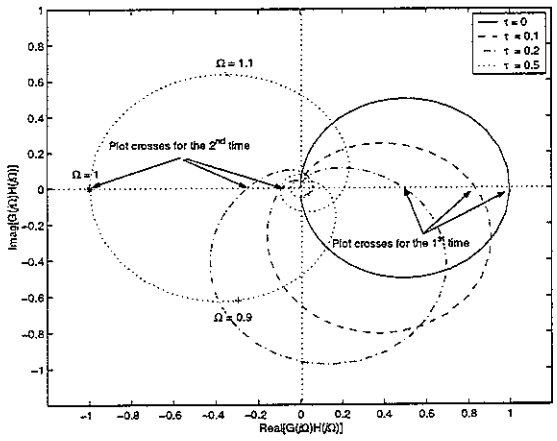

(b) Velocity feedback control with $\frac{g_v}{c} = 1$ *and* $\zeta = 0.05$.

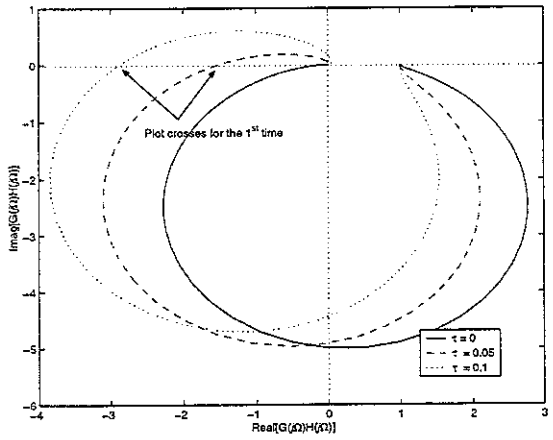

(c) Displacement feedback control with $\frac{g_d}{k} = 1$ *and* $\zeta = 0.05$.

Figure 4.1 the Nyquist plot of open loop transfer function for different time delay.

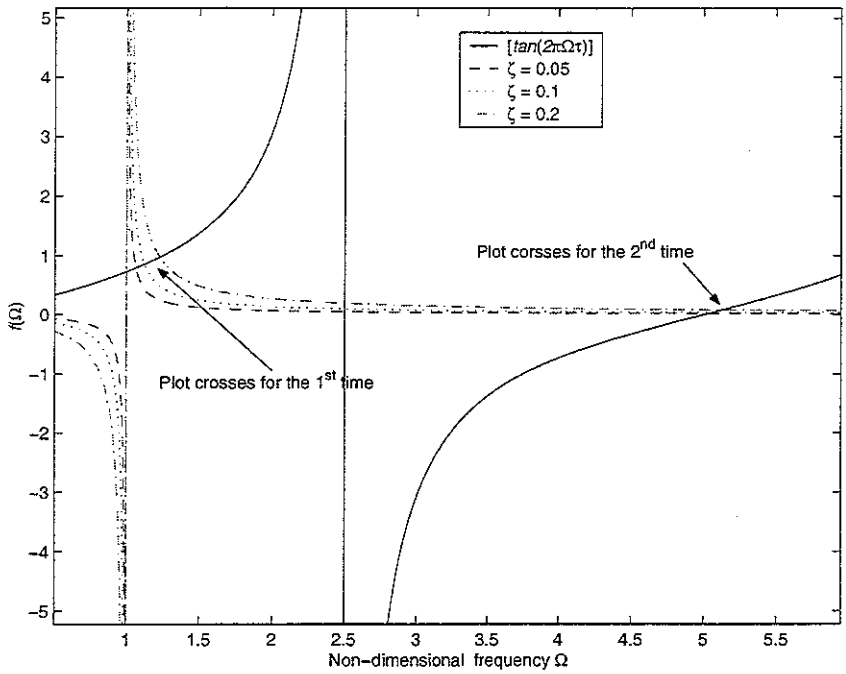

(a) Acceleration and displacement feedback control.

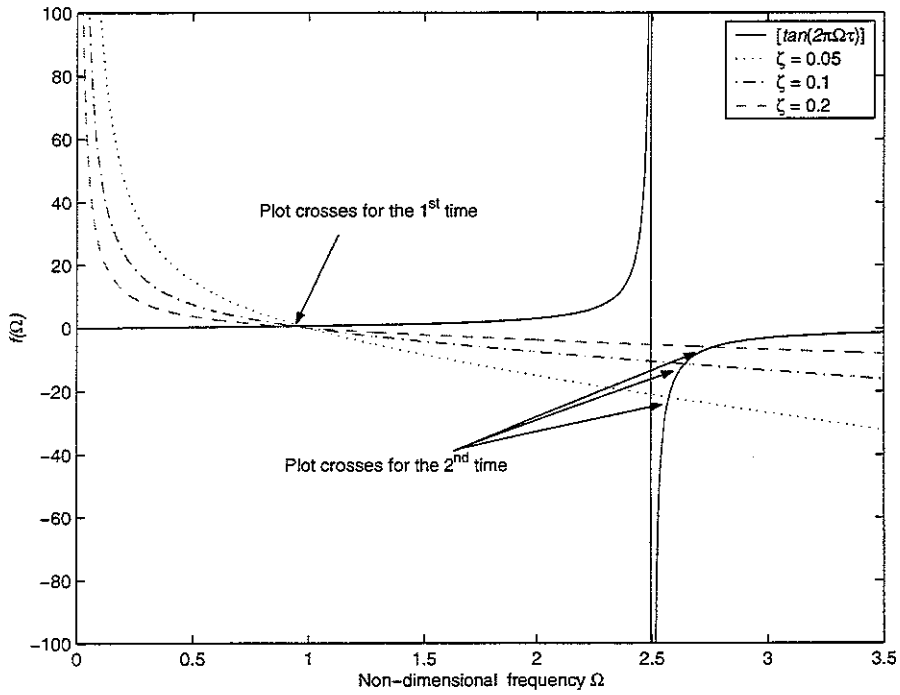

(b) Velocity feedback control.

Figure 4.2 graphical representations of the solutions for the equation of critical frequency (non-dimensional time delay $\tau = 0.1$)

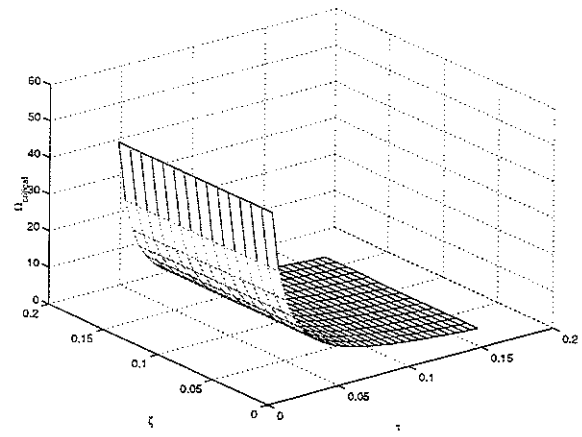

(a) Acceleration feedback control.

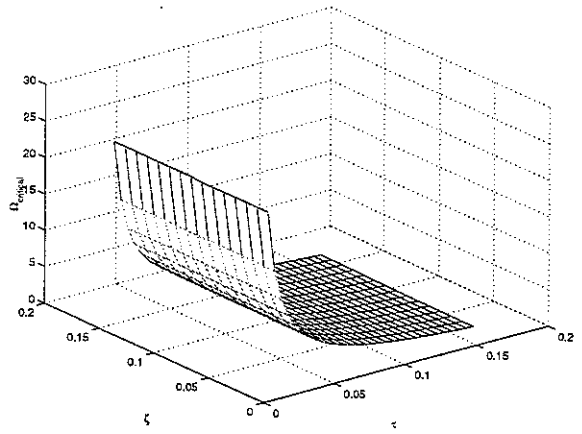

(b) Velocity feedback control

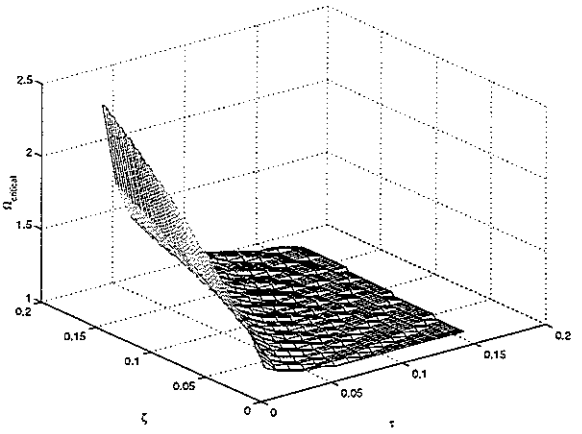

(c) Displacement feedback control

Figure 4.3 Critical frequencies as a function of time delay and damping ratio.

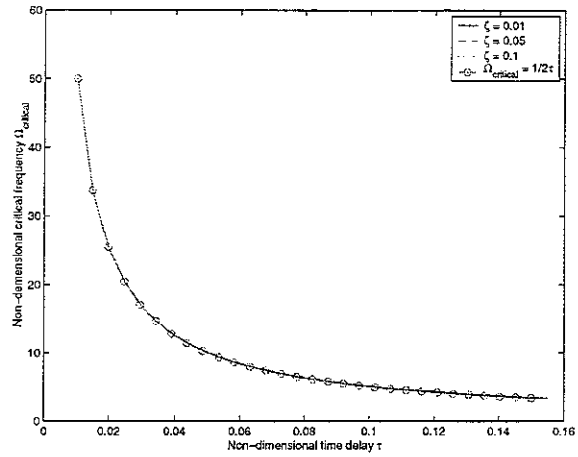

(a) Acceleration feedback control

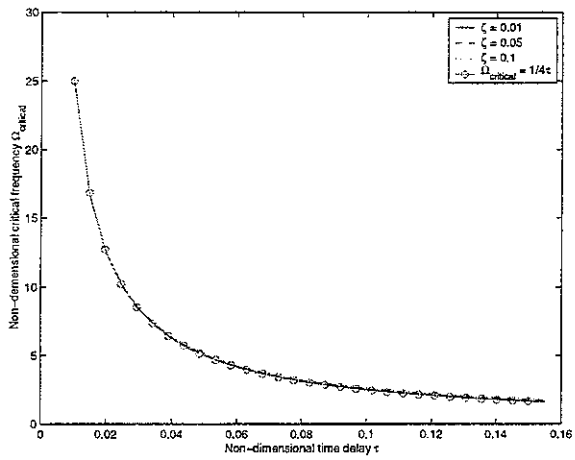

(b) Velocity feedback control

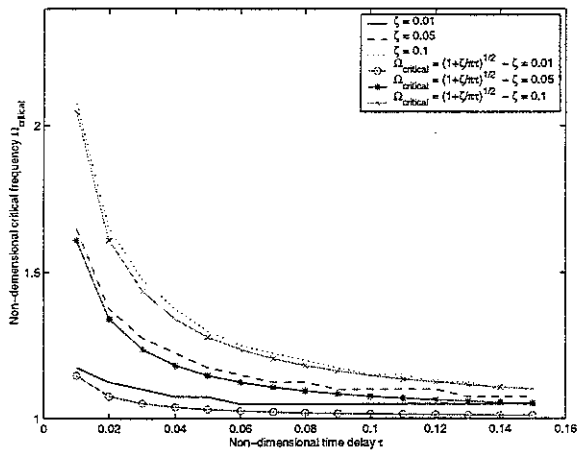

(c) Displacement feedback control

Figure 4.4 Critical frequencies as a function of time delay (with approximate models)

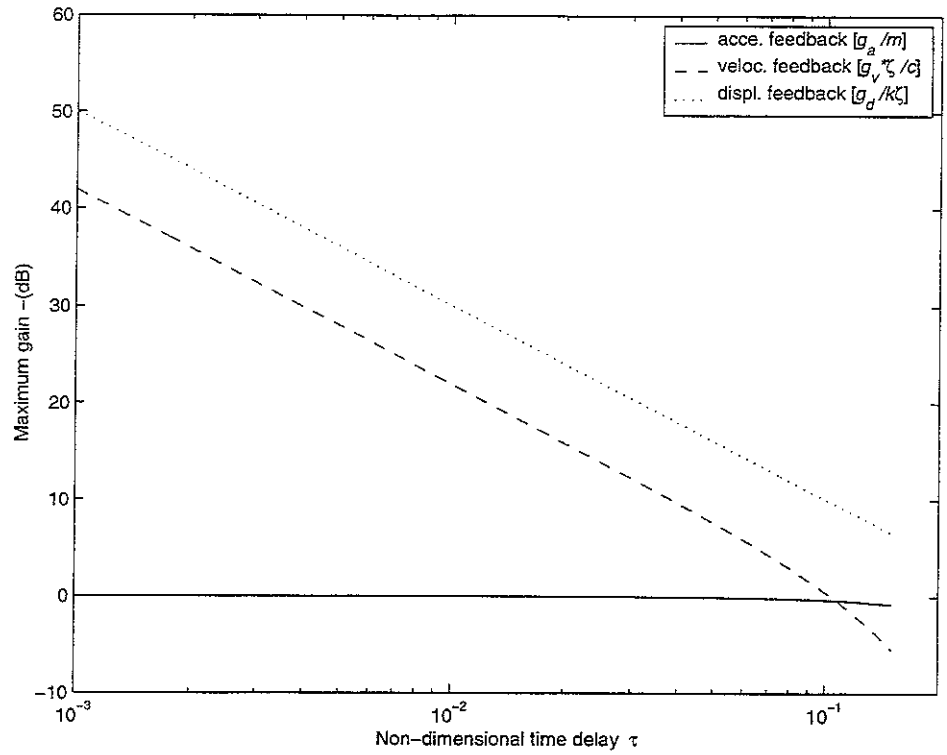

Figure 4.5. Maximum gain as a function of non-dimensional time delay. (damping ratio included with the maximum gain where applicable)

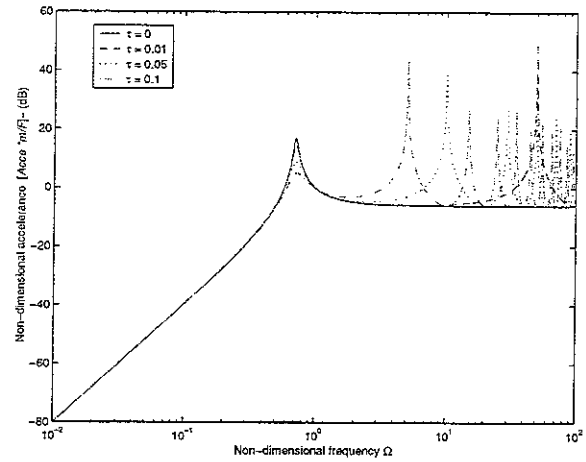

(a) Acceleration feedback control

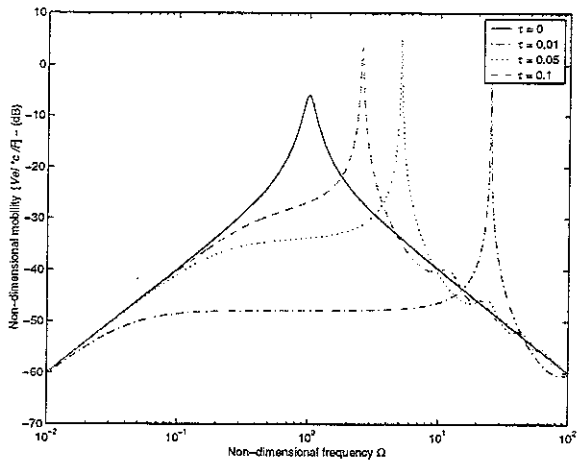

(b) Velocity feedback control

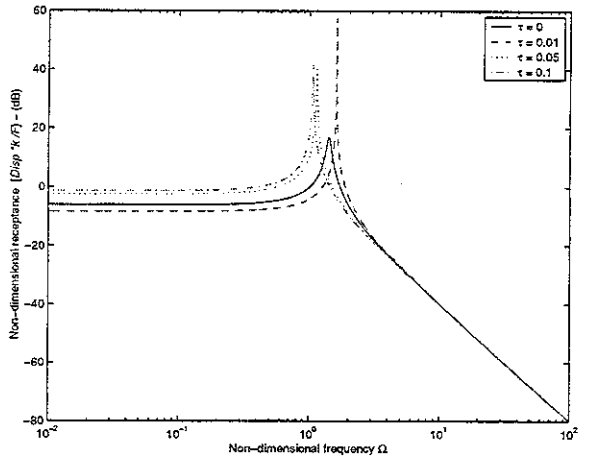

(c) Displacement feedback control

Figure 4.6 Closed loop frequency response function – effects of time delay (ζ =0.05) and maximum gain.

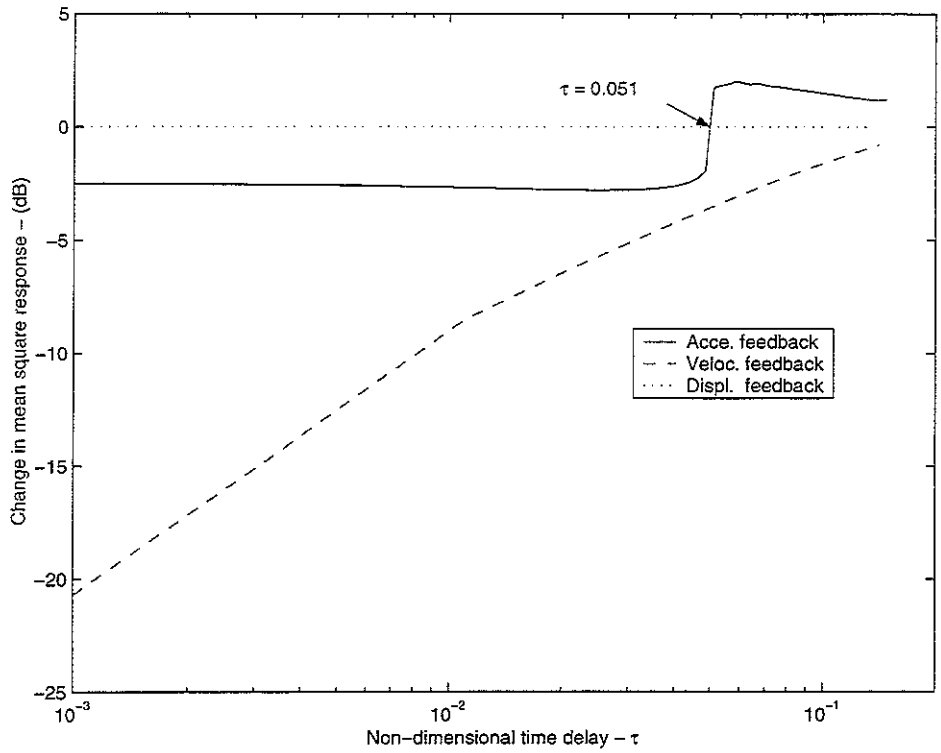

Figure 4.7 Change in mean square response as a function of time delay – for ζ *=0.05, maximum gain and a frequency band of* $0.01 \leq \Omega \leq 100$

5. Experimental work

5.1 Introduction

In this section the experimental work conducted to evaluate the active control of the single degree of freedom system discussed previously is outlined. The overall aim of this section is to compare qualitatively, theoretical analysis and experimental results to verify the conclusions on control strategies (acceleration, velocity and displacement feedback control) discussed in the previous sections. In order to achieve this experiments were conducted using a SDOF system set on a rigid foundation. Open and closed loop responses were measured with the feedback control strategies applied. The experiments were conducted with the following objectives

- To compare the open loop response of acceleration, velocity and displacement feedback control of a single degree of freedom system with theoretical analysis.
- To evaluate/judge the closed loop performances of acceleration, velocity and displacement feedback control.
- To compare the experimental open and closed loop response with predictions based on the characteristics of instruments to see whether the system exhibits any un-modelled characteristics.
- To investigate the effect of the high pass filter corner frequency (α) setting in feedback control. Only velocity feedback control is considered for this purpose.

Since low frequency instabilities were found to be the dominant source in the theoretical analysis, experiments were conducted for the low frequency range of 0~200 Hz.

5.2 Description of the experimental equipment

In this section the equipment and set up used to perform the experiments are described. Figure 5.1 shows the active mount system used in the experimental work. It consists of an aluminium plate, two mounts placed symmetrically underneath the aluminium plate and two electromagnetic shakers to produce the control force. The aluminium plate had previously been shown to behave as a rigid mass up to 1000 Hz

[1], which is well above the maximum frequency of interest in this experimental study.

Each of the mounts is composed of a passive as well as an active part. The passive part of the mount consists of a rubber cylinder fixed between two thin aluminium plates, one side of which is connected to the aluminium plate and the other is glued to a rigid base. The passive parts of both mounts were assumed to have the same mechanical properties and were each modelled as a parallel connection of spring and damper without mass.

The electromagnetic shakers of the system produce the active force, which is transmitted to the bottom disc by a thin rod through the rubber cylinder. Thus the force at the bottom and top of the discs attached to the rubber mount is produced. Since the shakers and rubber mounts are symmetrically placed with respect to the mass centre of the aluminium plate, it is therefore possible to treat the system as a SDOF system if both the control shakers are set to produce in-phase control forces. This can be practically achieved if both the shakers are excited by the same input signal.

In principle the aluminium plate will vibrate under influence of a primary force that will be counter acted by the secondary force generated by the actuators. Therefore eventually the aluminium plate will experience the difference of the primary and secondary forces. Hence in this experimental work, the actuators were set to generate both the primary and the secondary forces [1] by exciting them with the difference of the primary and feedback signal as shown in figure 5.2. A summing box, designed by Serrand [1] was connected as shown in figure 5.2 to produce the difference of the signals (negative feedback). The output signal from an accelerometer placed in the centre of the plate was fed into the charge amplifier, which was again fed through power amplifier 2 into the summing box ensuring negative feedback.

5.3. Characteristics of electrical components

Before any control technique is applied, identification of the experimental system and the characteristics of each instrument used are important. This helps to identify the correct interpretation of the coupling phenomena between the controller and the system dynamics in order to have a sensible assessment of the control performance. Figure 5.2 shows the feedback control system with instruments connected. It consists of a summing box, power amplifier 1, two shakers, an accelerometer, a charge amplifier and power amplifier 2 (model and serial numbers are given in table A2.1 in appendix 2). The accelerometer calibration chart supplied by the manufacture provides information on its gain, which is found to be unity up to 10 kHz. The shaker gain (g_s) is defined as the force generated by the two actuators for an input voltage. This information was taken from Serand's [1] work; which is 0.91. An attempt was made to study the characteristics of the rest of the instrument used in the active feedback control of the single degree of freedom system. These results were used to obtain their mathematical models.

White noise from analyser was fed into the summing box and the output was normalised by the input signal, in a simple experiment to measure the gain (g_b) of summing box. A gain of about 0.67 was observed. The details of experiments and the technique used to model the characteristics of power amplifier 1, power amplifier 2, the charge amplifier in integration mode with 1 and 10 Hz cut-off frequencies and the charge amplifier characteristics at double integration are given in appendix 2. Since the frequency range of interest in this experimental work is 0 ~ 200 Hz, the characteristics were measured in this range. The low pass filter of the charge amplifier does not have influence in this frequency range hence it is not included in the mathematical model. The mathematical model are given below (refer to appendix 2 and 3 for details),

- Power amplifier 1

$$Pa_1 = \frac{j0.2775\omega}{(1 + j0.0633\omega)} \tag{5.1}$$

Equation (5.1) shows the characteristic of power amplifier 1, which is as described in section 3, consists of a gain of 0.2775 and a high pass filter described by $\frac{j\omega}{(1+j0.0633\omega)}$.

- Power amplifier 2

$$Pa_2 = \frac{-g_{p2}\omega^2}{(1+j0.0633\omega)^2} \tag{5.2}$$

where g_{p2} = [0.002, 0.0045, 0.0075, 0.0131, 0.0162, 0.020].

Equation (5.2) shows the characteristics of power amplifier 2, which is the controller in this experimental work. The gain g_{p2} can take a range of discrete values, hence allowing an increase in the gain in the feedback system. It is seen that it has a second order high pass filter.

- The charge amplifier with 1 Hz and 10 Hz cut-off frequencies with single integration,

$$Ca_1 = \frac{j4.1539\omega}{(1+j0.159\omega)} \times \frac{1}{(1+j0.251\omega)} \quad \text{At cut off frequency 1 Hz.} \tag{5.3}$$

$$Ca_{10} = \frac{j0.0567\omega}{(1+j0.0159\omega)} \times \frac{1}{(1+j0.0333\omega)} \quad \text{At cut off frequency 10Hz.} \tag{5.4}$$

It was discussed in section 3 that the greater the value of α (ratio of natural frequency of the system to the corner frequency of electrical component) the better the system performance in closed loop. Equations (5.3), and (5.4) give the charge amplifier frequency response functions at two cut-off frequencies, it is seen that they are considerably different from each other. This allows the investigation of the effect of the magnitude of α as discussed in section 3.

- The charge amplifier frequency response function with double integration

$$Ca\_d_1 = \frac{j5.0752\omega}{(1+j0.159\omega)} \times \frac{1}{(1+j0.1757\omega)^2} \quad \text{At cut off frequency 1Hz.} \tag{5.5}$$

Equation (5.5) shows the characteristics of charge amplifier with double integration, which has a gain 5.0752, a first order high pass filter $\frac{j\omega}{(1+j0.159\omega)}$ and real double integrator $\frac{1}{(1+j0.1757\omega)^2}$.

In acceleration feedback the charge amplifier was assumed to have unity gain. In section 3, for the purpose of simplicity the corner frequencies of the electrical components were assumed to be same. However the measured characteristics of the electrical components are different from each other, this allows only a qualitative comparison of the experimental results with the theory explained in section 3.

5.4 Acceleration feedback control

The open and closed loop frequency response functions of the feed back system shown in figure 5.2 can be written as,

$$G(j\omega)H(j\omega) = Pa_1(j\omega)\times G_p(j\omega)\times Ca(j\omega)\times Pa_2(j\omega)\times g_s g_b \qquad (5.6)$$

where

$G(j\omega) = Pa_1(j\omega)\times G_p(j\omega)\times Ca(j\omega)\times g_b$ and

$H(j\omega) = Pa_2(j\omega)\times g_s$

Closed loop frequency response function (*CLFRF*) is given by,

$$CLFRF(j\omega) = \frac{G(j\omega)}{1+G(j\omega)H(j\omega)}, \qquad (5.7)$$

For acceleration feedback control $Ca(j\omega)=1$, $G_p(j\omega)$ is given by equation (2.14), Pa_1 by equation (5.1), Pa_2 by equation (5.2), $g_s = 0.91$ and $g_b = 0.67$. This system has a total mass (m) of 2.9 kg, natural frequency f_n of 20.2 Hz and damping ratio ζ of 0.05 [1]. Substituting these parameters in equations (5.6) and (5.7), the open and closed loop frequency response functions can be obtained.

As seen from figure 5.3, the Nyquist plot for acceleration feedback control, the system becomes unstable at very low gain (0.0045). As discussed in section 3, acceleration feedback control becomes unstable at lower gain than the velocity or the displacement feedback control systems. Although the charge amplifier was assumed to provide only gain, the system still has an overall high pass filter of order 3 (power amplifier 1 has

first order and power amplifier 2 has second order). It was seen in section 3, table 3.2 and table 3.3 that an acceleration feedback system with an overall high pass filter of order 0,1,2 has an approximate maximum total gain of infinity, $\frac{2\zeta\alpha^2}{\omega_n}$ and $\frac{\zeta\alpha^3}{\omega_n^2}$. It is this inclusion of the damping ratio in the expression for the maximum gain that reduces it in comparison with velocity and displacement feedback systems. Figure 5.4 shows the measured closed loop response of acceleration feedback control. It is seen that the reduction in the resonance peak is small.

5.5 Velocity feedback control

The open and closed loop frequency response functions for velocity feedback control with 1 Hz and 10 Hz charge amplifier cut-off frequency can be obtained by substituting equations (5.3) and (5.4) into equations (5.6) and (5.7) while all other conditions remains the same as acceleration feedback control.

It can be seen from figures 5.5(a) and 5.5(b) that when charge the amplifier cut-off frequency is increased from 1 Hz to 10 Hz the maximum attainable gain reduces considerably. With a 10 Hz cut off frequency the gain becomes comparable to acceleration feedback control. The closed loop response at 1 Hz shown in figure 5.6(a), (simulations) and 5.7(a) (measurement) shows that a reduction of about 20 dB at the uncontrolled resonance frequency is possible. It is also seen that the high frequency behaviour is not affected very much. At very low frequencies however the measurements are inaccurate because of the low sensitivity of actuator and sensor. As predicted in section 3, figure 3.5 as the gain is increased a downshift in resonance frequency and increase in response is observed. At the 10 Hz cut-off frequencies, although the open loop response is similar to acceleration feedback control the measured and simulated characteristics shows that the velocity feedback control has a better closed loop performance than acceleration feedback control.

5.6 Displacement Feedback

The open and closed loop frequency response functions for displacement feedback control with a 1 Hz charge amplifier cut-off frequency can be obtained by substituting equation (5.5) into equations (5.6) and (5.7) while all other conditions remains the same as acceleration feedback control. The theoretical analysis presented in section 3

suggested that such a system is more stable than the velocity feedback and acceleration feedback systems. Figure 5.8 shows the Nyquist plot (simulated and measured) of the open loop response for displacement feedback control. It is seen that displacement feedback control has a better open loop response than the other two. However it was mentioned in section three, that at higher frequencies the displacement feedback signal becomes very small with a reduced signal to noise ratio.

It is seen from figure 5.9, although the response is reduced near resonance with an increase of gain, at high frequencies the response contains noise, which is an undesirable effect.

5.7 Summary

Based on the experimental results and simulations presented in this section, it is evident that acceleration feedback control exhibits low gain and poor closed loop performance as predicted in section 3. Experiments with charge amplifier cut-off frequency set to1 Hz and 10 Hz for velocity feedback control show that the corner frequency setting of the charge amplifier has an effect on the attainable gain and associated closed loop control performance. When the cut-off frequency is set to10Hz it is closer to the system resonance frequency 20.2 Hz, and hence the maximum attainable gain reduces. Amongst the three-control strategies displacement feedback exhibits better open loop performance, however, its closed loop performance is influenced by noise. Hence among the three strategies velocity feedback is more attractive.

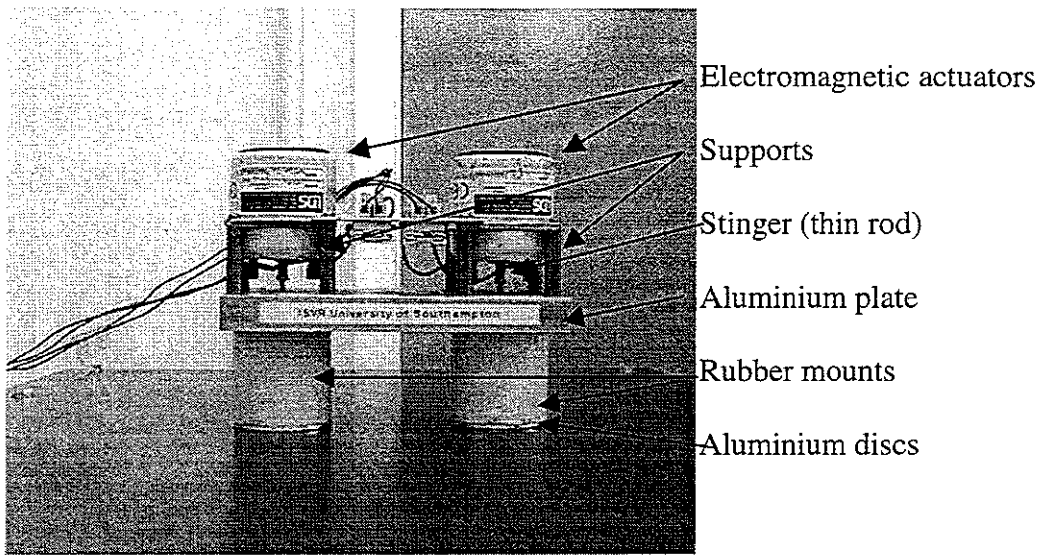

Figure 5.1 Two-mount active control system.

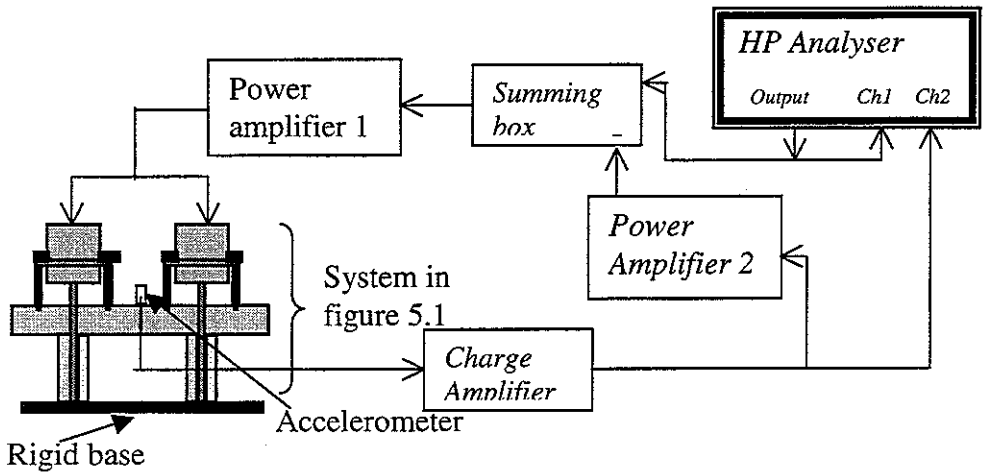

Figure 5.2 Experimental set-up for the control implementation of feedback control of a SDOF system

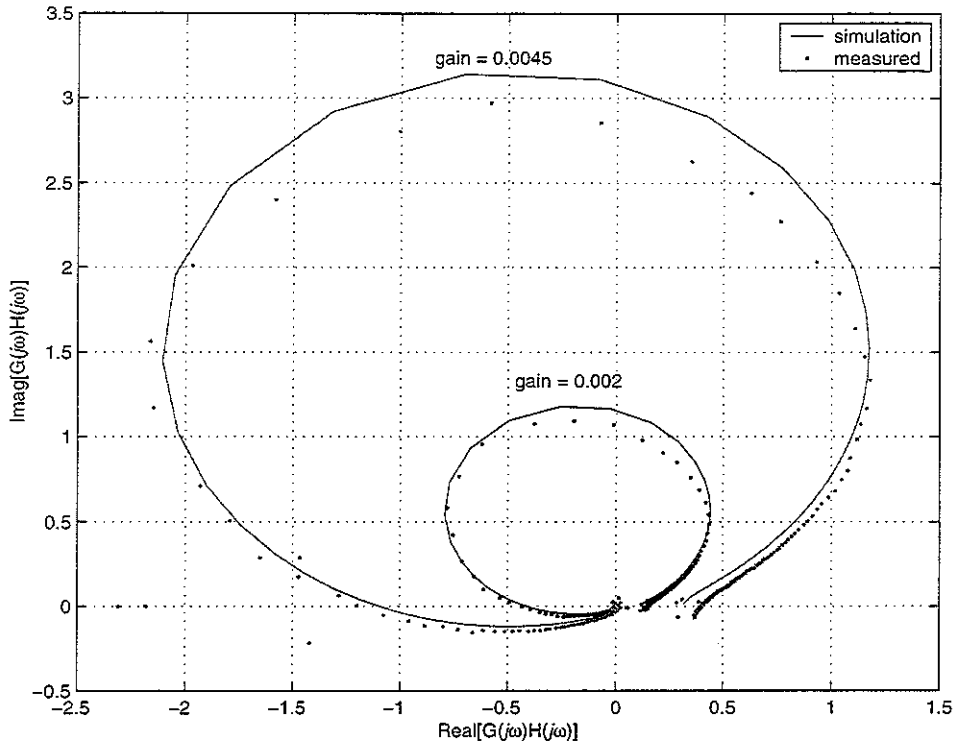

Figure 5.3, Nyquist plot of the open loop frequency response for acceleration feedback control (simulated and measured).

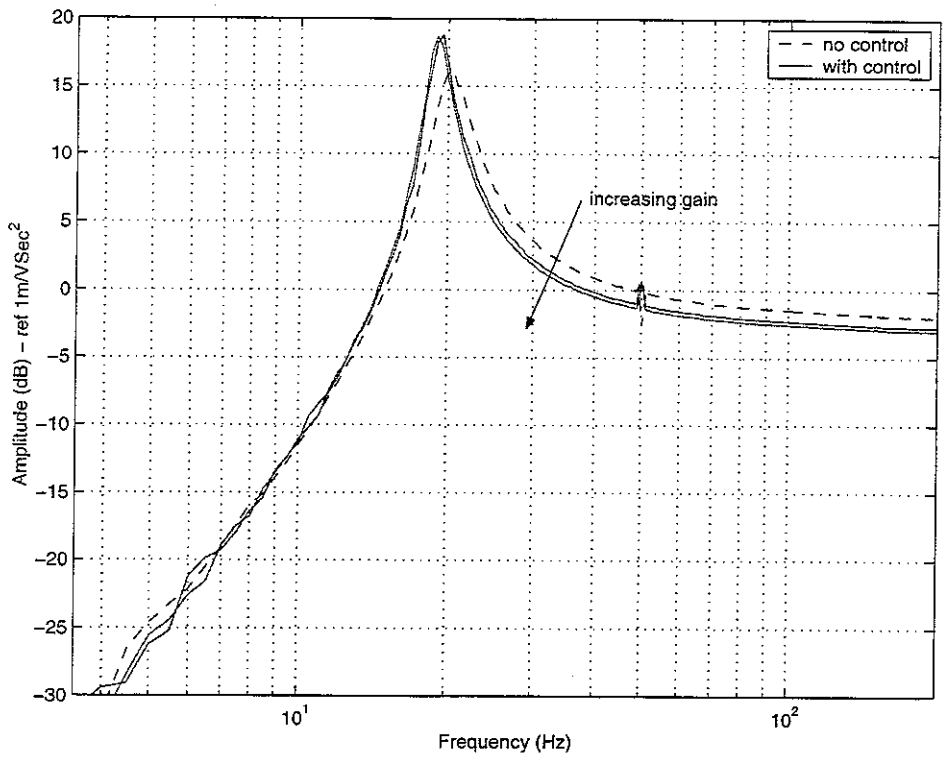

Figure 5.4, Closed loop frequency response function for acceleration feedback control (measured). Gains (0, 0.002 and a gain less than 0.0045)

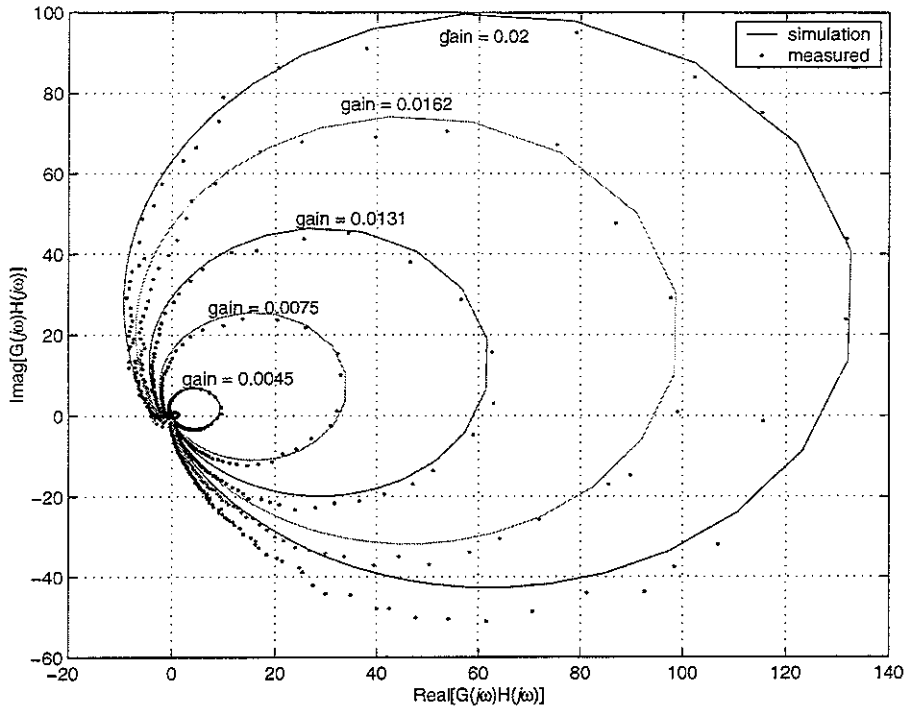

(a) Charge amplifier cut-off frequency set to 1 Hz.

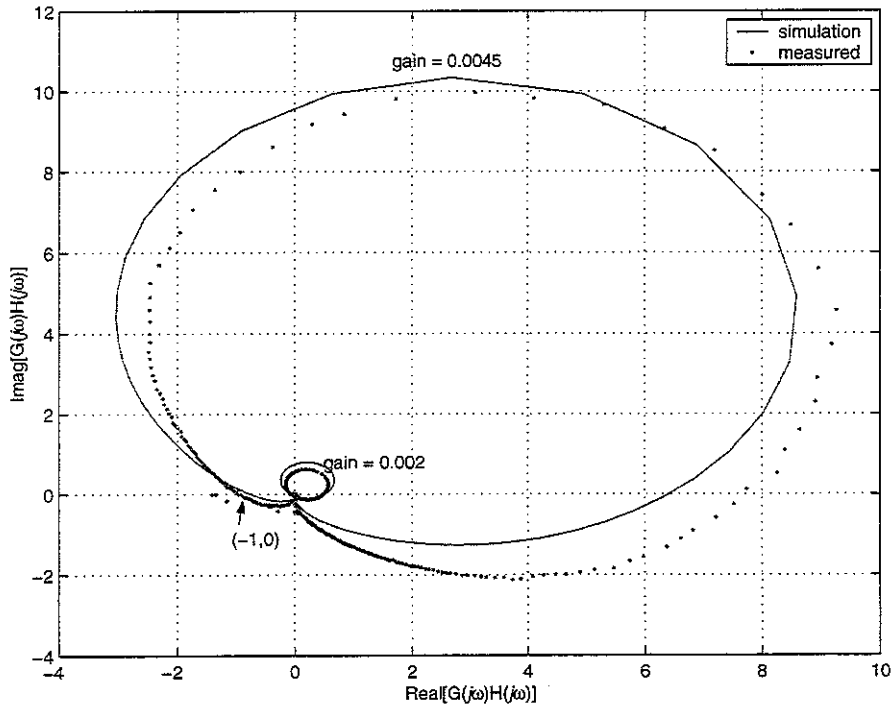

(b) Charge amplifier cut-off frequency set to 10 Hz.

Figure 5.5 Nyquist plot of the open loop frequency response for velocity feedback control (simulated and measured)

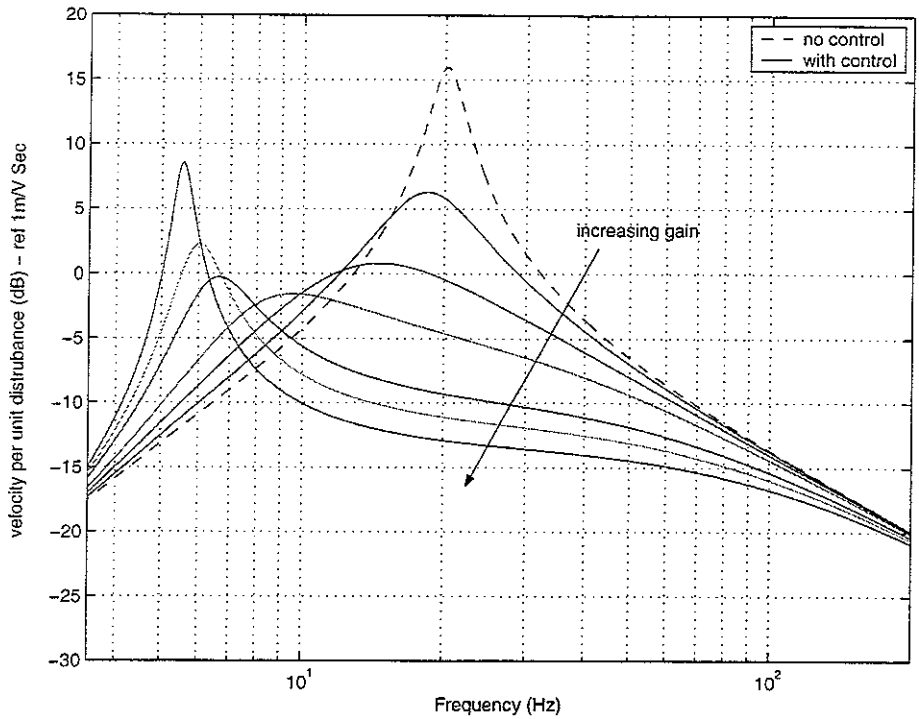

(a) Charge amplifier cut-off frequency set to 1 Hz. Gains = [0, 0.002, 0.0045, 0.0075, 0.0131, 0.0162, and 0.020].

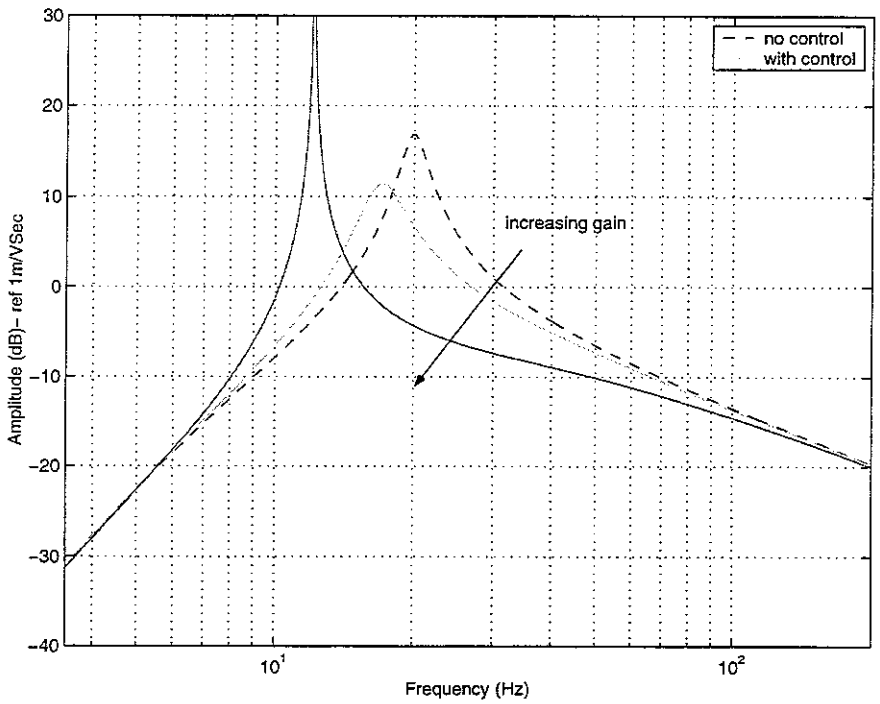

(b) Charge amplifier cut-off frequency set to 10 Hz. Gains = [0, 0.002 and 0.0045].

Figure 5.6 Closed loop frequency response for velocity feedback control (Simulated)

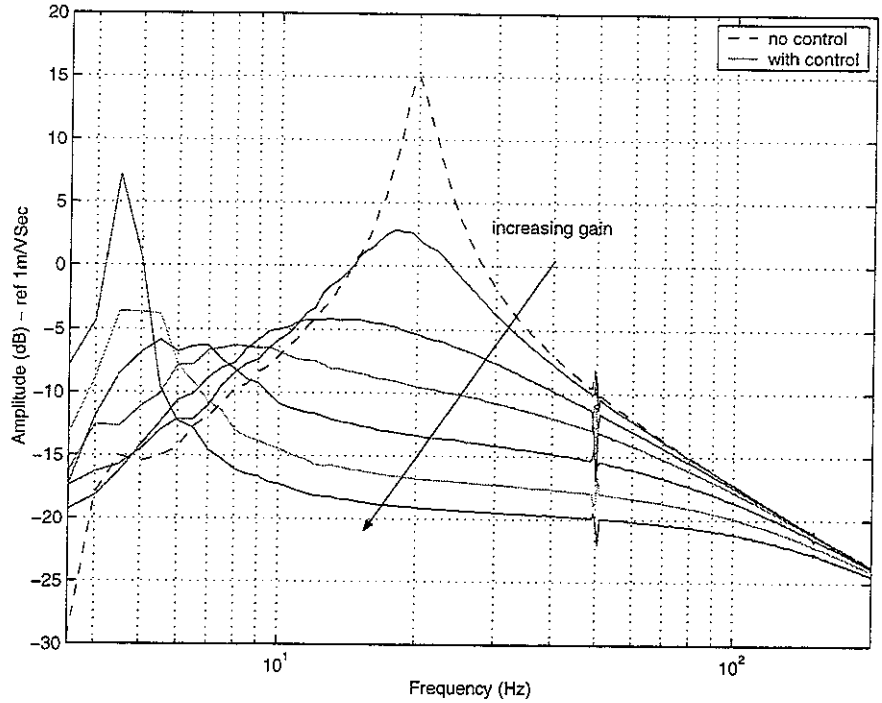

(a) Charge amplifier cut-off frequency set to 1 Hz. Gains = [0, 0.002, 0.0045, 0.0075, 0.0131, 0.0162, and 0.020].

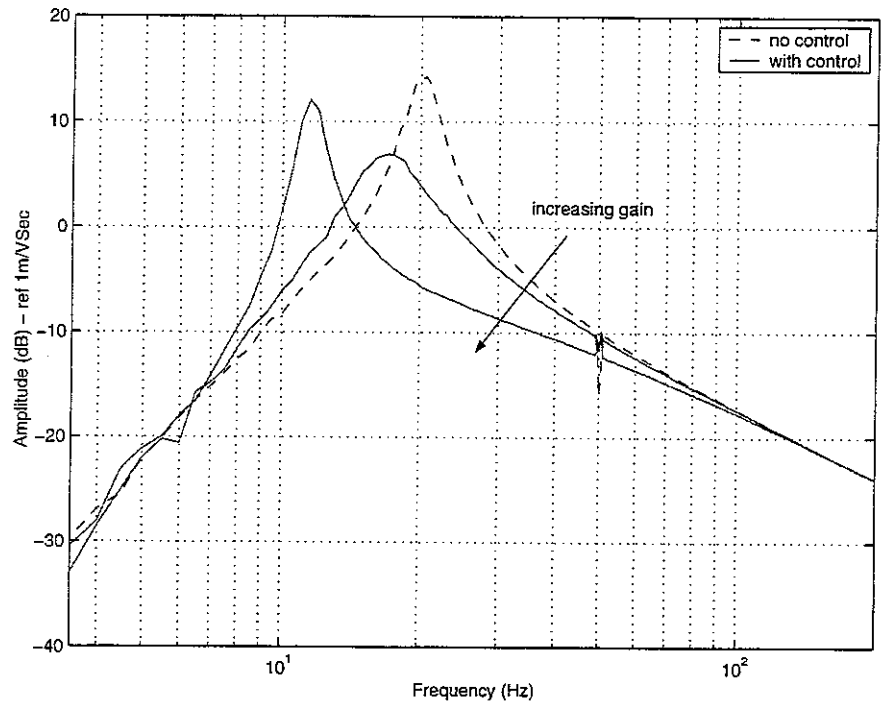

(b) Charge amplifier cut-off frequency set to 10 Hz. Gains = [0, 0.002 and a gain less than 0.0045].

Figure 5.7 Closed loop frequency response for velocity feedback control (measured)

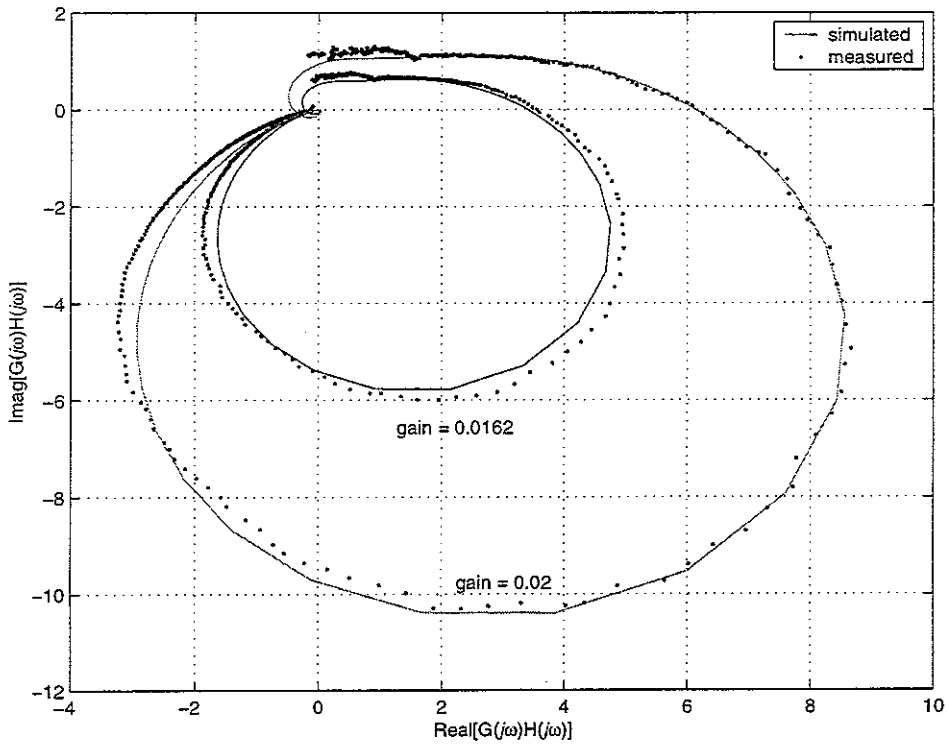

Figure 5.8, Nyquist plot of the open loop frequency response for displacement feedback control with charge amplifier cut-off frequency 1 Hz (simulated and measured).

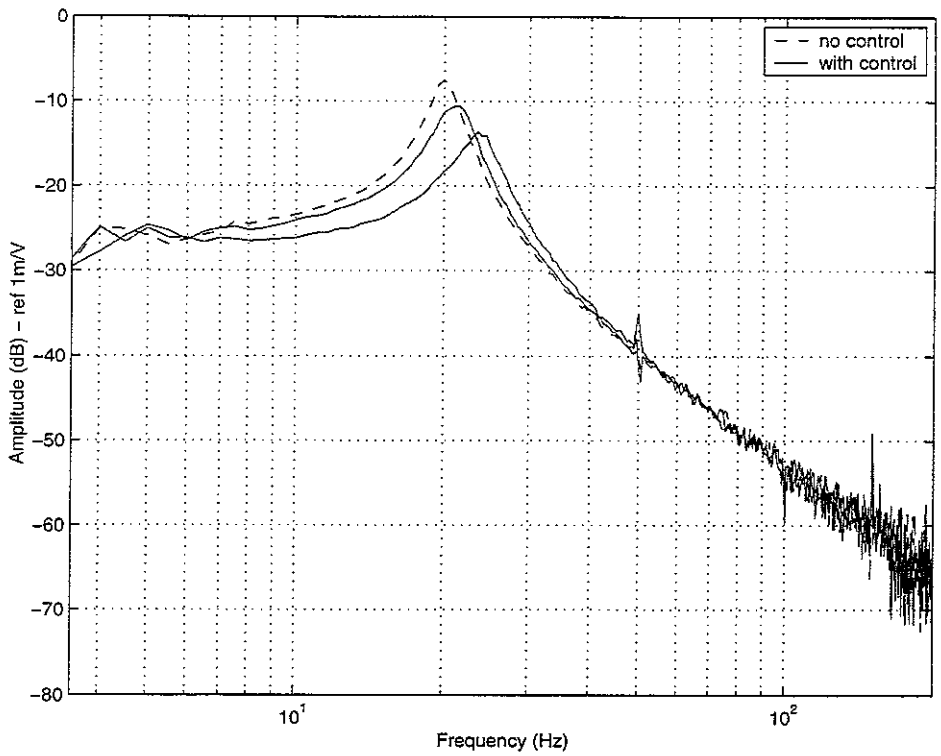

Figure 5.9, closed loop frequency response for displacement feedback control with charge amplifier cut-off frequency 1 Hz (measured). Gains = [0, 0.002 and 0.0045].

6. Conclusions

This report has described an investigation of the stability issues of acceleration, velocity and displacement feedback control of a SDOF system. The control strategy used is analogue feedback control. Low and high frequency sources of instability have been investigated.

An ideal system with perfect instruments is found to be unconditionally stable for acceleration, velocity and displacement feedback. When real components are connected, however, (a real system) it becomes conditionally stable for acceleration, velocity and displacement feedback control. Considering the three configurations the acceleration feedback control system exhibits the lowest maximum gain. Velocity and displacement feedback control systems are unconditionally stable even with a real integrator provided that there is no high pass filter connected. The addition of one high pass filter component for velocity and displacement feedback control brings these unconditionally stable systems to be conditionally stable. Increasing the number of such components reduces the maximum attainable gain. In comparison with velocity feedback, the displacement feedback control system has a higher maximum gain but both systems theoretically have a comparable overall performance. Although damping helps to improve the performance, it does not have a considerable effect in the overall performance.

As far as high frequency instability is concerned the low pass filter does not have significant effect in velocity feedback control. However it reduces the stability of the displacement feedback control system. In addition at high frequency, the displacement feedback control system is affected by noise due to double integration (reduced signal to noise ratio). Although control time delay is the dominant source of instability at high frequencies, it does not significantly affect the analogue feedback control system considered in this report. However for low damping relatively simple formulae have been established to estimate the maximum gain, if there is control time delay, for example in a digital system.

In summary, low frequency instability is dominant in analogue feedback systems, and is caused in particular by the high pass filter component. This provides low frequency phase advance, which is critical to the stability. Considering low and high frequency instabilities, velocity feedback control is more robust and hence considered to be more attractive.

References

1. M.Serrand, 1998, *Msc Dissertation, University of Southampton*, Active isolation of base vibration
2. S.M.Kim, S.J.Elliott and M.J Brennan, *Technical Memorandum No 845, 1999, University of Southampton*, Active vibration isolation of a 3-dimensional structure using velocity feedback control
3. S.J.Elliott, M.Serrand and P.Gardonio, 2001 *Transaction of the American Society of Mechanical Engineers. Vol. 123 pp 250 – 261.* Feedback stability limits for active isolation systems with reactive and inertial actuators
4. C.R. Fuller, S.J. Elliott and P.A. Nelson, 1996, *Active Control of Vibration*, Academic Press, London.
5. M. Serrand and S.J.Elliott, 2000, *Journal of Sound and Vibration, Vol. 234(4) pp 681-704.* Multi-channel feedback control for the isolation of base excited vibration.
6. S.A. Collins and A. H. Von Flotow 1991, *42nd Congress of the International Astronautical Federation, Montreal, Canada. Paper No IAF-91-289.* Active vibration isolation for spacecraft.
7. M.D. Jenkins, P.A. Nelson, R.J. Pinnington and S.J.Elliott, 1993, *Journal of Sound and Vibration Vol. 169, pp 117-140.* Active isolation of periodic machinery vibrations.
8. S.J. Elliott, T.J. Sutton, B. Rafaely and M. Johnson, 1995, *Active 95, pp 863-874.* Design of feedback controllers using a feed forward approach.
9. M.Z. Ren, K. Seto and F. Doi, 1997, *Journal of Sound and Vibration, 205, pp 57-80.* Feedback structure-borne sound control of a flexible plate with an electromagnetic actuator: the phase lag problem.
10. M.J.Brennan, J. Garcia-Bonito, S.J.Elliott, A. David and R.J. Pinnington, 1999, *Smart Mater. Struct. 8 pp 145-153.* Experimental investigation of different actuator technologies for active vibration control
11. Sang- Myeong Kim, Stephen J. Elliott and Michael J. Brennan, 2001, *IEEE Transactions on Control Systems Technology, vol. 9 NO.1 pp 93-100.* Decentralised control for multichannel active vibration isolation.

12. P. Gardonio, S.J Elliott R.J Pinnington, *Journal of Sound and Vibration vol. 207, pp 95-121*, Active isolation of structural vibration on a multiple - degree-of freedom system, Part II: Effectiveness of active control strategies.
13. S.A.Collins, D.W.Miller and A.H.Von Flotow, 1994, *Journal of Sound and Vibration vol. 173 (4) pp 471-501.* Distributed sensors as spatial filters in active structural control.
14. K.H. Baek and S.J.Elliott, 2000, *Journal of Sound and Vibration vol. 230(2), pp 261-289.* The effects of plant and disturbance uncertainties in active control systems on the placement of transducers.
15. Mark Serridge, Torben R Licht, 1986, *Piezoelectric Accelerometer and Vibration Preamplifier Handbook.* B&K.
16. Kenneth G. McConnell, 1995, *Vibration Testing: Theory and Practice*, John Wiley & sons Inc.
17. Richard C. Dorf, 1967, *Modern Control Systems*, Addison Wesley publishing company.
18. J.A.Haskam, G.R.Summers and D. Williams, 1981, *Engineering Instrumentation and Control*, Edward Arnold, London.
19. W. Bolton, 1996, *Measurement and Instrumentation Systems*, Newnes An Imprint of Butter Worth-Heinemann
20. C.F. Beards, 1988, *Vibration and Control Systems*, Ellis Horwood Limited.
21. Robert A. Bruns and Robert M. Saunders, 1955, Analysis *of Feedback Control Systems,* McGraw-hill publishing company ltd.
22. John J. D'azzo and Constantine H. Houpis, 1995, *Linear Control System Analysis and Design*, McGraw-Hill, Inc.
23. Ilene J. Busch-Vishniac, 1998, *Electromechanical Sensors and Actuators*, Springer
24. Gene H. Hostetter, Clement J. Savant, Jr, Raymond T. Stefani, 1982, *Design of Feedback Control System,* Holt, Rinehart and Winston

Appendix 1

A1.1 Analysis of maximum gain for systems in table 3.1

In table 3.1, different instrument conditions, which will form a feedback control system, are given. Cases A1, A2 and A3, which are ideal acceleration, velocity and displacement feedback control respectively, were discussed in section 2 and cases B1, B2 and B3 were discussed in section 3. In this appendix, the rest of the cases are considered. It was also discussed in section 3 that cases (A1 & C1), (B1, D1 &F1), (B2 & C2), (D2, E2 & F2), (C3 & E3) and (D3 & F3) are mathematically similar. Therefore the cases C3, D2, D3, G1, G2 and G3 are discussed here.

For case C3, which is displacement feedback, consisting of real double integrator and charge amplifier gain in the forward path, and pure gain power amplifier and shaker gain in the feedback path, the open loop frequency response function can be written as,

$$G(j\Omega)H(j\Omega)=\left(\frac{-\Omega^2}{m(1-\Omega^2)+j2\zeta\Omega}\right)\left(\frac{1}{1+j\alpha\Omega}\right)^2 g_c g_p g_s \qquad \text{(A1.1)}$$

Letting $g_{total}=\frac{g_c g_p g_s}{m}$, equation (A1.1) can be arranged into real and imaginary parts as follows,

$$\mathrm{Re}(G(j\Omega)H(j\Omega))=g_{total}\frac{\Omega^2\left(4\zeta\alpha\Omega^2+(1-\Omega^2)(\alpha^2\Omega^2-1)\right)}{\left((1-\Omega^2)^2+(2\zeta\Omega)^2\right)(1+\alpha^2\Omega^2)^2} \qquad \text{(A1.2)}$$

$$\mathrm{Im}(G(j\Omega)H(j\Omega))=-g_{total}\frac{2\Omega^3\left(\zeta(\alpha^2\Omega^2-1)+\alpha(\Omega^2-1)\right)}{\left((1-\Omega^2)^2+(2\zeta\Omega)^2\right)(1+\alpha^2\Omega^2)^2} \qquad \text{(A1.3)}$$

When the equation (A1.3) is zero,

$$\Omega^2=\frac{\alpha+\zeta}{\alpha(1+\zeta\alpha)} \qquad \text{(A1.4)}$$

Substituting equation (A1.4) into equation (A1.2) gives,

$$\mathrm{Re}(G(j\Omega)H(j\Omega))=g_{total}\frac{(\zeta\alpha+1)(\alpha+\zeta)}{\zeta\left(4\alpha^2\zeta^2+4\zeta\alpha(\alpha^2+1)+(\alpha^2+1)\right)} \qquad \text{(A1.5)}$$

Which is positive and hence the system is unconditionally stable.

For case D2, which is velocity feedback, consisting of a real integrator, a high pass filter and charge amplifier gain in the forward path, and pure gain power amplifier and shaker gain in the feedback path, the open loop frequency response function can be written as,

$$G(j\Omega)H(j\Omega)=\left(\frac{-\Omega^2}{m(1-\Omega^2)+j2\zeta\Omega}\right)\left(\frac{1}{1+j\alpha\Omega}\right)\left(\frac{j\omega_n\Omega}{1+j\alpha\Omega}\right)g_c g_p g_s \qquad \text{(A1.6)}$$

Letting $g_{total}=\frac{g_c g_p g_s \omega_n}{m}$, equation (A1.6) can be arranged into real and imaginary parts as follows,

$$\mathrm{Re}(G(j\Omega)H(j\Omega))=g_{total}\frac{2\Omega^4\left(\zeta\left(\alpha^2\Omega^2-1\right)+\alpha\left(\Omega^2-1\right)\right)}{\left(\left(1-\Omega^2\right)^2+(2\zeta\Omega)^2\right)\left(1+\alpha^2\Omega^2\right)^2} \qquad \text{(A1.7)}$$

$$\mathrm{Im}(G(j\Omega)H(j\Omega))=g_{total}\frac{\Omega^3\left(4\alpha\zeta\Omega^2+\left(1-\Omega^2\right)\left(\alpha^2\Omega^2-1\right)\right)}{\left(\left(1-\Omega^2\right)^2+(2\zeta\Omega)^2\right)\left(1+\alpha^2\Omega^2\right)^2} \qquad \text{(A1.8)}$$

When the equation (A1.8) is zero, and $\alpha>>1$, $\zeta<<1$ gives,

$$\Omega^2=\frac{1}{\alpha^2} \qquad \text{(A1.9)}$$

Substituting equation (A1.9) into equation (A1.7) gives,

$\mathrm{Re}(G(j\Omega)H(j\Omega))=-g_{total}\frac{\left(\alpha^2-1\right)}{2\alpha\left(4\alpha^2\zeta^2+\left(\alpha^2-1\right)^2\right)}$, equating this to -1 gives maximum total gain as,

$$g_{total\_max}=\frac{2\alpha\left(4\alpha^2\zeta^2+\left(\alpha^2-1\right)^2\right)}{\left(\alpha^2-1\right)} \qquad \text{(A1.10)}$$

Applying the condition $\alpha>>1$ and $\zeta<<1$ gives,

$$g_{total\_max}=2\alpha^3 \qquad \text{(A1.11)}$$

For case D3, which is displacement feedback, consisting of a real integrator, a high pass filter and charge amplifier gain in the forward path, and pure gain power amplifier and shaker gain in the feedback path, the open loop frequency response function can be written as,

$$G(j\Omega)H(j\Omega)=\left(\frac{-\Omega^2}{m(1-\Omega^2)+j2\zeta\Omega}\right)\left(\frac{1}{1+j\alpha\Omega}\right)^2\left(\frac{j\omega_n\Omega}{1+j\alpha\Omega}\right)g_c g_p g_s \qquad \text{(A1.12)}$$

Letting $g_{total}=\frac{g_c g_p g_s \omega_n}{m}$, equation (A1.12) can be arranged into real and imaginary parts as follows,

$$\mathrm{Re}(G(j\Omega)H(j\Omega))=g_{total}\frac{\Omega^4\left(2\zeta\left(3\alpha^2\Omega^2-1\right)+\alpha\left(\Omega^2-1\right)\left(\alpha^2\Omega^2-3\right)\right)}{\left(\left(1-\Omega^2\right)^2+(2\zeta\Omega)^2\right)\left(1+\alpha^2\Omega^2\right)^3} \qquad \text{(A1.13)}$$

$$\mathrm{Im}(G(j\Omega)H(j\Omega))=-g_{total}\frac{\Omega^3\left(2\alpha\zeta\Omega^2\left(\alpha^2\Omega^2-3\right)+\left(1-\Omega^2\right)\left(3\alpha^2\Omega^2-1\right)\right)}{\left(\left(1-\Omega^2\right)^2+(2\zeta\Omega)^2\right)\left(1+\alpha^2\Omega^2\right)^3} \qquad \text{(A1.14)}$$

When the equation (A1.14) is zero, and $\alpha>>1$, $\zeta<<1$ gives,

$$\Omega^2=\frac{1}{3\alpha^2} \qquad \text{(A1.15)}$$

Substituting equation (A1.9) into equation (A1.7) gives,

$\mathrm{Re}(G(j\Omega)H(j\Omega))=-g_{total}\frac{3\left(3\alpha^2-1\right)}{8\alpha\left(12\alpha^2\zeta^2+\left(3\alpha^2-1\right)^2\right)}$, equating this to –1 gives maximum total gain as,

$$g_{total\_max}=\frac{8\alpha\left(12\alpha^2\zeta^2+\left(3\alpha^2-1\right)^2\right)}{3\left(3\alpha^2-1\right)} \qquad \text{(A1.16)}$$

Applying the condition $\alpha>>1$ and $\zeta<<1$ gives,

$$g_{total\_max}=8\alpha^3 \qquad \text{(A1.17)}$$

For case G1, which is acceleration feedback, consisting of a high pass filter and charge amplifier gain in the forward path, and a high pass filter, power amplifier gain and shaker gain in the feedback path, the open loop frequency response function can be written as,

$$G(j\Omega)H(j\Omega)=\left(\frac{-\Omega^2}{m(1-\Omega^2)+j2\zeta\Omega}\right)\left(\frac{j\omega_n\Omega}{1+j\alpha\Omega}\right)^2 g_c g_p g_s \qquad \text{(A1.18)}$$

Letting $g_{total}=\frac{g_c g_p g_s \omega_n^2}{m}$, equation (A1.18) can be arranged into real and imaginary parts as follows,

$$\mathrm{Re}(G(j\Omega)H(j\Omega))=g_{total}\frac{\Omega^4\left(4\zeta\alpha\Omega^2+\left(1-\Omega^2\right)\left(\alpha^2\Omega^2-1\right)\right)}{\left(\left(1-\Omega^2\right)^2+(2\zeta\Omega)^2\right)\left(1+\alpha^2\Omega^2\right)^2} \qquad \text{(A1.19)}$$

$$\mathrm{Im}(G(j\Omega)H(j\Omega)) = g_{total}\frac{2\Omega^5\left(\zeta\left(\alpha^2\Omega^2-1\right)+\alpha\left(1-\Omega^2\right)\right)}{\left(\left(1-\Omega^2\right)^2+(2\zeta\Omega)^2\right)\left(1+\alpha^2\Omega^2\right)^2} \quad \text{(A1.20)}$$

When the equation (A1.14) is zero,

$$\Omega^2 = \frac{\alpha+\zeta}{\alpha(\alpha\zeta+1)} \quad \text{(A1.21)}$$

Substituting equation (A1.21) into equation (A1.20) gives,

$\mathrm{Re}(G(j\Omega)H(j\Omega)) = -g_{total}\dfrac{(\alpha+\zeta)^2}{\alpha\zeta\left(1+\alpha^2+2\alpha\zeta\right)^2}$, equating this to –1 gives maximum total gain as,

$$g_{total\_\max} = \frac{\alpha\zeta\left(1+\alpha^2+2\alpha\zeta\right)^2}{(\alpha+\zeta)^2} \quad \text{(A1.22)}$$

Applying the condition $\alpha >> 1$ and $\zeta << 1$ gives,

$$g_{total\_\max} = \alpha^3\zeta \quad \text{(A1.23)}$$

For case G2, which is velocity feedback, consisting of a high pass filter, real integrator and charge amplifier gain in the forward path, and a high pass filter, power amplifier gain and shaker gain in the feedback path, the open loop frequency response function can be written as,

$$G(j\Omega)H(j\Omega) = \left(\frac{-\Omega^2}{m\left(1-\Omega^2\right)+j2\zeta\Omega}\right)\left(\frac{j\omega_n\Omega}{1+j\alpha\Omega}\right)^2\left(\frac{1}{1+j\alpha\Omega}\right)g_c g_p g_s \quad \text{(A1.24)}$$

Letting $g_{total} = \dfrac{g_c g_p g_s \omega_n^2}{m}$, equation (A1.24) can be arranged into real and imaginary parts as follows,

$$\mathrm{Re}(G(j\Omega)H(j\Omega)) = g_{total}\frac{\Omega^4\left(2\zeta\alpha\Omega^2\left(\alpha^2\Omega^2-3\right)+\left(\Omega^2-1\right)\left(3\alpha^2\Omega^2-1\right)\right)}{\left(\left(1-\Omega^2\right)^2+(2\zeta\Omega)^2\right)\left(1+\alpha^2\Omega^2\right)^3} \quad \text{(A1.25)}$$

$$\mathrm{Im}(G(j\Omega)H(j\Omega)) = g_{total}\frac{\Omega^5\left(2\zeta\left(3\alpha^2\Omega^2-1\right)+\alpha\left(1-\Omega^2\right)\left(\alpha^2\Omega^2-3\right)\right)}{\left(\left(1-\Omega^2\right)^2+(2\zeta\Omega)^2\right)\left(1+\alpha^2\Omega^2\right)^3} \quad \text{(A1.26)}$$

When the equation (A1.26) is zero and $\alpha >> 1$ and $\zeta << 1$,

$$\Omega^2 = \frac{3}{\alpha^2} \quad \text{(A1.27)}$$

Substituting equation (A1.27) into equation (A1.25) gives,

$\mathrm{Re}(G(j\Omega)H(j\Omega)) = -g_{total}\dfrac{9(\alpha^2-3)}{8\alpha^2\left(12\alpha^2\zeta^2+(\alpha^2-3)^2\right)}$, equating this to -1 gives maximum total gain as,

$$g_{total\_max} = \frac{8\alpha^2\left(12\alpha^2\zeta^2+(\alpha^2-3)^2\right)}{9(\alpha^2-3)} \tag{A1.28}$$

Applying the condition $\alpha >> 1$ and $\zeta << 1$ gives,

$$g_{total\_max} = \frac{8\alpha^4}{9} \tag{A1.29}$$

For case G3, which is displacement feedback, consisting of a high pass filter, real double integrator and charge amplifier gain in the forward path, and a high pass filter, power amplifier gain and shaker gain in the feedback path, the open loop frequency response function can be written as,

$$G(j\Omega)H(j\Omega) = \left(\frac{-\Omega^2}{m(1-\Omega^2)+j2\zeta\Omega}\right)\left(\frac{j\omega_n\Omega}{1+j\alpha\Omega}\right)^2\left(\frac{1}{1+j\alpha\Omega}\right)^2 g_c g_p g_s \tag{A1.30}$$

Letting $g_{total} = \dfrac{g_c g_p g_s \omega_n^2}{m}$, equation (A1.30) can be arranged into real and imaginary parts as follows,

$$\mathrm{Re}(G(j\Omega)H(j\Omega)) = g_{total}\frac{\Omega^4\left(8\zeta\alpha\Omega^2(\alpha^2\Omega^2-1)+(\Omega^2-1)(\alpha^4\Omega^4-6\alpha^2\Omega^2+1)\right)}{\left((1-\Omega^2)^2+(2\zeta\Omega)^2\right)(1+\alpha^2\Omega^2)^4} \tag{A1.31}$$

$$\mathrm{Im}(G(j\Omega)H(j\Omega)) = -g_{total}\frac{2\Omega^5\left(\zeta(\alpha^4\Omega^4-6\alpha^2\Omega^2+1)+2\alpha(1-\Omega^2)(\alpha^2\Omega^2-1)\right)}{\left((1-\Omega^2)^2+(2\zeta\Omega)^2\right)(1+\alpha^2\Omega^2)^3} \tag{A1.32}$$

When the equation (A1.32) is zero and $\alpha >> 1$ and $\zeta << 1$,

$$\Omega^2 = \frac{1}{\alpha^2} \tag{A1.33}$$

Substituting equation (A1.33) into equation (A1.31) gives,

$\mathrm{Re}(G(j\Omega)H(j\Omega)) = -g_{total}\dfrac{(\alpha^2-1)}{4\alpha^2\left(4\alpha^2\zeta+(\alpha^2-1)^2\right)}$, equating this to -1 gives maximum total gain as,

$$g_{total\_max} = \frac{4\alpha^2\left(4\alpha^2\zeta + (\alpha^2-1)^2\right)}{(\alpha^2-1)} \tag{A1.34}$$

Applying the condition $\alpha >> 1$ and $\zeta << 1$ gives,

$$g_{total\_max} = 4\alpha^4 \tag{A1.35}$$

A1.2 Maximum gain in system with more high pass filter components

Consider equation 3.27 from section 3. It is rewritten here,

$$G(j\omega)H(j\omega) = \left(\frac{g_c g_p g_s}{m}\right)\left(\frac{-\Omega^2}{1-\Omega^2}\right)\left(\frac{1}{1+j\alpha\Omega}\right)\left(\frac{j\omega_n\Omega}{1+j\alpha\Omega}\right)^m \tag{A1.36}$$

Consider m = 3;

Substituting m = 3, rearranging equation (A1.36) into real and imaginary and then equating imaginary part to zero gives the critical frequency as,

$\Omega_{cri} = \frac{\sqrt{2}+1}{\alpha}$, Substituting this critical frequency into the real part of equation (A1.36) gives

$$\mathrm{Re}\{G(j\Omega)H(j\Omega)\} = -g_{total}\omega_n^3\left(\frac{(5\sqrt{2}+7)}{8\alpha^3(\alpha^2-2\sqrt{2}-3)}\right) \tag{A1.37}$$

where $g_{total} = \left(\frac{g_c g_p g_s}{m}\right)$

When equation (A1.37) is equal to –1 maximum gain occurs. This gives,

$$g_{total\_max} = \frac{1}{\omega_n^3}\left(\frac{8\alpha^3(\alpha^2-2\sqrt{2}-3)}{(5\sqrt{2}+7)}\right) \tag{A1.38}$$

This can be approximated as,

$$g_{total\_max} \approx \frac{8\alpha^3(\alpha^2-6)}{14\omega_n^3} \tag{A1.39}$$

For $\alpha >> 1$, equation (A1.39) can be approximated to give,

$$g_{total\_max} \approx \frac{8\alpha^5}{14\omega_n^3} \tag{A1.40}$$

Consider m = 4;

Substituting m = 4, rearranging equation (A1.36) into real and imaginary and then equating imaginary part to zero gives the critical frequency as,

$\Omega_{cri}^2 = \frac{2\sqrt{5}+5}{\alpha^2}$, Substituting this critical frequency into the real part of equation (A1.36) gives

$$\mathrm{Re}\{G(j\Omega)H(j\Omega)\} = -g_{total}\omega_n^4\left(\frac{5\sqrt{5}(3\sqrt{5}+7)}{64\alpha^4(\alpha^2-2\sqrt{5}-5)}\right) \tag{A1.41}$$

where $g_{total} = \left(\frac{g_c g_p g_s}{m}\right)$

When equation (A1.41) is equal to –1, the maximum gain occurs. This gives,

$$g_{total\_max} = \frac{1}{\omega_n^4}\left(\frac{64\alpha^4(\alpha^2-2\sqrt{5}-5)}{5\sqrt{5}(3\sqrt{5}+7)}\right) \tag{A1.42}$$

This can be approximated as,

$$g_{total\_max} \approx \frac{8\alpha^4(\alpha^2-9)}{19\omega_n^4} \tag{A1.43}$$

For $\alpha >> 1$, equation (A1.43) can be approximated to give,

$$g_{total\_max} \approx \frac{8\alpha^4}{19\omega_n^4} \tag{A1.44}$$

Consider m = 5;

Substituting m = 5, rearranging equation (A1.36) into real and imaginary and then equating imaginary part to zero gives the critical frequency as,

$\Omega_{cri}^2 = \frac{7+4\sqrt{3}}{\alpha^2}$, Substituting this critical frequency into the real part of equation (A1.36) gives,

$$\mathrm{Re}\{G(j\Omega)H(j\Omega)\} = -g_{total}\omega_n^5\left(\frac{56\sqrt{3}+97}{64\alpha^5(\alpha^2-4\sqrt{3}-7)}\right) \tag{A1.45}$$

where $g_{total} = \left(\frac{g_c g_p g_s}{m}\right)$

When equation (A1.45) is equal to –1, the maximum gain occurs. This gives,

$$g_{total\_max} = \frac{1}{\omega_n^5}\left(\frac{64\alpha^5(\alpha^2-4\sqrt{3}-7)}{56\sqrt{3}+97}\right) \tag{A1.46}$$

This can be approximated as,

$$g_{total\_max} \approx \frac{8\alpha^5(\alpha^2-14)}{24\omega_n^5} \tag{A1.47}$$

For $\alpha >> 1$, equation (A1.47) can be approximated to give,

$$g_{total\_max} \approx \frac{8\alpha^7}{24\omega_n^5} \tag{A1.48}$$

Appendix 2

A2. Analysis of instruments used in active control of single degree of freedom system

Before any control technique is applied, identification of the experimental plant and the characteristic of each instruments used is important. This helps to identify the correct interpretation of the coupling phenomena between the controller and the system dynamics in order to have a sensible assessment of the control performance. An attempt was made to study the characteristic of each instrument used in active feedback control of single degree of freedom system and mathematically model their characteristics that were obtained experimentally.

A2.1 Power Amplifiers

A simple experiment, as depicted in figure A2.1, was conducted to measure the frequency response function of the power amplifiers. White noise from a Hewlett Packard analyser (analyser C) was fed into the power amplifier and the output was normalised by the input white noise signal. Figure A2.2 shows the measured characteristic of power amplifier 1, which was used in the experiment discussed in section 5.

It can be seen that the phase of the system tends to zero after 100 Hz. In addition at low frequencies the phase trends to 90 degrees. It suggests that the power amplifier has a high pass filter of first order and a mathematical model can take the following form in the frequency domain.

$\frac{jg_{p1}\omega}{(1+j\tau_{p1}\omega)}$, where g_{p1} is the gain of power amplifier 1 and τ_{p1} is the time constant.

This function can be expressed as magnitude and phase to give,

The magnitude is $PA1 = \frac{g_{p1}\omega}{\sqrt{(1+\tau_{p1}^2\omega^2}}$ and the phase is $\phi = 90 - \tan^{-1}(\tau_{p1}\omega)$.

where $PA1$ and ϕ denote the magnitude and phase of power amplifier 1 respectively. From measurement of power amplifier characteristics, the phase angle ϕ_i and the magnitude $PA1_i$ are known for each frequency points f_i in the range 0~200 Hz. Where i goes from 1 to the number of frequency lines in the measurements n. Using the

phase relationship above, the time constant τ_{p1i} can be calculated for each frequency points f_i. It τ_{p1i} becomes,

$$\tau_{p1i} = \frac{\tan(90 - \phi_i)}{\omega_i} \tag{A2.1}$$

Now using magnitude relationship and equation (A2.1), the coefficient g_{p1i} can be calculated for each frequency points. It becomes,

$$g_{p1i} = \frac{PA1_i \sqrt{(1 + \tau_{p1i}^2 \omega_i^2}}{\omega_i} \tag{A2.2}$$

An estimate of the time constant τ_{p1} and gain g_{p1} are the average of τ_{p1i} and g_{p1i} over the frequency range. It is a good estimate since it takes into account the measurement over the frequency range considered. It can be expressed as follows,

$$\tau_{p1} = \frac{\sum_{i=1}^{n} \tau_{p1i}}{n} \tag{A2.3}$$

$$g_{p1} = \frac{\sum_{i=1}^{n} g_{p1i}}{n} \tag{A2.4}$$

The frequency response function of the power amplifier 1 then becomes,

$$Pow\_amp1 = \frac{j0.2775\omega}{(1 + j0.0633\omega)} \tag{A2.5}$$

Figure A2.2 also shows the Bode magnitude plot and phase plot for this model. It can be seen that this plot is in good agreement with the measured characteristic of the power amplifier 1.

After setting a suitable gain in the power amplifier 1, which is in the forward path, it was intended to change the gain in power amplifier 2 to study the effect of active control. Hence the characteristic of the amplifier 2 was measured for various settings. These are shown in figure A2.3. The phase difference between the low and high frequency of the power amplifier characteristics suggests that it has a high pass filter of order 2. Hence the frequency response function can be written as,

$$Pow\_amp2 = \frac{-g_{p2}\omega^2}{(1 + j\tau_{p2}\omega)^2} \tag{A2.6}$$

where g_{p2} is the gain and τ_{p2} is the time constant of power amplifier 1

Similar to power amplifier 1, equation (A2.6) can be simplified to obtain the time constant τ_{p2} and the gain g_{p2}.

From the phase relationship the coefficient e_i at each frequency point becomes,

$$\tau_{p2_i} = \frac{\tan\left(90 - \frac{\phi_i}{2}\right)}{\omega_i} \tag{A2.7}$$

Now using magnitude relationship,

$$g_{p2i} = \frac{PA2_i(1+\tau_{p2i}^2\omega_i^2)}{\omega_i^2} \tag{A2.8}$$

where $PA2_i$ and ϕ_i are measured magnitude and phase at each frequency points.

Now the time constant τ_{p2} and gain g_{p2} can be calculated using equations (A2.3) and (A2.4) with appropriate modifications. Repeating the procedure for each gain settings, g_{p2} for each gain can be found. The frequency response function for the power amplifier 2 then becomes,

$$Pow\_amp2 = \frac{-g_{p2}\omega^2}{(1+j0.0633\omega)^2}. \tag{A2.9}$$

Where g_{p2} = [0.002, 0.0045, 0.0075, 0.0131, 0.0162, 0.020].

The mathematical model is plotted in the form of Bode magnitude plot and phase plot as shown in figure A2.3. It can be seen that these plots are in good agreement with the measured characteristic of the power amplifier. Due to low sensitivity of accelerometer at very low frequencies, the measurement of power amplifier 1 and 2 is not shown at very low frequencies. It is also interesting to note that the phase is independent of gain. This is because the characteristics of power amplifier are linear. Small peaks at frequencies 50 Hz and 150 Hz are due to the line effect.

A2.2. Charge Amplifier with integrator module

As discussed in section 2 and 3 the charge amplifiers play a crucial role in this experiment. The output charge from a piezo-electric accelerometer is converted into voltage by the charge amplifier. The output voltage is directly proportional to the input charge. Its very high resistance reduces the problem of charge leakage from the piezo-electric crystal and its very high capacitance completely dominates the effect of the cable capacitance.

The charge amplifier can also be used to integrate the accelerometer output so that the output is proportional to the velocity or displacement. Hence velocity or displacement feedback control can also be studied. Since it is intended to study acceleration, velocity and displacement feedback it is useful to study the characteristic of a single integrator and a double integrator. Kim et el. [4] measured the characteristic of a single integrator of charge amplifier using the following approach.

In the frequency domain acceleration and velocity are related by,

$$\ddot{X} = j\omega\dot{X}$$

This can be rearranged to give,

$$\frac{\dot{X}}{\ddot{X}} = \frac{1}{j\omega}$$

Where $\ddot{X}$ and $\dot{X}$ denote acceleration and velocity respectively. Therefore dividing the velocity response measured at a point by acceleration response measured at the same point gives the integrator characteristics. Similarly dividing the displacement response measured at a point by acceleration response measured at the same point gives the double integrator characteristics.

The B&K (type 2635) charge amplifier was used for this purpose. It contains a high pass filter and an integrator module. For velocity and displacement response the high pass filter can be set to a cut-off frequency of 1Hz or 10Hz. The measured characteristics of single and double integrators are shown in figure A2.5 and A2.6. Due to the low sensitivity of the actuator and sensor at low frequencies, the response at low frequencies are not shown. Even with a 1Hz cut off frequency there is a small phase advance at very low frequencies. However the phase approximately tends to -90 degree at high frequencies.

The integrator module in the charge amplifier performs integrations of the filtered signals electronically. It is assumed that the integrator module and high pass filter can be represented separately in a mathematical model (Refer Appendix 3).

Therefore the charge amplifier together with its high pass filter can be modelled as,

$$cha\_amp1 = \frac{jg_c\omega}{(1+j\tau_c\omega)}\frac{1}{(1+j\tau_i\omega)} \qquad \text{(A2.10)}$$

where g_c is the gain of the charge amplifier and $1/\tau_c$ and $1/\tau_i$ are the corner frequency of the high pass filter and integrator respectively.

There are three unknown in equation (A2.13), only two can be found using magnitude and phase information. Hence one of the coefficients has to be fixed to a suitable value. The most appropriate is to fix the time constant τ_c to the setting of the charge amplifier cut-off frequency. The time constant τ_c can be related to the cut-off frequency of the charge amplifier by $\tau_c = \frac{1}{2\pi f_c}$, where f_c is the cut-off frequency. For 1 Hz and 10 Hz cut-off frequencies τ_c is 0.159 and 0.0159 respectively.

Therefore the overall mathematical model of the charge amplifier becomes,

$$Cha\_amp1 = \frac{jg_{c1}\omega}{(1+j0.159\omega)} \times \frac{1}{(1+j\tau_{i1}\omega)} \qquad \text{(A2.11)}$$

$$Cha\_amp10 = \frac{jg_{c2}\omega}{(1+j0.0159\omega)} \times \frac{1}{(1+j\tau_{i2}\omega)} \qquad \text{(A2.12)}$$

Using a similar approach to the power amplifier, the charge amplifier characteristics can be written as,

$$Cha\_amp1 = \frac{j4.1539\omega}{(1+j0.159\omega)} \times \frac{1}{(1+j0.251\omega)} \quad \text{At cut off 1Hz} \qquad \text{(A2.13)}$$

$$Cha\_amp10 = \frac{j0.0567\omega}{(1+j0.0159\omega)} \times \frac{1}{(1+j0.0333\omega)} \quad \text{At cut off 10Hz} \qquad \text{(A2.14)}$$

A2.3. Charge Amplifier with double integrator module

Figure A2.6 shows the charge amplifier characteristic at double integration. A cut-off frequency of 1 Hz was used. Therefore, it can be assumed that the high pass model in equation (A2.16) is unchanged. Therefore a mathematical model for the charge amplifier at double integration can be written as,

$$Cha\_amp\_double = \frac{jg_{dc}}{(1+j0.159\omega)} \times \frac{1}{(1+j\tau_{id}\omega)^2} \qquad \text{(A2.15)}$$

Using the phase and magnitude relationship and applying a similar argument presented for power amplifier, the double integration model can be expressed as,

$$Cha\_amp\_double = \frac{j5.0752\omega}{(1+j0.159\omega)} \times \frac{1}{(1+j0.1757\omega)^2} \qquad \text{(A2.16)}$$

Fig A2.6 also shows the Bode plot of this mathematical model. It can be seen that the representation up to about 3Hz does not reflect the measured characteristic exactly. However apart from that it is a reasonable representation. One reason may be the inaccuracy of the measured response at low frequency. As mentioned above at low frequencies the accelerometer has low sensitivity.

Table A2.1 Equipments used for experimental work

Name	Manufacturer and model	Serial Number
Accelerometer	B& K type 4375	1760059
Charge amplifier	B& K type 2635	1446895
Power amplifier (1)	H/H electronic TPA 50-D	14415
Power amplifier (2)	H/H electronic TPA 100-D	15397
Shakers	Ling dynamic systems ltd Model V101	40326.21
Analyser	Harvard Packard	Analyser B

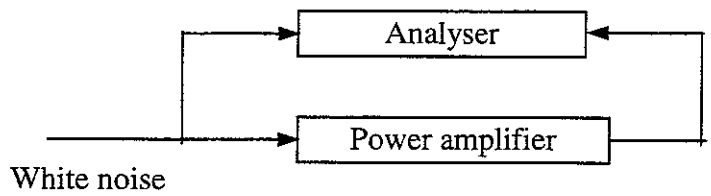

Figure A2.1 the arrangement for measuring frequency response function of Power amplifier

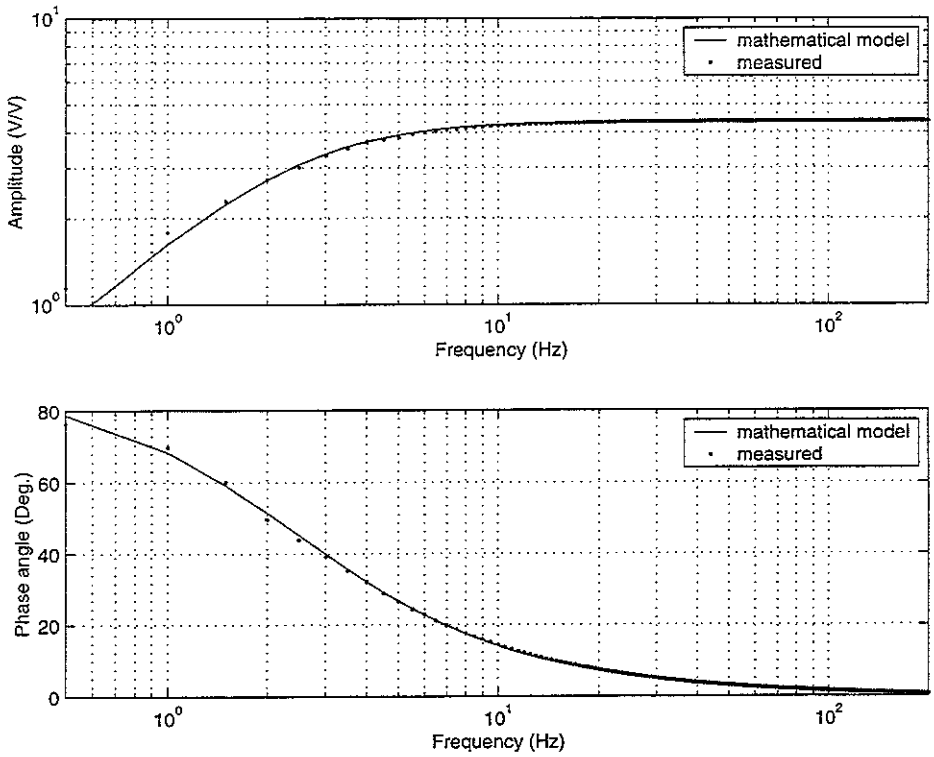

Figure A2.2 Measured and mathematical model of the characteristic of power amplifier 1

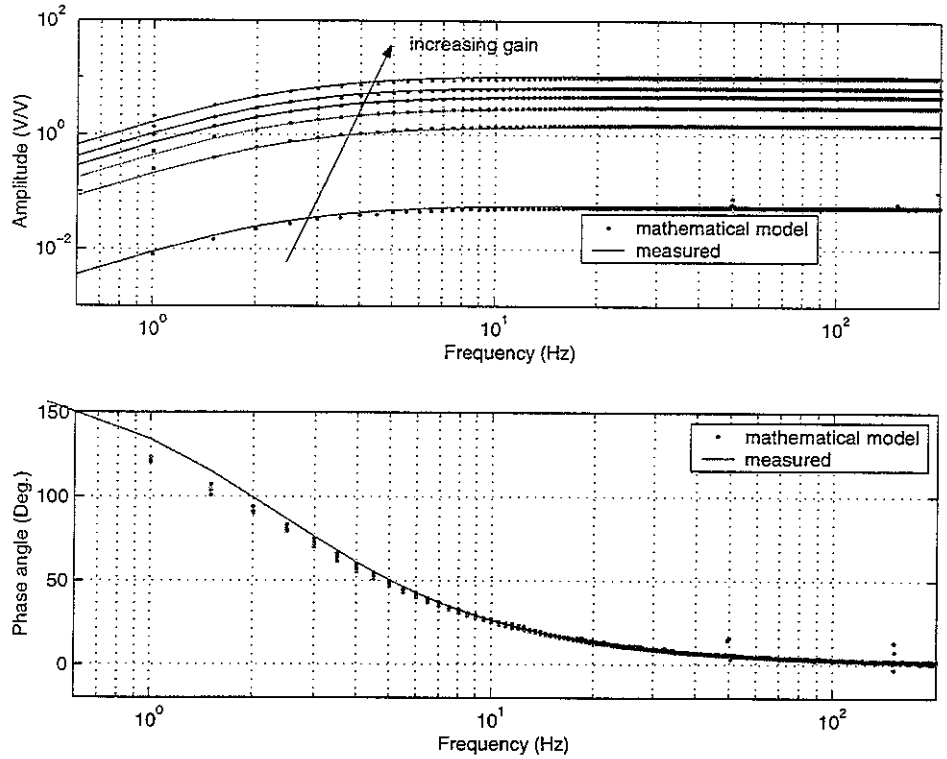

Figure A2.3 Measured and mathematical model of the characteristic of power amplifier 2

(Each curve in the magnitude plot corresponds to the gain settings in the power amplifier from its lowest position. As the gain increased the plots shifts upwards in the direction shown. Corresponding gains are -

`[0.002,0.0045,0.0075,0.0131,0.0162,0.020])`

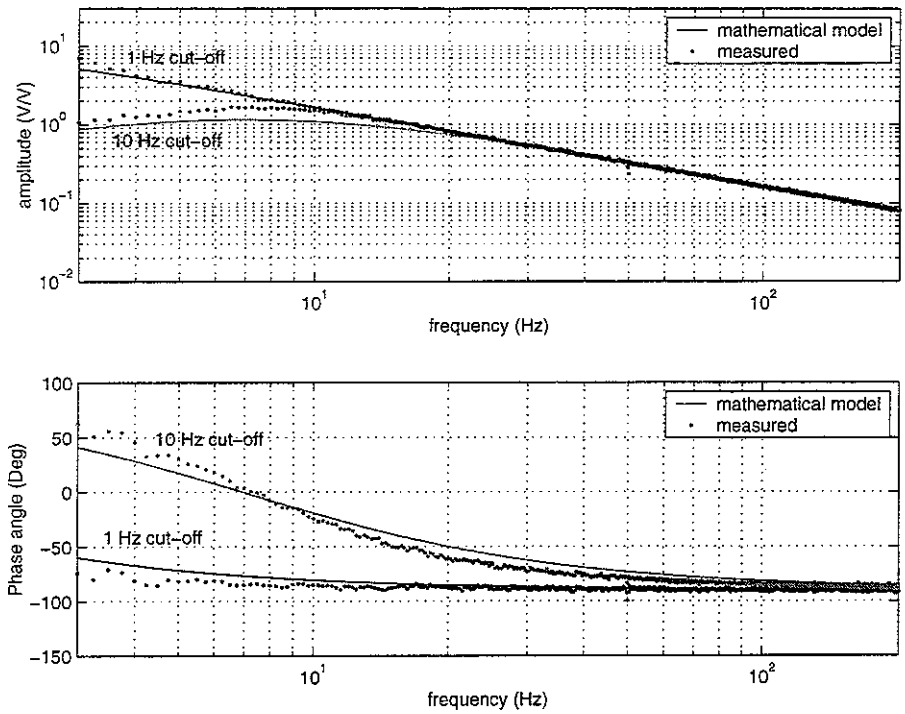

Figure A2.5 Measured and mathematical model of charge amplifier characteristics at 1Hz and 10Hz cut-off frequencies.

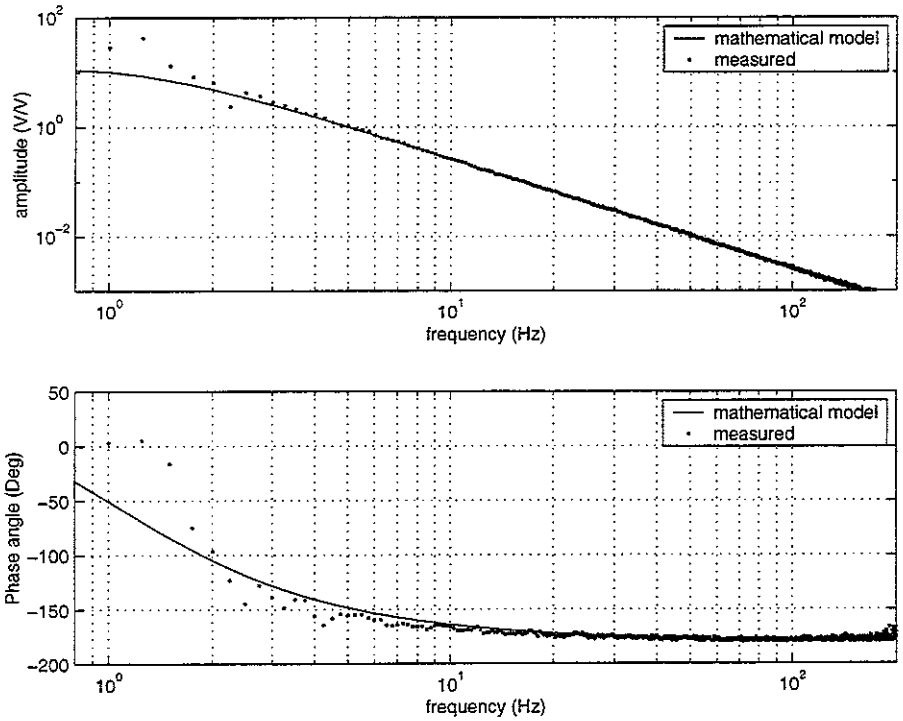

Figure A2.6 Measured and mathematical model of Charge Amplifier characteristic at double integration

Appendix 3

A3. Integrators and filters

As mentioned previously power amplifiers and charge amplifiers consist of high pass filters. In addition the charge amplifier also consists of low a pass filter and an electronic integrator. In this appendix their basic mathematical models are discussed.

A3.1 Electronic integrator

Electronic integration, at the most basic level can be achieved using a circuit similar to the one shown in figure A3.1, where R and C denotes resistance and capacitance respectively.

When a voltage V_{in} is applied at the input, the voltage across the capacitor V_{out} can be shown to be,

$$\frac{V_{out}}{V_{in}} = \frac{1}{1 + j\omega RC} \tag{A3.1}$$

Letting $\tau_i = RC$ equation (A3.1) can be written as,

$$\frac{V_{out}}{V_{in}} = \frac{1}{1 + j\tau_i\omega} \tag{A3.2}$$

When $\tau_i\omega \succ\succ 1$ then,

$$V_{out} \approx \left(\frac{1}{j\tau_i}\right)\frac{V_{in}}{\omega} \tag{A3.3}$$

Similarly when $\tau_i\omega \prec\prec 1$ then

$$V_{out} = V_{in} \tag{A3.4}$$

Comparing equations (A3.2), (A3.3) , it can be seen that an electronic integration has taken place only when $\tau_i\omega \succ\succ 1$. The factor $1/\tau_i$ is usually taken care of in internal calibration [18]. It is also clear that there is no true integration below a certain frequency (i.e. when $\tau_i\omega \prec\prec 1$) and there is almost true integration above a certain frequency (i.e. when $\tau_i\omega \succ\succ 1$). Hence there exists a frequency range in which only a partial integration is taking place. As all of the experiments were in frequency range

0 ~ 200 Hz, it is appropriate to model the integrator module as $\frac{1}{(1+j\tau_i\omega)}$. This model will also deal with the region of partial integration. Whereas a model of $\frac{1}{j\tau_i\omega}$, although theoretically a good representation it will not include the region of partial integration. However in high frequency models $\frac{1}{j\tau_i\omega}$, can be used.

A3.2 High pass filter

High pass filtering can be achieved using a circuit similar to the one shown in figure A3.2, where R and C denotes resistance and capacitance respectively.

When a voltage V_{hin} is applied at the input, the voltage across the capacitor V_{hout} can be shown to be,

$$\frac{V_{hout}}{V_{hin}} = \frac{jRC\omega}{1+j\omega RC} \qquad \text{(A3.5)}$$

Letting $\tau_h = RC$ and substituting in equation (3.4) gives,

$$\frac{V_{hout}}{V_{hin}} = \frac{j\tau_h\omega}{1+j\tau_h\omega} \qquad \text{(A3.6)}$$

where τ_h is called time constant

Equation (A3.5) gives the frequency response function of first order high pass filter. The constant in the numerator of equation (A3.6) can be grouped with gains of the instrument to which it is attached.

A3.3 Low pass filter

Basically Circuit for low pass filter is same as integration circuit, but the difference is that the product RC is very small compared to the integration circuit RC product. Hence the frequency response function for low pass filter can be written as,

$$\frac{V_{lout}}{V_{lin}} = \frac{1}{1+j\tau_l\omega} \qquad \text{(A3.7)}$$

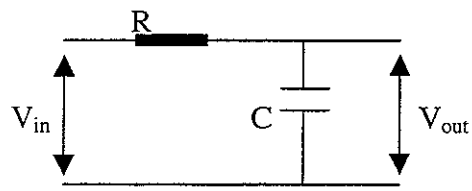

Figure A3.1 a simple RC integration network

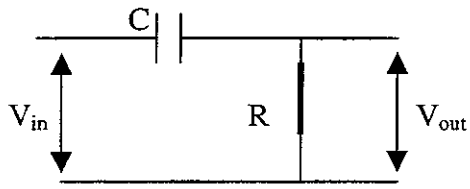

Figure A3.2 a simple RC high pass filter network